2018-01-01

# Comparison Of Mesoscopic Fracture Analysis Techniques: A Case Study Near Onion Creek Diapir, Paradox Basin, Utah

Muhammed Tarik Iraz
*University of Texas at El Paso*, mtiraz@miners.utep.edu

# COMPARISON OF MESOSCOPIC FRACTURE ANALYSIS TECHNIQUES: A CASE STUDY NEAR ONION CREEK DIAPIR, PARADOX BASIN, UTAH

MUHAMMED TARIK IRAZ

Master's Program in Geological Sciences

APPROVED:

Terry Pavlis, Ph.D., Chair

Katherine Giles, Ph.D.

Mark P. Fischer, Ph.D.

Charles Ambler, Ph.D.
Dean of the Graduate School

# Dedication

To my family for encouraging me and making me trust myself and my fiancée for being patient for years despite the peer pressures because of our long-distance relationship.

# COMPARISON OF MESOSCOPIC FRACTURE ANALYSIS TECHNIQUES: A CASE STUDY NEAR ONION CREEK DIAPIR, PARADOX BASIN, UTAH

by

MUHAMMED TARIK IRAZ, B.E.

THESIS

Presented to the Faculty of the Graduate School of

The University of Texas at El Paso

in Partial Fulfillment

of the Requirements

for the Degree of

MASTER OF SCIENCE

Department of Geological Sciences

THE UNIVERSITY OF TEXAS AT EL PASO

December 2018

# Acknowledgements

First of all, I would like to thank Turkish Petroleum Corporation for their financial support, and for providing me with this incredible opportunity to learn English which helped me to accomplish my master's degree in the USA.

I would like to thank my committee members, Dr. Terry Pavlis, Dr. Katherine Giles, and especially Dr. Mark P. Fischer for supporting me from Northern Illinois University by emails and video calls, as well as Dr. Rick Allmendinger for the great free software, Stereonet 10, and responding to my question right away.

I would also like to mention my family and fiancée by being patient and encouraging me.

Finally, I am grateful to those who contributed in my academic and personal life in the USA, including I.T.S research group, specifically Nila Matsler; ExxonMobil for supporting me financially during my field work; David Lankford, Kate Grisi, Garrett Goff and Alex Eddy for assisting me in the field work; Galen Kaip for teaching me how to use surveying DGPS (digital Global Positioning System) equipment and both Kinematic and RTK collection methods in the field work; and Dr. Annette Veilleux for answering my questions stoically since I got the acceptance from UTEP.

# Abstract

Faults and fractures are abundant along the diapir contact in the Onion Creek Diapir in eastern Utah and relate to the mechanisms of diapir formation. Western Onion Creek exhumes two spectacular exposures of the diapir contact and adjacent wall rocks providing two nearly orthogonal transects oriented ~E-W and S-N. In this study, I used field measurements from natural outcrops and a 3D model developed using Structure-from-Motion/Multiview Stereo photogrammetry to evaluate fracture reservoir development along diapir margins. The 3D-Model was developed using Agisoft Photoscan from ~3200 ground-based images and was georeferenced using 76 ground control points located with a GPS unit capable of cm level accuracy. Simultaneous measurements of ground control points with a handheld WAAS enabled GPS allowed a comparison of model accuracy with this lower resolution GPS. Although horizontal positions of the handheld GPS were in line with known errors in differential GPS, the vertical estimates from the handheld produced a systematic error. The origin of this error is uncertain but likely is related to local terrain affecting the handheld GPS. The 3-D models were interpreted using Maptek I-site Studio, allowing 3D mapping of fractures and bedding as well as measurements of strike and dip from fractures visible on the model. This allowed direct comparison of model based measurements to field measurements at focus sites. This comparison of model results with field data showed comparable results at all sites where fractures formed clear surfaces on the model and arguably the model results were superior at one site where a second fracture set was revealed by allowing measurements at the top of a cliff, above the site. At complexly deformed sites near the diapir contact, however, measurements made on the model were unsatisfactory, producing measurements that were inconsistent with the field data due to

insufficient 3D control and resolution of the model at this site. This problem could have been eliminated had we taken high resolution images of this site as a virtual outcrop, allowing sufficient point density for resolving surfaces on the model. Future studies should consider this approach of developing higher resolution models within larger models where this kind of assessment is needed.

# Table of Contents

# List of Tables

# List of Figures

# 1. Introduction

The understanding of near salt stratigraphy in salt diapir systems is a key exploration issue for the oil and gas industry (Cook, 2017). Sediments that are affected by salt diapirs can have spectacular structural traps (Figure 1), stratigraphic traps, or both. Unfortunately, deformation at the salt interface is complex and fracture networks in the vicinity of the salt contact can complicate local permeability near the salt margin, confounding industry attempts to model subsurface petroleum systems with potentially expensive results when these models are in error. As a part of this effort to evaluate this type of problem, this paper concentrates on western Onion Creek in eastern Utah where a salt diapir contacts the Permian Cutler Formation with spectacular exposures of the deformed rocks along the contact. The Cutler Formation in the Paradox Basin has been widely studied for more than five decades (eg. Baars, 1966; Baars et al, 1981; Barbeau, 2003; Bromley, 1991; Condon, 1997; Elston et al, 1960, 1962, 1963; Friedman et al, 1994; Goldhammer et al, 1994; Hazel, 1994; Hite et al, 1981; Hudec, 1995; Kluth et al, 2009; Lawton et al, 2006; Moore et al, 2008; Nuccio et al, 1996; Ohlen, 1965; Rasmussen, 2006; Rasmussen et al, 2009; Raup et al 1992; Trudgill et al, 2009; Trudgill, 2011; Wengerd, 1962; White et al, 1983). The Onion Creek diapir (Figure 2) is one of many NW-SE salt walls in Paradox Basin (Figure 3) (Doelling, 1985; Trudgill, 2011). The details of what happens at the salt sediment interface at Onion Creek, however, are poorly understood and it is this problem that is the subject of this study.

Fracture is defined by Narr et al (2006) as discontinuity or parting of a material that is a direct product of brittle failure. In this study, fractures along the contact of the Salt Diapir and Cutler Fm were investigated to see how fracturing changes near the diapir margin and to

determine if any variations are related to salt movement. To analyze a fracture network, it is required to have many fractures which might be grouped based on orientations, types, and ages and there is a need to asses how fracture branches interact with each other (Peacock et al., 2018). The characterization of fracture interactions is listed as Fracture type (opening, closing, shearing or mixed-mode displacements), geometry and topology, chronology, kinematics (Peacock, 2018).

In this study I examine a well-exposed contact zone between the Onion Creek diapir and adjacent Cutler Formation. The focus of the study was on use of new technology, primarily 3D Structure-from Motion/Multiview Stereo modeling of the outcrops but also rapid field measurement of orientations using an Iphone, to asses the fracture systems within the outcrop.

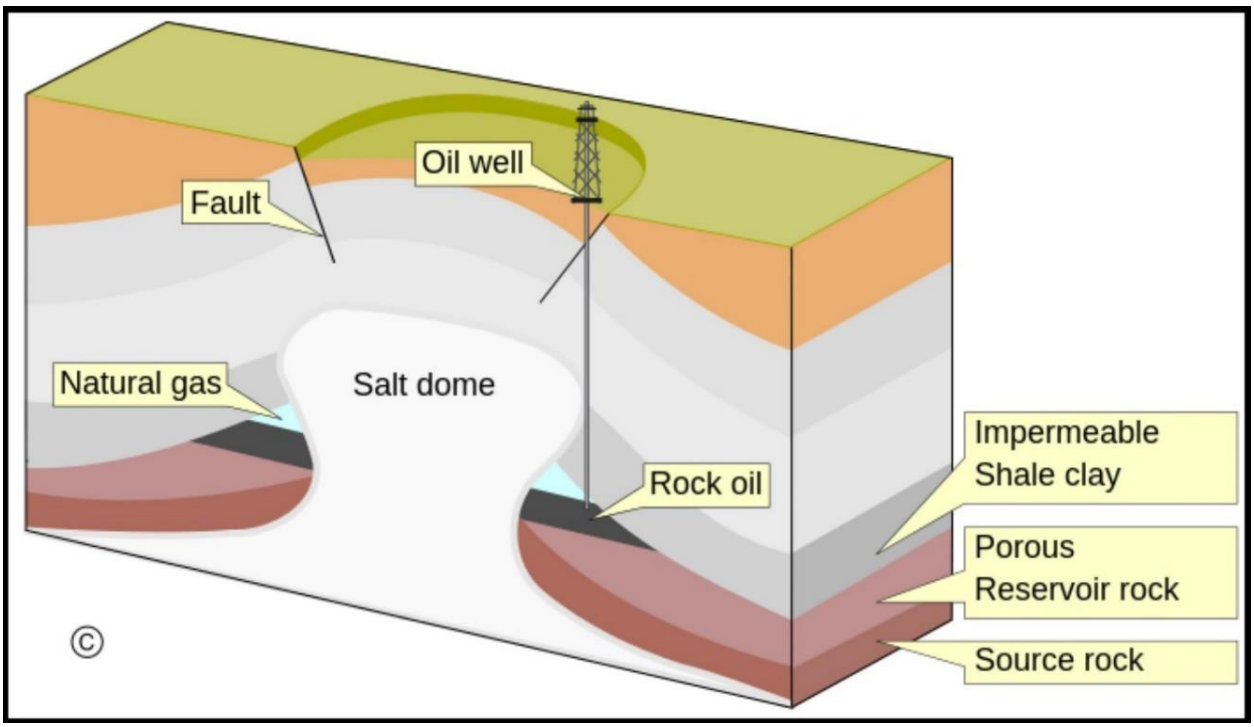


*Figure 1: Salt dome trap (Green, 2014)*

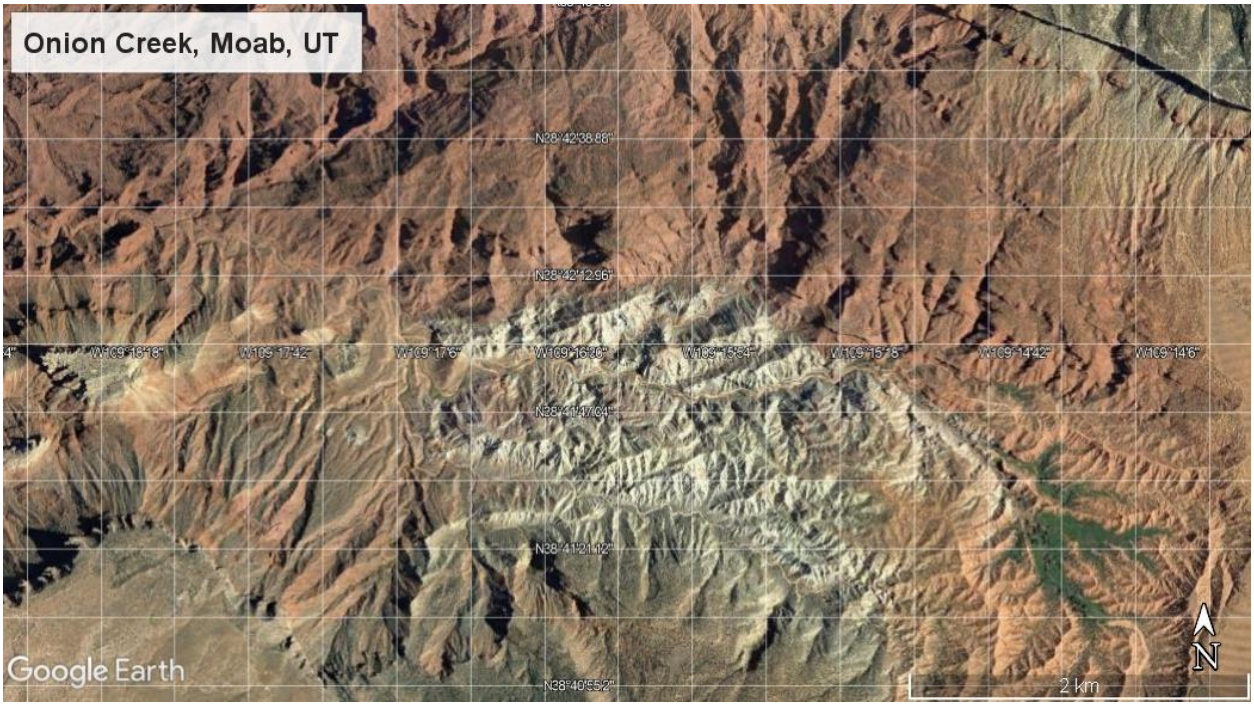


*Figure 2: Location of Onion Creek from Google Earth*

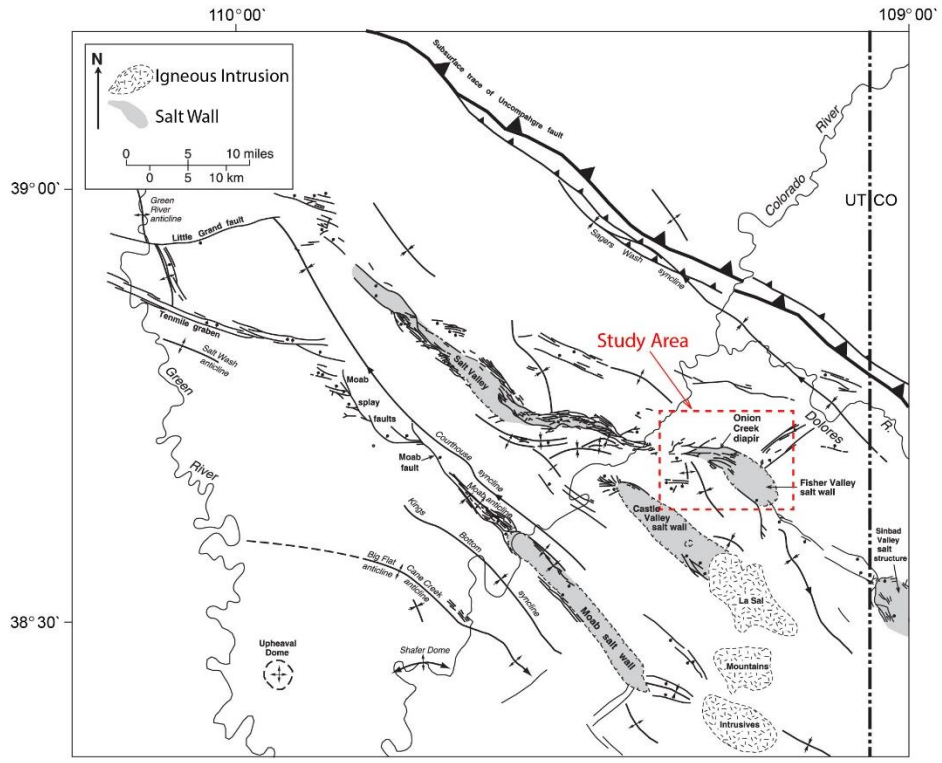


*Figure 3: A structural map of the Paradox Basin. The map illustrates the salt domes and Uncompahgre Front. (modelled from Trudgill, 2011; after Doelling, 2001)*

# 2. Background: Previous Work and Importance of Fracture Network Systems

## 2.1. The Importance of the Area

In the Paradox Basin, petroleum has been extracted from stratigraphic traps in rocks of Devonian and Carboniferous (Mississippian and Pennsylvanian) ages (Baars and Stevenson, 1982). A massive sequence (~up to 4300m (Trudgill, 2011)) of Pennsylvanian rocks with organic-rich black shales form petroleum source rocks of the basin with younger Pennsylvanian-Permian clastic strata forming the primary reservoir rocks. The black shales generated over 400 MMbbl (millon barrels of oil) and 1 TCF gas (trillion cubic feet) within the basin (Baars and Stevenson, 1982; Hite et al., 1984; Nuccio and Condon, 1996; Grisi, 2018). Thus, understanding this petroleum system is important for the oil and gas industry (Cook, 2017).

## 2.2. Fracture Network

The significance of fractures is understood in engineering, geotechnical, and hydrogeological applications because they can play a role as hydraulic conductors, providing pathways for fluid flow or a barrier which can inhibit flow toward them. Many reservoirs of petroleum, gas, geothermal, and water are developed in fractured rocks (NRC, 1996). Fractures form in a variety of modes and can record a stress history within rock bodies, but separating fracture generation and fracture type within individual outcrops can be challenging in complexly deformed rocks. Here I attempt to evaluate this type of problem using a new approach in which limited field time is supplemented by extensive study of the outcrop post-field work, using a 3D model of the outcrop and remotely sensed fracture measurements.

The way to identify, locate and characterize the fractures that are important hydraulic conductors or barriers is through determination of their orientation and connectivity. Rock properties have a significant function in both the creation of fractures and in the structure of fault zones. Within the inner structures of the fractures as well as the fracture zones in various lithologic sections, there exist distinct differences (NRC, 1996).

There are numerous ways to determine fracture properties such as surface methods, borehole-borehole/borehole-surface methods, single-hole methods, or fluid flow monitoring using geophysical methods. Subsurface methods, however, are always a poor estimator of fracture systems because of limited sampling. Hence, excellent natural exposures provide critical information to asses subsurface data when only those data are available. In this study neither well data nor seismic data are available, but excellent surface exposures allow careful assessment of fracture systems in situ. Specifically, after field reconnaissance we recognized that a river cut provided two nearly orthogonal transects oriented ~E-W and S-N that produced exceptional exposures of fractured rocks along the Onion Creek diapir contact. Therefore, I used these natural outcrops to evaluate fracture reservoir development along diapir margins.

## 2.3. Geology of the Paradox basin

The Paradox Basin is a large asymmetric basin. Onion Creek exposes one of the salt diapirs in the basin. The Paradox Basin developed from middle of Pennsylvanian to Permian time as part of the Ancestral Rocky Mountain (ARM) orogenic event (Kelley, 1958; Doelling, 1988; Barbeau, 2003). The basin exhibits similarities to intraforeland flexural basins developed by basement-cored thrusting which formed the Uncompahgre Uplift. The basin is elongate in a NW-SE direction and it is bounded to the northeast by the Uncompahgre Thrust. Evaporites, black shale, and halite of the Pennsylvanian Paradox Formation were mobilized by sediment

loading and displaced upward through salt diapirism (Trudgill, 2011). The Onion Creek diapir in particular is located within 16 km of the Uncompahgre Thrust (Table 1 from Trudgill, 2011, modified from Banbury, 2005) (Figure 3). The diapir exposes evaporites of Paradox Fm and large carbonate blocks of Honaker Trail Fm which were distorted whilst Undifferentiated Permian Cutler Fm was deposited across the basin as progradational alluvial to fluvial fans (Cook, 2017). Diapirism continued through deposition of younger rocks as well, at least through Late Tertiary and Quaternary time during deposition of Upper Triassic of the Chinle Formation, Jurassic Morrison Formation, Tertiary burial, and Late Tertiary-Quaternary, erosion and dissolution of salt (Doelling, 1988; Hazel, 1994; Doelling, 2002; Trudgill, 2011).

Deposition of the Cutler Group had a well know effect on formation of the salt domes and has been studied for some time (Barbeau, 2003; Condon, 1997; Elston et al, 1962; Hazel, 1994; Nuccio et al, 1996; Trudgill et al, 2009; Trudgill, 2011 etc.). Before salt movement, Honaker Trail Fm (Pennsylvanian) was deposited and therefore is the mostly strongly deformed rock unit above the Paradox Formation (Trudgill and Paz, 2009; Trudgill, 2011).

The Onion Creek salt diapir is one of a linear trend of salt structures. Specifically, it creates a structural high within the Fisher Valley salt wall (Figure 3), and has the best exposures of the evaporites in the Paradox Basin. At the surface more than 4 $km^2$ of evaporites are revealed in the core of the diapir and with outcrops of the Paradox Formation composed primarily of gypsum, with minor anhydrite and clastic rocks (Trudgill, 2011).

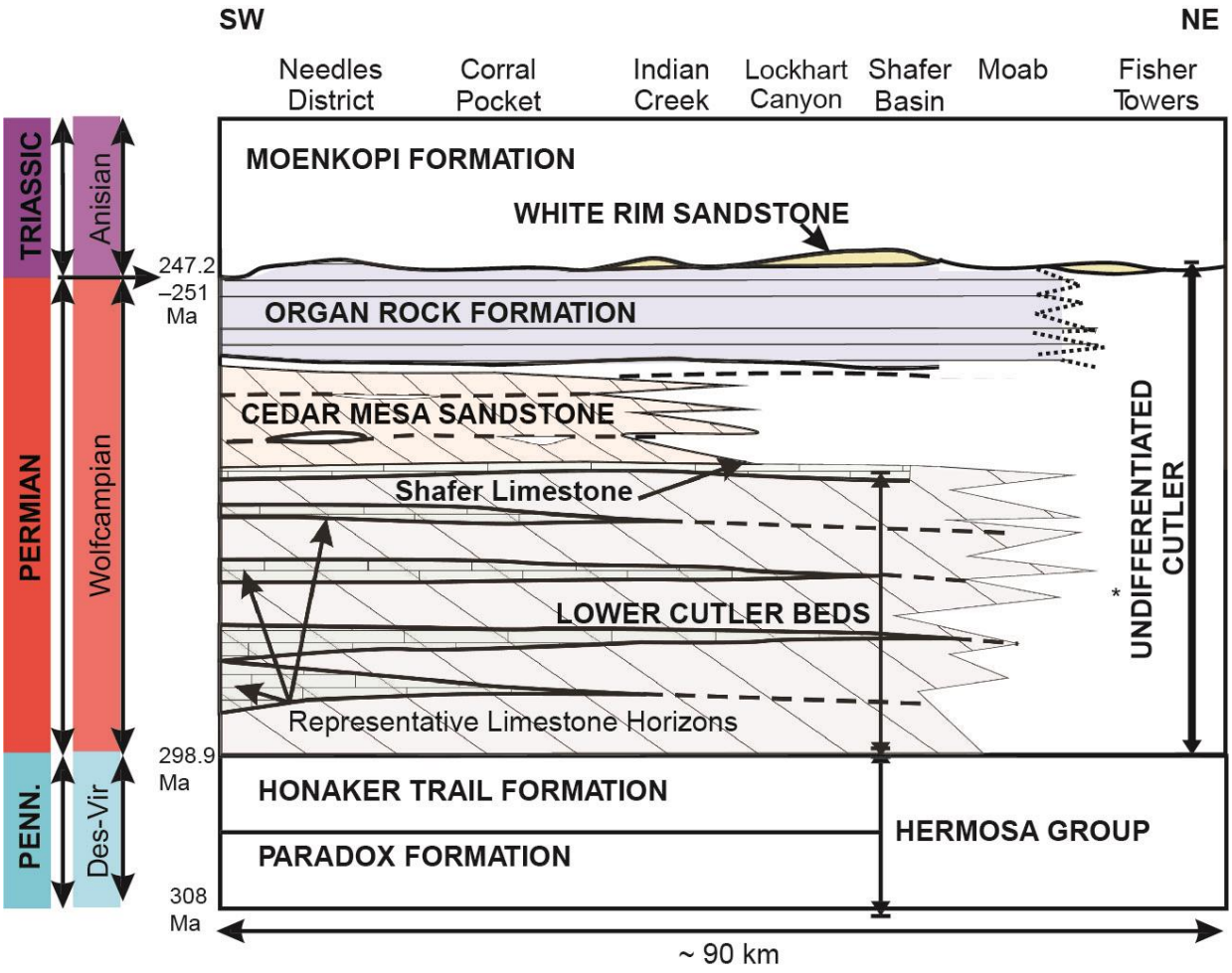


*Figure 4: The stratigraphic column of the study area (Modified from Venus et al., 2015)*

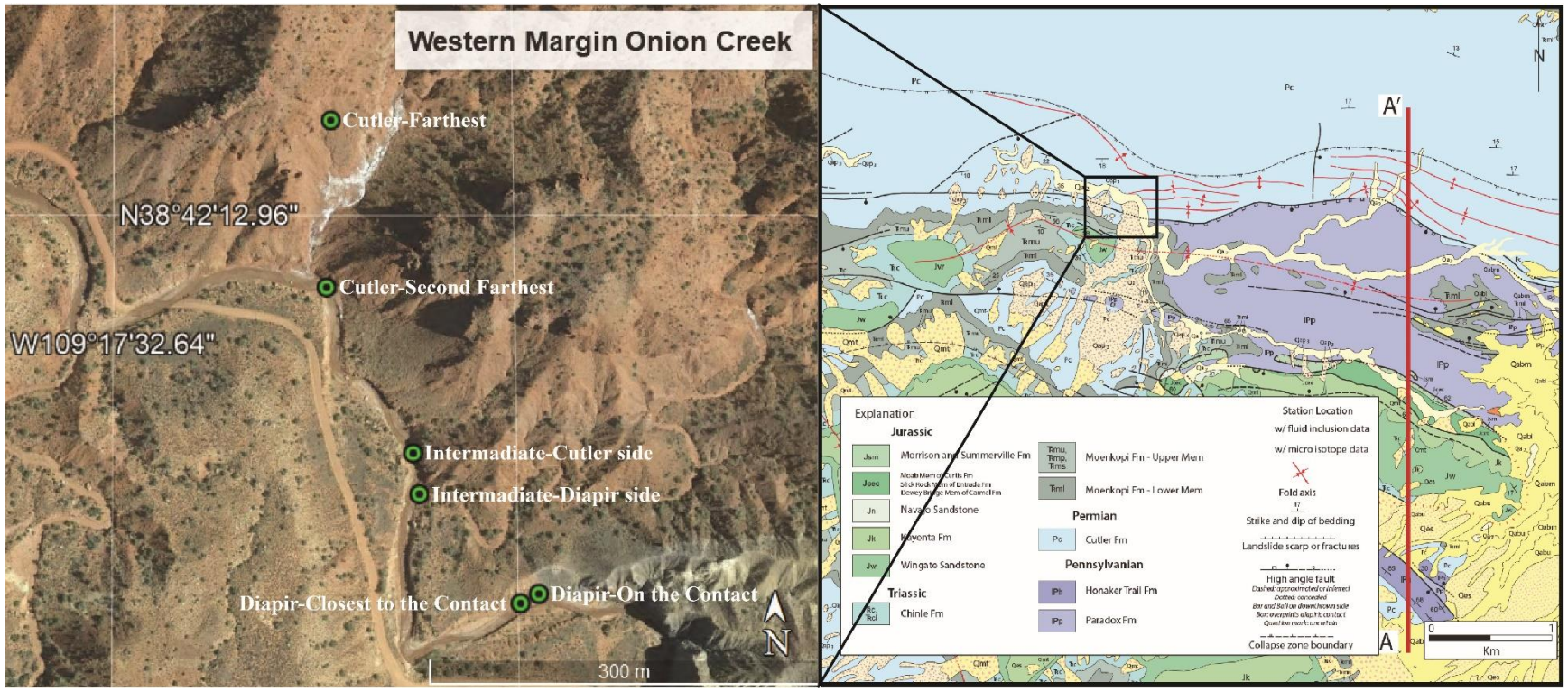


*Figure 5: Left-hand figure shows the location of the area and the stations of collected fracture data from Google Earth Pro and right-hand figure shows the geological map of the area (Modified from Doelling 2002, Trudgill, 2011 and Kenroy 2013)*

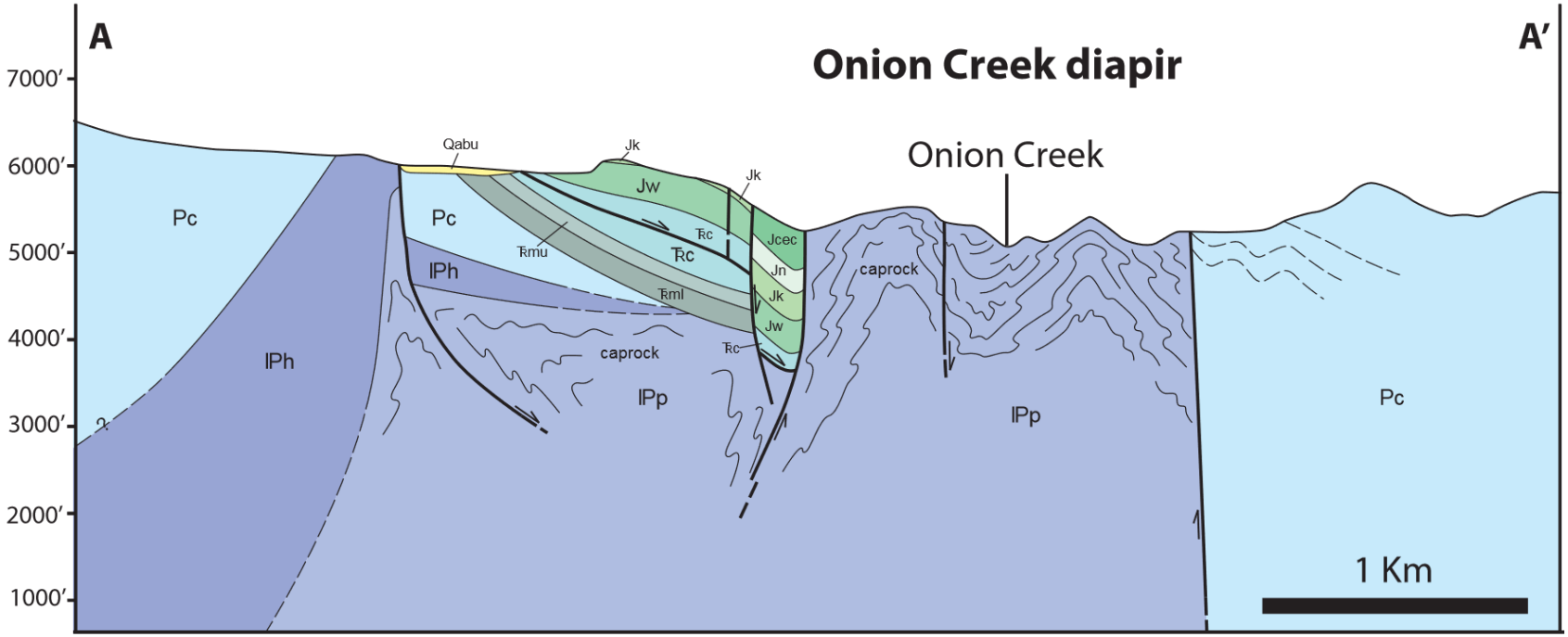


*Figure 6: Cross section of the eastern part of the Onion Creek Diapir. The location and legend of the cross section is in the Figure 5. A is South and A' is North (from Kenroy (2013) after Doelling (2002)).*

# 3. Methodology and Results

For the field work I emphasized two complementary approaches: 1) a study of fracture systems in situ such as measuring the orientation of fractures along some segments of focus study outcrops while at the same time acquiring GPS data and photos for photogrammetric modeling, 2) obtaining data for a 3D model using photogrammetry and using this model as a base for macroscopic fracture analysis. For the in-situ fracture studies I measured fracture systems, focusing on details in 6 stations, chosen from sites ranging from at the diapir contact across complexly deformed rocks of the Cutler Fm into more intact Cutler Formation approximately 500m from the diapir. Whilst making measurements, I used three different sized circular scan lines that were located in the same center. This allowed me to spatially reference fracture measurements to estimate other fracture parameters instead of measuring every single fracture. In this method the number of fractures intersecting the circumference ($n$) of the circle and the number of fracture traces terminating in the circle interior ($m$) give a quantitative estimate of fracture parameters such as density, size and intensity, (Reiss, 1982; Nelson, 1985; Dershowitz and LaPointe, 1994; Narr, 1996; Rohrbaugh Jr, 2002). These parameters are important for deduction of patterns that would assist in the evaluation of hydrocarbon flow and storage in fractured reservoirs. Through this I would know whether the fractures cross the circle lines which would give the estimated lengths. Unfortunately, I did not count n nor m in the field under an assumption that I could use the 3D model to estimate these parameters, thus, increasing field time for other studies. Ultimately, technology limitations prevented clear application of this method.

Because of the need to collect many strike and dip measurements in a limited time, I chose to use a digital compass. To determine if my device (iPhone 7 Plus) was comparable with an analog compass I collected comparison data sets (Figure 30).

For the macroscopic fracture studies, I began by developing 3D models of the outcrop using photogrammetry methods of Structure from Motion/Multiview Stereo (SfM/MvS) methods (Carrivick et al, 2016). For these studies I began by placing markers throughout the study area and used a high-resolution DGPS Survey (Digital Global Positioning System) (Figure 7) to accurately locate the markers –which has an estimated accuracy of 1 cm or better. At the same time I used a handheld GPS to provide approximate locations for later reference, which provided an opportunity to compare the accuracy of the handheld unit relative to the DGPS. To get a ground control data from DGPS, I needed to make tripod stable and push the bottom. In the beginning, I set it for 30 sec to let communicate with satellite for each data. While I was waiting

*Figure 7: A view from the base station of Topcon GB1000 GPS equipment to diapir contact.*

for DGPS. I let the handheld GPS to run 15-20 sec, so I could write down latitude, longitude and elevation. The handheld GPS was always running next to the tripod, it could expect to have maximum 1 m difference on X-Y axises of DGPS because of the cable of DGPS with its antenna. However, I would not expect to see meters difference on the elevation axis.

I then used the department's camera to acquire ground-based images of the exposure, I scanned across the exposure from as many camera positions as possible. For example, images were acquired at distances of a maximum of 4m. These data formed the basis for 3D model development, using the SfM/MvS software Photoscan from Agisoft Ltd.

In the office I used the photos acquired in the field and the DGPS data to process the imagery using Agisoft Photoscan, in a computer Intel Xeon 12 CPU E5, 1,.60 GHz, and 64 GB RAM. Processing times for this effort was at least a week for each wall of the focus outcrops in medium resolution cloud density. I used the workflow of Matthews et al (2016) to insure high model accuracy, and through use of the high-resolution DGPS positioning of the markers, the resultant model should be accurate to the mm level. Later, once the model was developed, I used a combination of Maptek i-site Studio and CloudCompare to interpret the fracture systems. This included superimposing the field fracture data onto the model as well as digitizing features on the model, including fractures visible on the model. For fractures visible on the model, I use multipoint methods for estimating fracture orientations, together with fracture mapping to analyze the fracture systems.

To interpret the fracture data collected in the field I used the traditional method of orientation analysis on a stereonet. After exporting my phone data to the computer, I used Stereonet 10.0 and Adobe Illustrator CC 2018 to compare the six fracture stations to each other. All figures refer to the sequence of stations as you walk in the river cut from the diapir contact to

northern side (Figure 5): *On the Contact/First station, Closest to the Contact, Intermediate Diapir Side, Intermediate Cutler Side, Cutler Mouth Canyon, and Cutler Farthest Canyon* respectively. None of the stations had open fracture aperture, nor mineralization, but partly sulfuric oxidation.

## 3.1. Data acquisition

For the photos, the camera used in this study to obtain ground-based images of the exposure was a NIKON D5300. This camera is a DSLR with a 24.2 MP (megapixel) sensor. I used a 35mm, fixed focal length Nikkor lens (Online Reference 1).

For the ground control on the 3D models I placed surveying flags at GCP points and used the following tools. For high resolution positioning I used the DGPS Topcon GB1000 (the differential kinematic GPS set). It is a dual frequency and GPS+ receiver. It is one of the most advanced receivers and can combine real time kinematic measurements (RTK) accurately (Online Reference 2). Also, a Garmin eTrex10 was used as a handheld GPS which is common device with only limited differential correction from a WAAS signal.

I collected 76 ground control points using GPS equipment obtained in a kinematic survey with Topcon GB 1000, and with Garmin eTrex10 to compare the results and reference the data to a map. Topcon GB1000's base station was set up on the top of the North and East transects' hill (Figure 5). The data shown in Tables are in WGS84 UTM 12N coordinate system.

The original intent of the using the handheld GPS was as a backup GCP solution in the event of data loss as well as a tool to get real time positions to aid in finding markers on the model without the data processing needs of the DGPS data. This allowed, however, an evalution of the handheld GPS accuracy in this site relative to the high- resolution kinematic survey (Table 1), which is discussed below.

For the photogrammetric models I took 3290 photos of the study area. The outcrop geometry made it advantageous to process the data in four "chunks" (Agisoft terminology for related pieces of a model that are more easily processed independently); 1) the Canyon chunk used 485 images - this site contains the fracture station called *Farthest/Canyon* Figure 22Figure 17*)*, 2) the northern and eastern chunk 1428 images – this area has the rest of the fracture stations, 3) the western chunk used 608 images, and the southern chunk has two sets one taken in the early morning and another taken in the afternoon with 388, 381 images respectively – the two imaging times produced different shadow patterns that affected the result. Once the individual chunks were processed and georeferenced, the individual chunks were merged into a single model. For interpretation, however, visualizing the entire model at once challenged most computers, thus, the model was ultimately subdivided into segments using tools in CloudCompare.

For fracture measurements I chose six stations in advance from the diapir contact across complexly deformed rocks of Cutler Fm into intact Cutler Formation almost half a km (map distance on Google Earth) away from the diapir. At each station I measured strike and dip for all fractures visible at the site. For the fracture measurements, I followed Rohrbaugh et al. (2002)'s measurement methods. Specifically, I had three different sizes of circular scanlines that were located in the same center -radius 25cm, 50cm, and 75cm- instead of measuring every single fracture's length. Then I collected 119 measurements, in total, from the same location with a Brunton compass and the smartphone to compare these two devices (Novakova and Pavlis, 2017; Allmendinger et al, 2017) (Figure 30). After the result of this test was positive, I started using the smartphone for the remainder of the data collection. A total of 412 fractures and bedding data were measured in the field (Figure 9 and Figure 10). These fracture measurement stations served

as reference sites for direct comparison of field measurements to measurements made on the 3D model. For the 3D model, however, the measurement areas were expanded beyond the limited radii of the specific stations because resolution was not always sufficient to make 1:1 comparisons.

Upon returning to the office, I processed the DGPS data and compared these data with handheld GPS (Tables 1-3). I used the photos obtained in the field and the DGPS data to process the imagery using Agisoft Photoscan by using the workflow of Matthews et al (2016). Once I made the models, I exported dense points of the models as ".las" format to import them to Maptek I-site Studio to digitize, collect same fracture measurements, and analyze from the same stations via remote analysis of the point cloud, using the geotech utilities in I-site studio. I imported the measurements from the phone to Stereonet 10 for further analysis.


*Figure 8: Intermediate and Diapir Sections from Google Earth (the image is oblique view)*

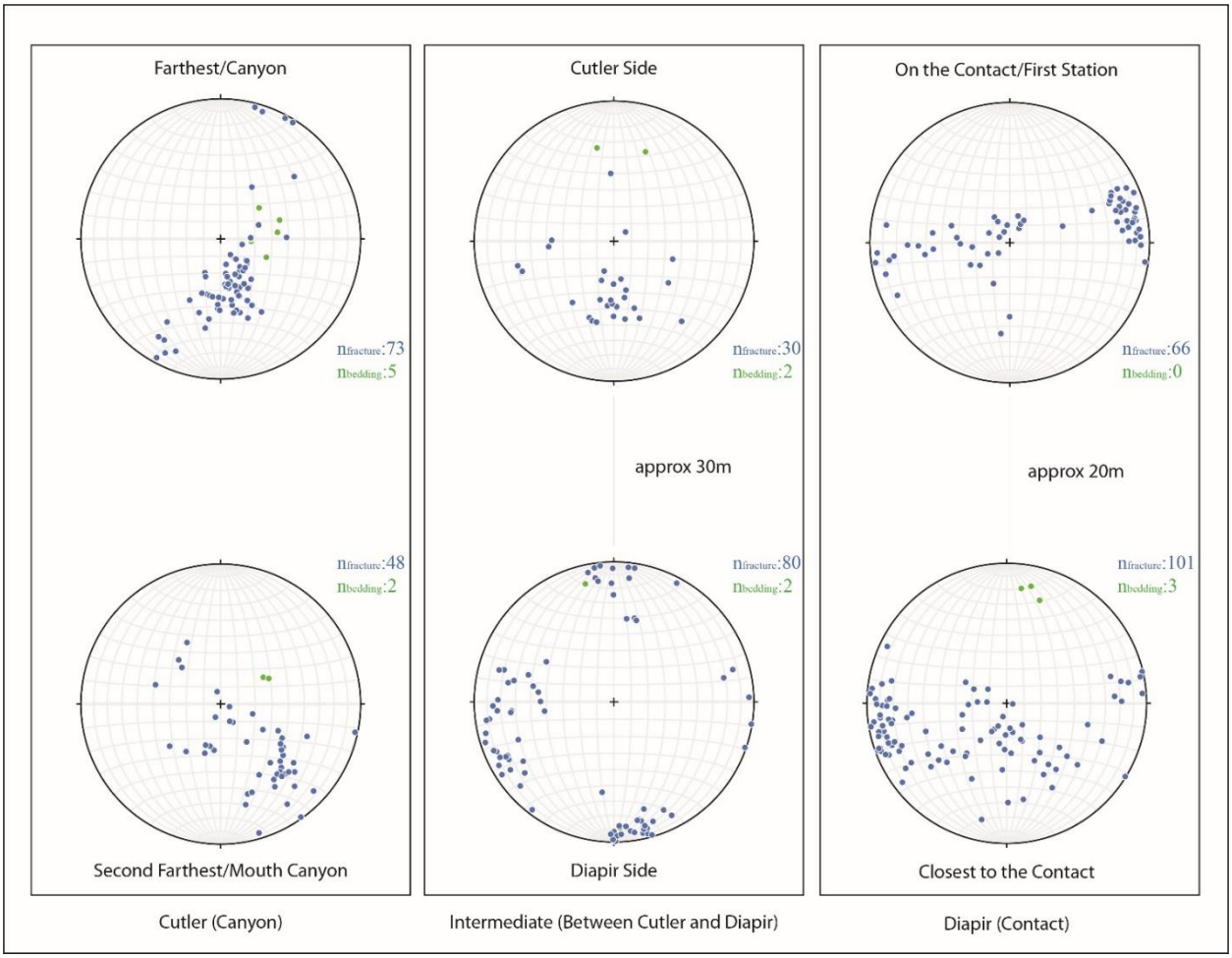


*Figure 9: The stereonets illustrates bedding and fracture's strike and dip raw data from the field. n shows the number of the data point in the stereonets. (Figure 10 shows the location of the stations)*

## 3.2. Results

### *3.2.1. DGPS vs WAAS corrected GPS positions on Ground Control Points*

Looking at horizontal errors the UTM Northing and Easting errors can be used with Pythagorean theorem to estimate total horizontal error. The average error (Table 1) is 1.80m with a S.D. of 1.03m; which is consistent with the generally estimated error for WAAS corrected GPS (Online Reference 4). When I took elevation into account to estimate the total error, the error increases to 8-11m (Table 2-3). This is consistent with well-known errors in vertical vs

horizontal positioning with GPS, but these data revealed a surprising result. The reason there are two different tables for the elevation is because I compared the handheld GPS elevations to two reference elevations in the DGPS survey: ellipsoidal height (Table 2), which is calculated based on the theoretical ellipsoidal earth shape reference (Online Reference 5), and orthometric height (Table 3), which is calculated based on height above geoid, which is determined by the earth's gravity and approximates Mean Sea Level (MSL) at a given site (Online Reference 5), from the DGPS survey. The handheld GPS was set to record a WGS ellipsoidal height, and therefore should directly compare to Table 2. This comparison produces a systematic error of elevation in both cases. In Table 3, the error is consistent with a vertical datum mismatch with the orthometric height consistently above the handheld's height estimated for an ellipsoid; that is, regional low gravity over the continents produces a geoid high and thus, orthometric height should be above ellipsoid height as seen in the height estimates for the DGPS data between Tables 2 and 3. What is surprising is that in Table 2, where both heights are estimated relative to an ellipsoid, there is a systematic error between the handheld and DGPS with the handheld consistently above the DGPS estimate by an average of 8.7m. The origin of this discrepancy is unknown but is greater than generally accepted estimate for WAAS corrected GPS values.

*Table 1: Comparison of GPS data points of survey and handheld (Elevation did not apply)*

| | Survey GPS | | Hand held GPS | | | | | | | |
|---|---|---|---|---|---|---|---|---|---|---|
| Name | Northing | Easting | Northing | Easting | Northing defe | Easting defer | Distance defer | Avarage | Stand dev | STD error |
| OCT100 | 4284972.541 | 648754.5011 | 4284971.4 | 648754.7 | 1.140682 | -0.198882 | 1.157890125 | | | |
| OCT101 | 4284967.101 | 648755.1168 | 4284968 | 648753.9 | -0.898646 | 1.2168092 | 1.512676014 | | | |
| OCT102 | 4284949.546 | 648732.5809 | 4284949.9 | 648732.5 | -0.354208 | 0.0808675 | 0.363321655 | | | |
| OCT103 | 4285000.04 | 648721.7588 | 4284999.6 | 648721.1 | 0.4403371 | 0.6587753 | 0.792389856 | | | |
| OCT104 | 4285033.919 | 648728.5245 | 4285034.1 | 648725.7 | -0.18055 | 2.8244746 | 2.830239398 | | | |
| OCT105 | 4285051.448 | 648724.7789 | 4285052.9 | 648724.5 | -1.452404 | 0.2789321 | 1.478945546 | | | |
| OCT106 | 4285012.751 | 648718.2036 | 4285014 | 648717.4 | -1.248997 | 0.8036248 | 1.48519568 | | | |
| OCT107 | 4285022.346 | 648710.3281 | 4285023.8 | 648711.1 | -1.453895 | -0.771855 | 1.646077281 | | | |
| OCT108 | 4285022.968 | 648710.6072 | 4285023.8 | 648711.1 | -0.831672 | -0.492787 | 0.966704174 | | | |
| OCT109 | 4285065.595 | 648719.7684 | 4285067.2 | 648717.3 | -1.604523 | 2.4684384 | 2.944093005 | | | |
| OCT110 | 4284969.646 | 648712.2678 | 4284968.4 | 648713 | 1.2459687 | -0.73224 | 1.445203418 | | | |
| OCT111 | 4284948.441 | 648720.0655 | 4284950.7 | 648719.5 | -2.259174 | 0.5655008 | 2.328874775 | | | |
| OCT112 | 4284944.163 | 648713.0959 | 4284943.9 | 648713.5 | 0.2625641 | -0.404064 | 0.481879164 | | | |
| OCT113 | 4284956.985 | 648760.8691 | 4284957 | 648759.4 | -0.015044 | 1.4691371 | 1.469214106 | 1.804941727 | 1.029220175 | 0.19807352 |
| OCT114 | 4284952.842 | 648783.3488 | 4284954.1 | 648781.2 | -1.257876 | 2.1488322 | 2.489926176 | | | |
| OCT115 | 4284971.811 | 648798.8434 | 4284972.2 | 648798.2 | -0.388505 | 0.6433691 | 0.751571765 | | | |
| OCT116 | 4284984.104 | 648828.3711 | 4284982.7 | 648827.6 | 1.4038431 | 0.7710928 | 1.601674048 | | | |
| OCT117 | 4284968.034 | 648858.1232 | 4284966.6 | 648859.2 | 1.434269 | -1.07684 | 1.793519157 | | | |
| OCT118 | 4284964.778 | 648857.8477 | 4284963.3 | 648858.4 | 1.4784232 | -0.552314 | 1.578222225 | | | |
| OCT119 | 4284952.032 | 648783.8294 | 4284950.8 | 648781.2 | 1.2319212 | 2.629429 | 2.903709103 | | | |
| OCT120 | 4284973.552 | 648786.0534 | 4284973 | 648784.3 | 0.5516777 | 1.7533818 | 1.838122936 | | | |
| OCT200 | 4284970.287 | 648755.4923 | 4284972.5 | 648755.6 | -2.213097 | -0.107679 | 2.215715492 | | | |
| OCT201 | 4284997.075 | 648810.3205 | 4284999 | 648810.8 | -1.924713 | -0.479545 | 1.983553407 | | | |
| OCT202 | 4284949.104 | 648707.4598 | 4284950.5 | 648706.4 | -1.395973 | 1.0598212 | 1.752701506 | | | |
| OCT203 | 4284980.548 | 648708.2958 | 4284981.6 | 648708.4 | -1.051765 | -0.104167 | 1.056910821 | | | |
| OCT204 | 4285035.49 | 648710.9313 | 4285040.4 | 648708.2 | -4.91003 | 2.7312575 | 5.618555206 | | | |
| OCT205 | 4285066.161 | 648715.7119 | 4285068.3 | 648716.4 | -2.138565 | -0.688101 | 2.246540598 | | | |

*Table 2: Comparison of GPS data points of survey and handheld according Ellipsoidal Height*

| | Survey GPS | | | Hand held GPS | | | | | | | | | |
|---|---|---|---|---|---|---|---|---|---|---|---|---|---|
| Name | Northing | Easting | Ellipsoidal Ht. | Northing | Easting | Elevation | Northing defer | Easting defer | Elevation defer | Distance defer | Avarage | Stand dev | STD error |
| OCT100 | 4284972.541 | 648754.5011 | 1440.34 | 4284971.4 | 648754.7 | 1449 | 1.14068201 | -0.19888211 | -8.66 | 8.73706527 | | | |
| OCT101 | 4284967.101 | 648755.1168 | 1439.965 | 4284968 | 648753.9 | 1450 | -0.89864574 | 1.21680917 | -10.035 | 10.14837 | | | |
| OCT102 | 4284949.546 | 648732.5809 | 1438.089 | 4284949.9 | 648732.5 | 1445 | -0.35420767 | 0.08086749 | -6.911 | 6.92054359 | | | |
| OCT103 | 4285000.04 | 648721.7588 | 1436.151 | 4284999.6 | 648721.1 | 1443 | 0.44033707 | 0.65877534 | -6.849 | 6.8946851 | | | |
| OCT104 | 4285033.919 | 648728.5245 | 1435.472 | 4285034.1 | 648725.7 | 1448 | -0.18055026 | 2.82447458 | -12.528 | 12.8437159 | | | |
| OCT105 | 4285051.448 | 648724.7789 | 1430.803 | 4285052.9 | 648724.5 | 1442 | -1.452403801 | 0.27893212 | -11.197 | 11.2942503 | | | |
| OCT106 | 4285012.751 | 648718.2036 | 1430.85 | 4285014 | 648717.4 | 1440 | -1.24899696 | 0.80362479 | -9.15 | 9.26975222 | | | |
| OCT107 | 4285022.346 | 648710.3281 | 1430.654 | 4285023.8 | 648711.1 | 1438 | -1.45389498 | -0.77185478 | -7.346 | 7.52816621 | | | |
| OCT108 | 4285022.968 | 648710.6072 | 1430.632 | 4285023.8 | 648711.1 | 1438 | -0.83167174 | -0.49278705 | -7.368 | 7.43114668 | | | |
| OCT109 | 4285065.595 | 648719.7684 | 1428.975 | 4285067.2 | 648717.3 | 1437 | -1.60452346 | 2.46843839 | -8.025 | 8.54800027 | | | |
| OCT110 | 4284969.646 | 648712.2678 | 1432.436 | 4284968.4 | 648713 | 1444 | 1.245968729 | -0.73223961 | -11.564 | 11.6539568 | | | |
| OCT111 | 4284948.441 | 648720.0655 | 1432.58 | 4284950.7 | 648719.5 | 1442 | -2.25917386 | 0.56550083 | -9.42 | 9.70361055 | | | |
| OCT112 | 4284944.163 | 648713.0959 | 1432.539 | 4284943.9 | 648713.5 | 1443 | 0.26256409 | -0.40406389 | -10.461 | 10.4720928 | | | |
| OCT113 | 4284956.985 | 648760.8691 | 1434.831 | 4284957 | 648759.4 | 1445 | -0.01504426 | 1.46913708 | -10.169 | 10.2745876 | 8.71884 | 2.39669 | 0.46124 |
| OCT114 | 4284952.842 | 648783.3488 | 1434.085 | 4284954.1 | 648781.2 | 1442 | -1.257876219 | 2.14883219 | -7.915 | 8.29740666 | | | |
| OCT115 | 4284971.811 | 648798.8434 | 1434.934 | 4284972.2 | 648798.2 | 1442 | -0.38850522 | 0.64336911 | -7.066 | 7.10585787 | | | |
| OCT116 | 4284984.104 | 648828.3711 | 1436.484 | 4284982.7 | 648827.6 | 1448 | 1.40384315 | 0.77109284 | -11.516 | 11.6268489 | | | |
| OCT117 | 4284968.034 | 648858.1232 | 1436.101 | 4284966.6 | 648859.2 | 1440 | 1.43426895 | -1.07683961 | -3.899 | 4.29172599 | | | |
| OCT118 | 4284964.778 | 648857.8477 | 1441.039 | 4284963.3 | 648858.4 | 1440 | 1.47842318 | -0.55231358 | 1.039 | 1.88952544 | | | |
| OCT119 | 4284952.032 | 648783.8294 | 1436.324 | 4284950.8 | 648781.2 | 1445 | 1.23192118 | 2.62942898 | -8.676 | 9.14901648 | | | |
| OCT120 | 4284973.552 | 648786.0534 | 1441.276 | 4284973 | 648784.3 | 1450 | 0.55167771 | 1.75338177 | -8.724 | 8.91554103 | | | |
| OCT200 | 4284970.287 | 648755.4923 | 1440.29 | 4284972.5 | 648755.6 | 1449 | -2.21309745 | -0.10767924 | -8.71 | 8.98740759 | | | |
| OCT201 | 4284997.075 | 648810.3205 | 1454.902 | 4284999 | 648810.8 | 1464 | -1.92471306 | -0.47954536 | -9.098 | 9.31171779 | | | |
| OCT202 | 4284949.104 | 648707.4598 | 1441.353 | 4284950.5 | 648706.4 | 1449 | -1.39597338 | 1.05982116 | -7.647 | 7.84528977 | | | |
| OCT203 | 4284980.548 | 648708.2958 | 1437.071 | 4284981.6 | 648708.4 | 1447 | -1.05176509 | -0.10416659 | -9.929 | 9.98509396 | | | |
| OCT204 | 4285035.49 | 648710.9313 | 1436.432 | 4285040.4 | 648708.2 | 1446 | -4.910030031 | 2.73125753 | -9.568 | 11.0957103 | | | |
| OCT205 | 4285066.161 | 648715.7119 | 1434.324 | 4285068.3 | 648716.4 | 1439 | -2.13856542 | -0.68810072 | -4.676 | 5.18767006 | | | |

*Table 3: Comparison of GPS data points of survey and handheld according Orthometric Height*

| | Survey GPS | | | Hand held GPS | | | | | | | | | |
|---|---|---|---|---|---|---|---|---|---|---|---|---|---|
| Name | Northing | Easting | Orthometric Ht. | Northing | Easting | Elevation | Northing defer | Easting defer | Elevation defer | Distance defer | Avarage | Stand dev | STD error |
| OCT100 | 4284972.541 | 648754.5011 | 1459.796 | 4284971.4 | 648754.7 | 1449 | 1.14068201 | -0.19888211 | 10.796 | 10.8579153 | | | |
| OCT101 | 4284967.101 | 648755.1168 | 1459.421 | 4284968 | 648753.9 | 1450 | -0.89864574 | 1.21680917 | 9.421 | 9.54166808 | | | |
| OCT102 | 4284949.546 | 648732.5809 | 1457.546 | 4284949.9 | 648732.5 | 1445 | -0.35420767 | 0.08086749 | 12.546 | 12.5512596 | | | |
| OCT103 | 4285000.04 | 648721.7588 | 1455.61 | 4284999.6 | 648721.1 | 1443 | 0.44033707 | 0.65877534 | 12.61 | 12.6348717 | | | |
| OCT104 | 4285033.919 | 648728.5245 | 1454.931 | 4285034.1 | 648725.7 | 1448 | -0.18055026 | 2.82447458 | 6.931 | 7.48658908 | | | |
| OCT105 | 4285051.448 | 648724.7789 | 1450.262 | 4285052.9 | 648724.5 | 1442 | -1.452403801 | 0.27893212 | 8.262 | 8.39332615 | | | |
| OCT106 | 4285012.751 | 648718.2036 | 1450.309 | 4285014 | 648717.4 | 1440 | -1.24899696 | 0.80362479 | 10.309 | 10.415435 | | | |
| OCT107 | 4285022.346 | 648710.3281 | 1450.113 | 4285023.8 | 648711.1 | 1438 | -1.45389498 | -0.77185478 | 12.113 | 12.2243339 | | | |
| OCT108 | 4285022.968 | 648710.6072 | 1450.091 | 4285023.8 | 648711.1 | 1438 | -0.83167174 | -0.49278705 | 12.091 | 12.1295836 | | | |
| OCT109 | 4285065.595 | 648719.7684 | 1448.435 | 4285067.2 | 648717.3 | 1437 | -1.60452346 | 2.46843839 | 11.435 | 11.8079172 | | | |
| OCT110 | 4284969.646 | 648712.2678 | 1451.894 | 4284968.4 | 648713 | 1444 | 1.245968729 | -0.73223961 | 7.894 | 8.02520086 | | | |
| OCT111 | 4284948.441 | 648720.0655 | 1452.037 | 4284950.7 | 648719.5 | 1442 | -2.25917386 | 0.56550083 | 10.037 | 10.3036414 | | | |
| OCT112 | 4284944.163 | 648713.0959 | 1451.997 | 4284943.9 | 648713.5 | 1443 | 0.26256409 | -0.40406389 | 8.997 | 9.00989548 | | | |
| OCT113 | 4284956.985 | 648760.8691 | 1454.286 | 4284957 | 648759.4 | 1445 | -0.01504426 | 1.46913708 | 9.286 | 9.40150978 | 11.2859 | 2.679 | 0.51557 |
| OCT114 | 4284952.842 | 648783.3488 | 1453.539 | 4284954.1 | 648781.2 | 1442 | -1.257876219 | 2.14883219 | 11.539 | 11.8045861 | | | |
| OCT115 | 4284971.811 | 648798.8434 | 1454.387 | 4284972.2 | 648798.2 | 1442 | -0.38850522 | 0.64336911 | 12.387 | 12.4097796 | | | |
| OCT116 | 4284984.104 | 648828.3711 | 1455.936 | 4284982.7 | 648827.6 | 1448 | 1.40384315 | 0.77109284 | 7.936 | 8.09601481 | | | |
| OCT117 | 4284968.034 | 648858.1232 | 1455.551 | 4284966.6 | 648859.2 | 1440 | 1.43426895 | -1.07683961 | 15.551 | 15.6540829 | | | |
| OCT118 | 4284964.778 | 648857.8477 | 1460.489 | 4284963.3 | 648858.4 | 1440 | 1.47842318 | -0.55231358 | 20.489 | 20.5496936 | | | |
| OCT119 | 4284952.032 | 648783.8294 | 1455.778 | 4284950.8 | 648781.2 | 1445 | 1.23192118 | 2.62942898 | 10.778 | 11.1622941 | | | |
| OCT120 | 4284973.552 | 648786.0534 | 1460.73 | 4284973 | 648784.3 | 1450 | 0.55167771 | 1.75338177 | 10.73 | 10.8863031 | | | |
| OCT200 | 4284970.287 | 648755.4923 | 1459.746 | 4284972.5 | 648755.6 | 1449 | -2.21309745 | -0.10767924 | 10.746 | 10.9720514 | | | |
| OCT201 | 4284997.075 | 648810.3205 | 1474.356 | 4284999 | 648810.8 | 1464 | -1.92471306 | -0.47954536 | 10.356 | 10.5442506 | | | |
| OCT202 | 4284949.104 | 648707.4598 | 1460.811 | 4284950.5 | 648706.4 | 1449 | -1.39597338 | 1.05982116 | 11.811 | 11.9403385 | | | |
| OCT203 | 4284980.548 | 648708.2958 | 1456.529 | 4284981.6 | 648708.4 | 1447 | -1.05176509 | -0.10416659 | 9.529 | 9.58743456 | | | |
| OCT204 | 4285035.49 | 648710.9313 | 1455.891 | 4285040.4 | 648708.2 | 1446 | -4.910030031 | 2.73125753 | 9.891 | 11.375414 | | | |
| OCT205 | 4285066.161 | 648715.7119 | 1453.784 | 4285068.3 | 648716.4 | 1439 | -2.13856542 | -0.68810072 | 14.784 | 14.9537153 | | | |

### *3.2.2. Geology of the Study Area*

The Onion Creek area exhumes an elongate salt diapir with an ~W-E long axis. The study area is along the western edge of the Onion Creek salt diapir core exposures of gypsum, but structures related to the diapir continue well westward from the study site. To the north of the diapir is intact, but deformed Cutler Fm, which is distinctly folded near the diapir while overlying strata typically dip northward, away from the diapir (Figure 5). In the study area the Cutler Fm is in fault contact with complexly deformed rocks near the contact. In our work in this area, we informally referred to these complexly deformed rocks as Domain 0, which forms a mappable unit along the diapir contact. The rocks in the study area between gypsum exposures and the intact Cutler can all be considered part of Domain 0. This study was chosen because of excellent rock exposures in the river cuts. Although not exposed, it is clear that the diapir underlies the exposures of Domain 0 in the study area. From diapir contact, across Domain 0 to

the Cutler Fm, the rocks are highly fractured and faulted, bedding orientations change abruptly across faults, and fractures vary between fault blocks.

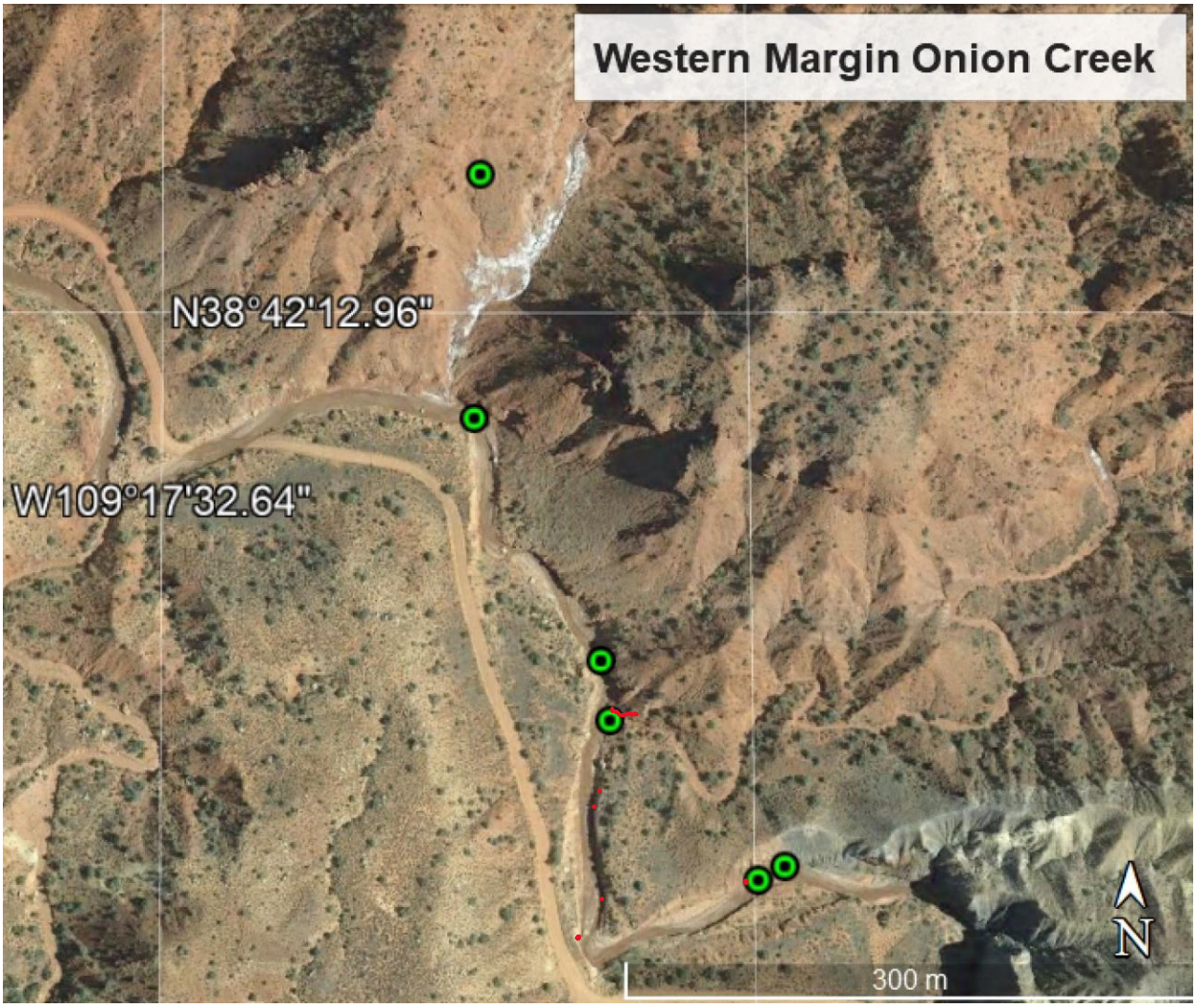


*Figure 10: The study area from Google Earth (red dots show the intact fault locations while green show the location of the stations)*

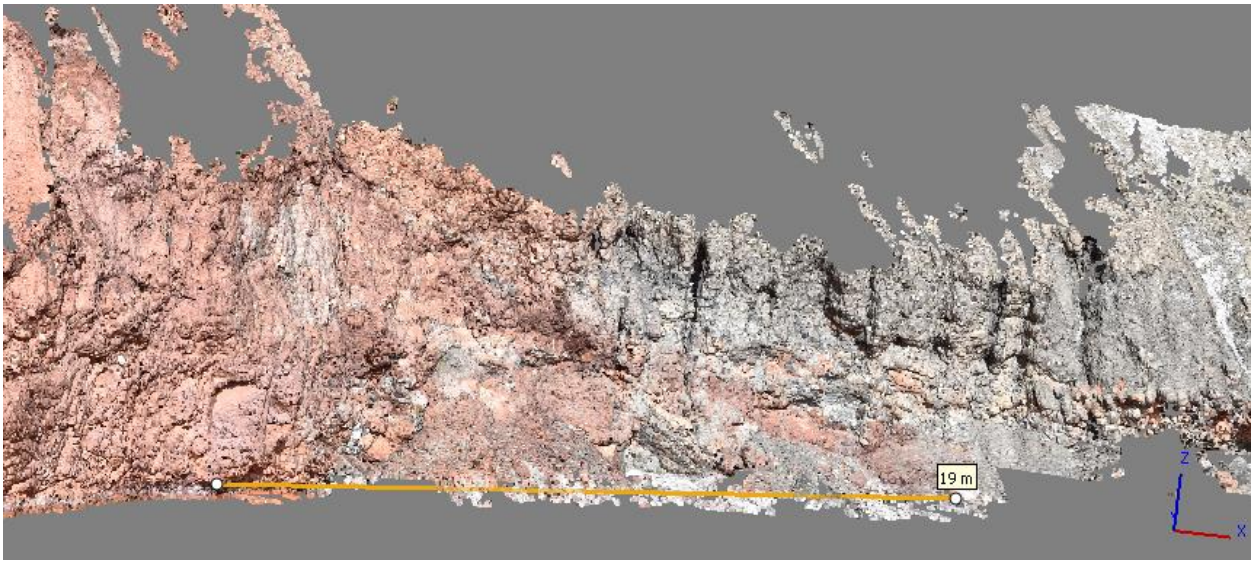


*Figure 11: The figure shows the contact of the salt diapir with Domain 0. The orange line joints the two fracture stations "On the Contact" to the right and "Closest to the Contact" on the left, a distance of 19m*

Figure 12 shows a part of the 3D model at the diapir contact looking NNW. Here the bedding-strikes NE and dips steeply northwest. Approximately 20 m west of the contact, (Figure 11-Figure 13) bedding changes abruptly to ~EW strikes with south dips. These dip changes indicate distinct faults cutting the section, but in this area bedding is typically indistinct, suggesting extensive cataclastic across this 20-30m side zone along the contact.

Figure 14 shows a view of the 3D model at the third fracture analysis site (labeled Intermediate-Diapir side Figure 10). This site is located just south of the fault contact with the Cutler Fm. At this site a fault is present in the deep shadow part of the model (Figure 14) but the fault is recognized by bedding truncations and abrupt change in strike and dip of bedding. Unfortunately, the field fracture station is not visible in the 3D model due to a gap in the model produced by deep shadow under the big rock on the right hand of the figure. The actual station is under the red circle shown on Figure 14.

Figure 15 shows a view of the 3D model at the fourth station (Intermediate-Cutler Side, Figure 10) located within the Cutler Fm outside the domain 0 zone. At this site bedding strikes ~EW and dips moderately south. Fracture sets can be clearly seen intersecting bedding at this site (Figure 15) with a sub horizontal intersection line.

Figure 16 and Figure 17 show the 3D model at the sites “Cutler, Second Farthest” and “Cutler Farthest” respectively. Both of these sites show similar bedding orientations to that seen in Figure 15Figure 17, with similar prominent fracture systems visible at high angle to bedding planes. These last three sites proved critical for comparisons of fracture orientations determined on the model and in the field because the fractures form prominent 3D surface visible on the model (Figure 15Figure 17).

There were many faults within the domain 0 part of the study area but these faults are difficult to trace beyond the limits of the outcrop due to alluvial cover separating the two cliff-walls along the creek bed. Figure 18, from the western river cut at the edge, there is a remarkable fault (shown on the map, Figure 8) in this study area. This fault is marked by a distinct gouge zone, ~15 cm thick, with the gouge strongly affected by a Sulphur oxidation (Figure 18). The result of this fluid interaction is the development of a very soft and wet clay gouge. Presumably this alteration reflects fluid migration from the diapir.

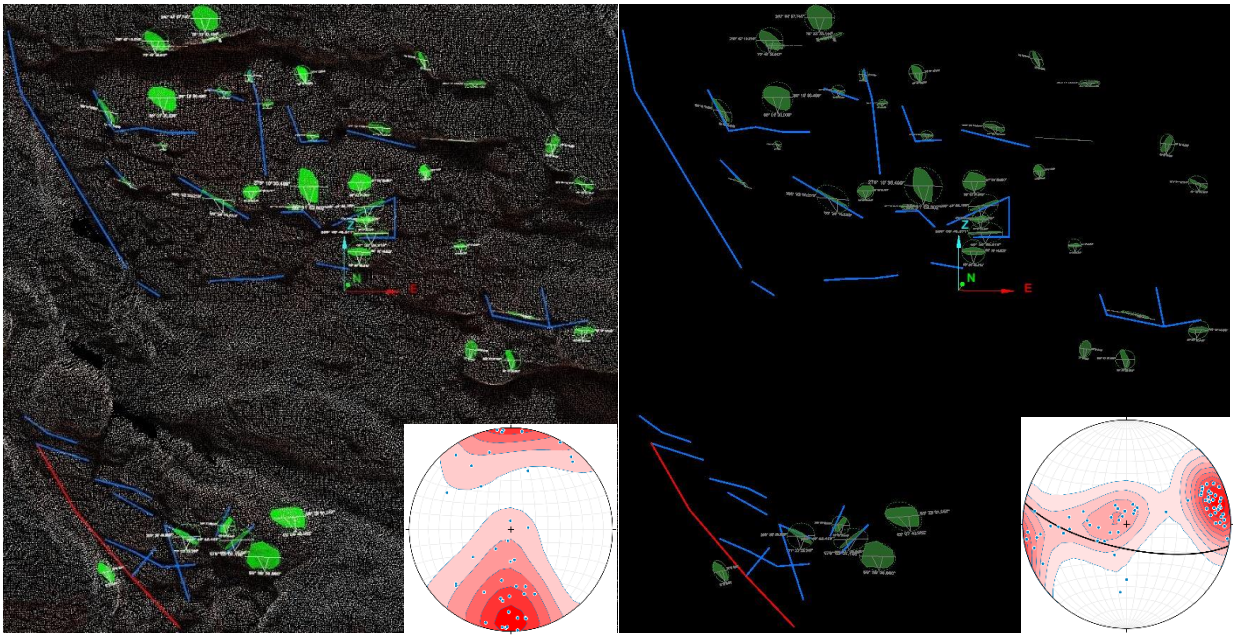

*Figure 12: Diapir contact focus site with view zoomed in to the exact area of the field fracture measurements. Left figure shows point cloud with measurements where the right figure shows only patches for orientation estimates. Note the relative sparsity of the point cloud at this zoom level. Figure shows a visualization of remotely sensed fracture orientations developed from 3D model as well as mapped traces of fractures (blue) and faults (red). The stereoplots show the data collected from 3D model (Left) and in situ (right) (see Appendix 1-2 for the data).*

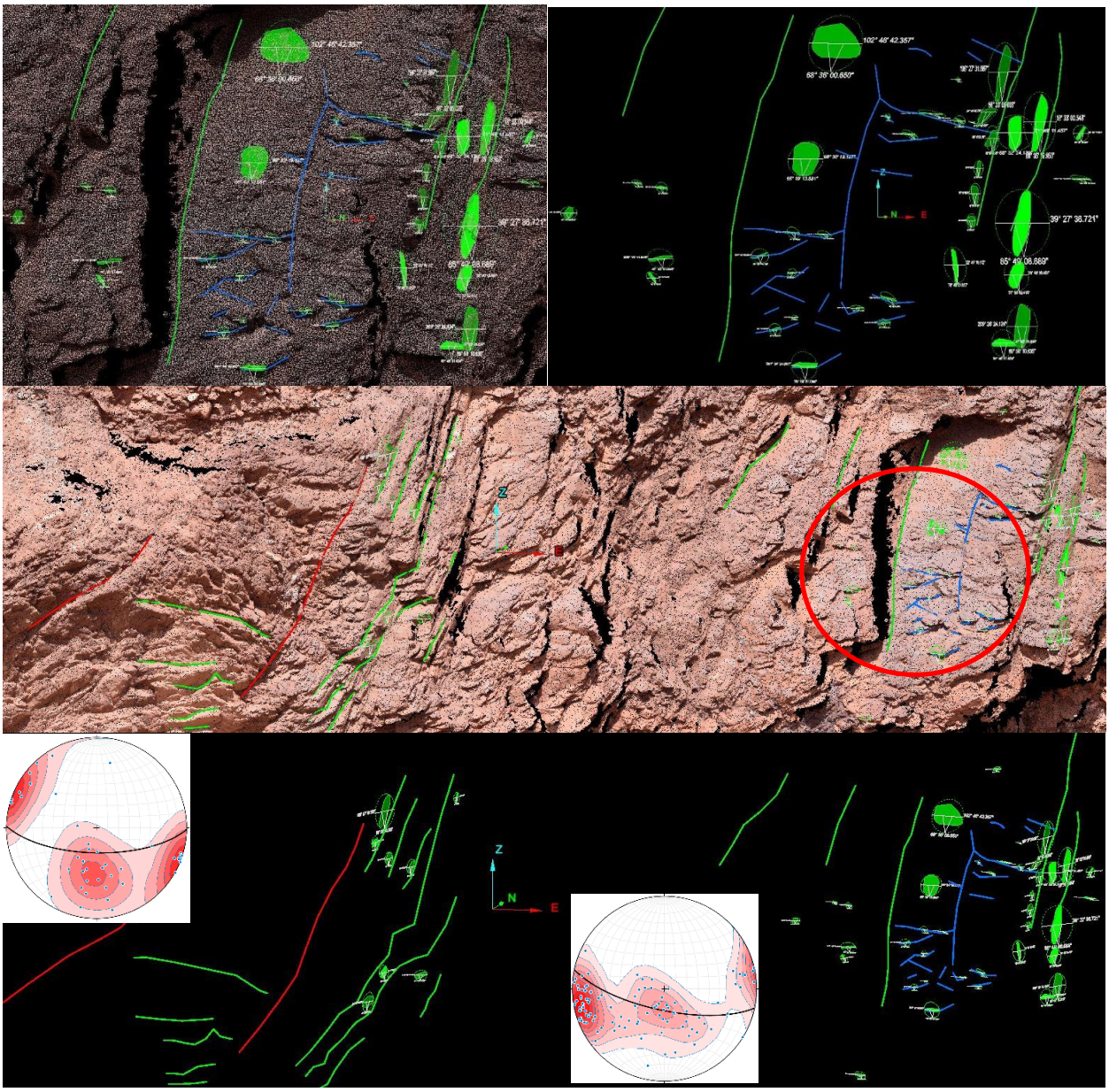

*Figure 13: Closest to the Contact focus site (second fracture station from the diapir, about 20m). Center and lower thirds of the figure are a visualization of ~20m of the model near the fracture focus site outlined by the red circle. Central figure shows the model with interpreted traces of bedding (green), fractures (blue) and faults (red, with fractures only mapped in the focus site (red circle). The lower 1/3 of the figure is the same view as the central figure with the point cloud visualization removed and showing patches where fractures were measured on the model. Upper third of the figure is a zoomed in view of the area of the field measurements with the point cloud include on the left and interpretation only on the right (color scheme and green patches are the same as the lower figure). The*

*stereoplot insesrts show the fracture data collected from 3D model (left) and in situ (right). All views are looking to the north along an approximately horizontal line. (see Appendix 1-2 for the data)*

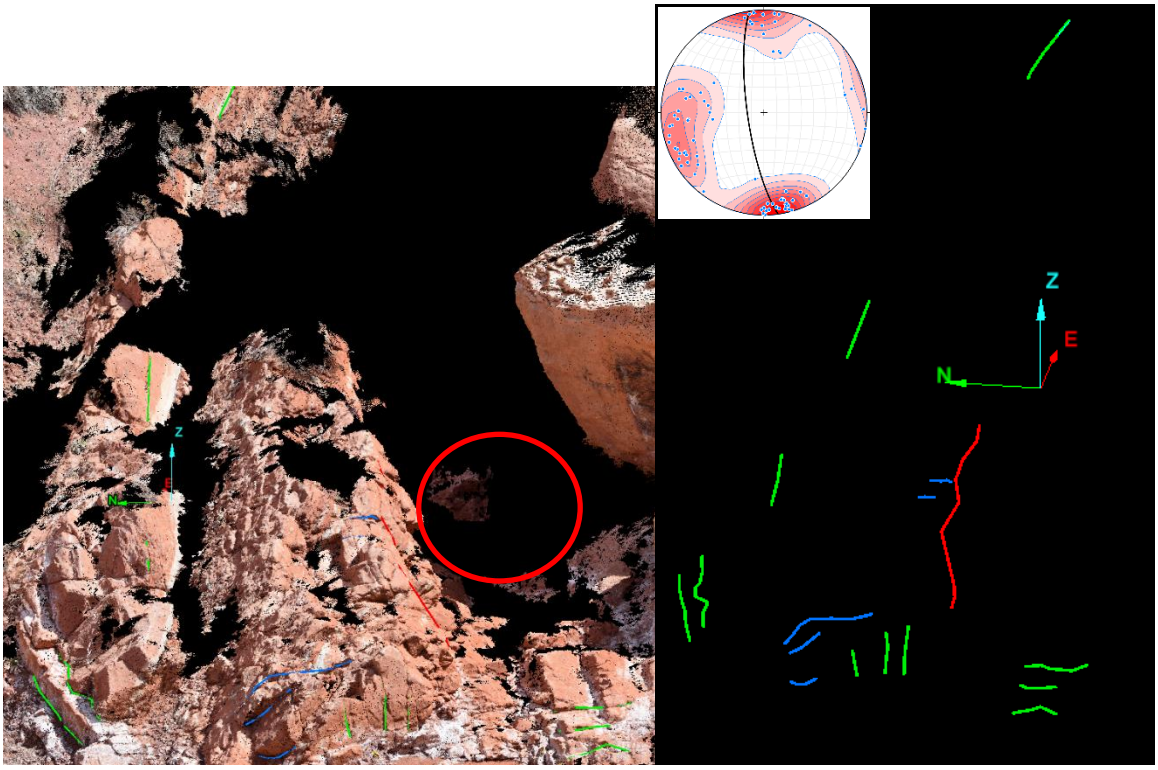


*Figure 14: Intermediate-Diapir side focus site (third station from the diapir). The color is the same as Figure 12Figure 13with fracture traces (blue) and beds (green). The red circle shows the approximate fracture station that collected data in situ, but Photoscan left as a gap because of deep shadow (see text for discussion)*

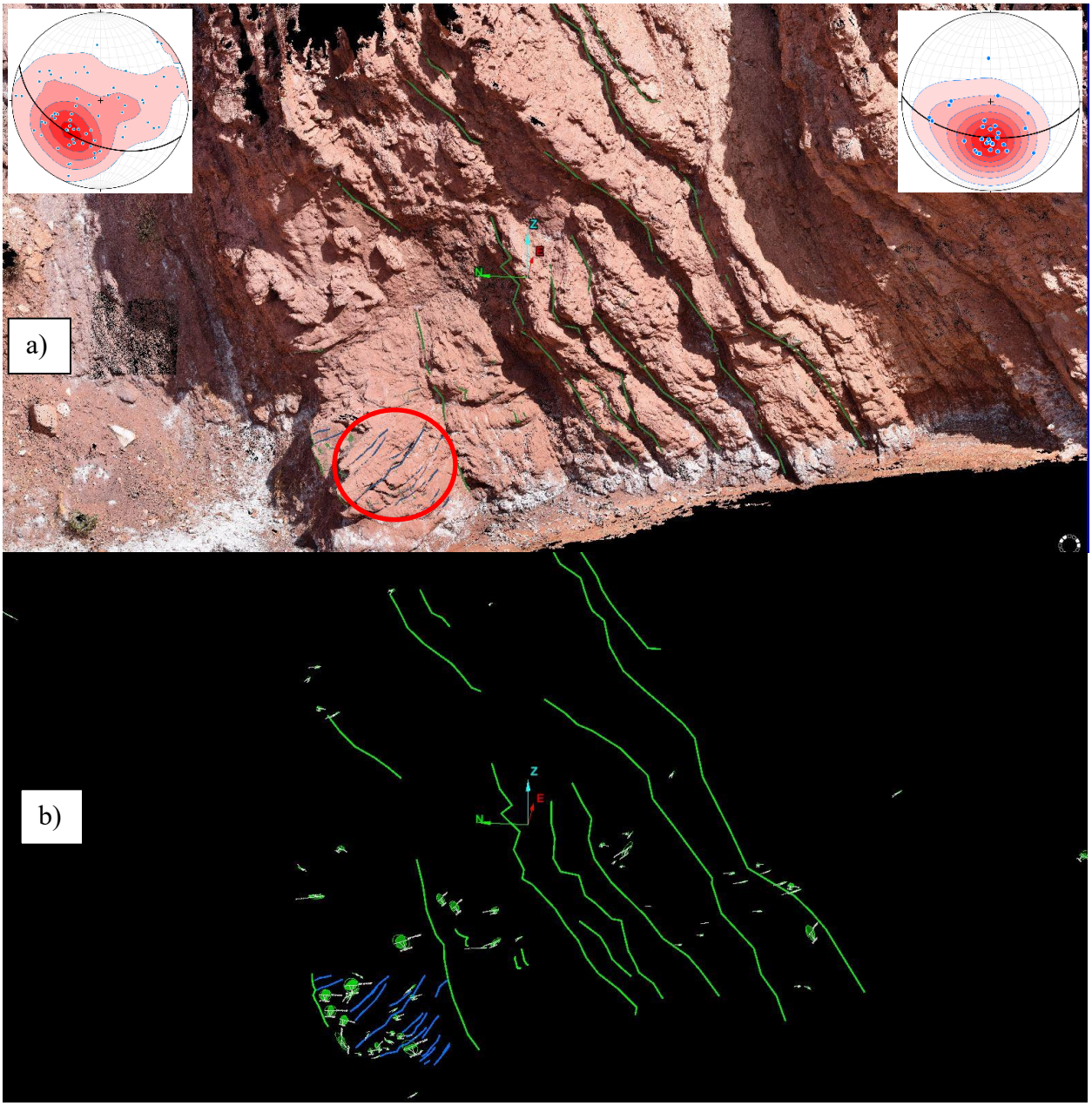
a)
Z
E
N
b)
Z
E
N

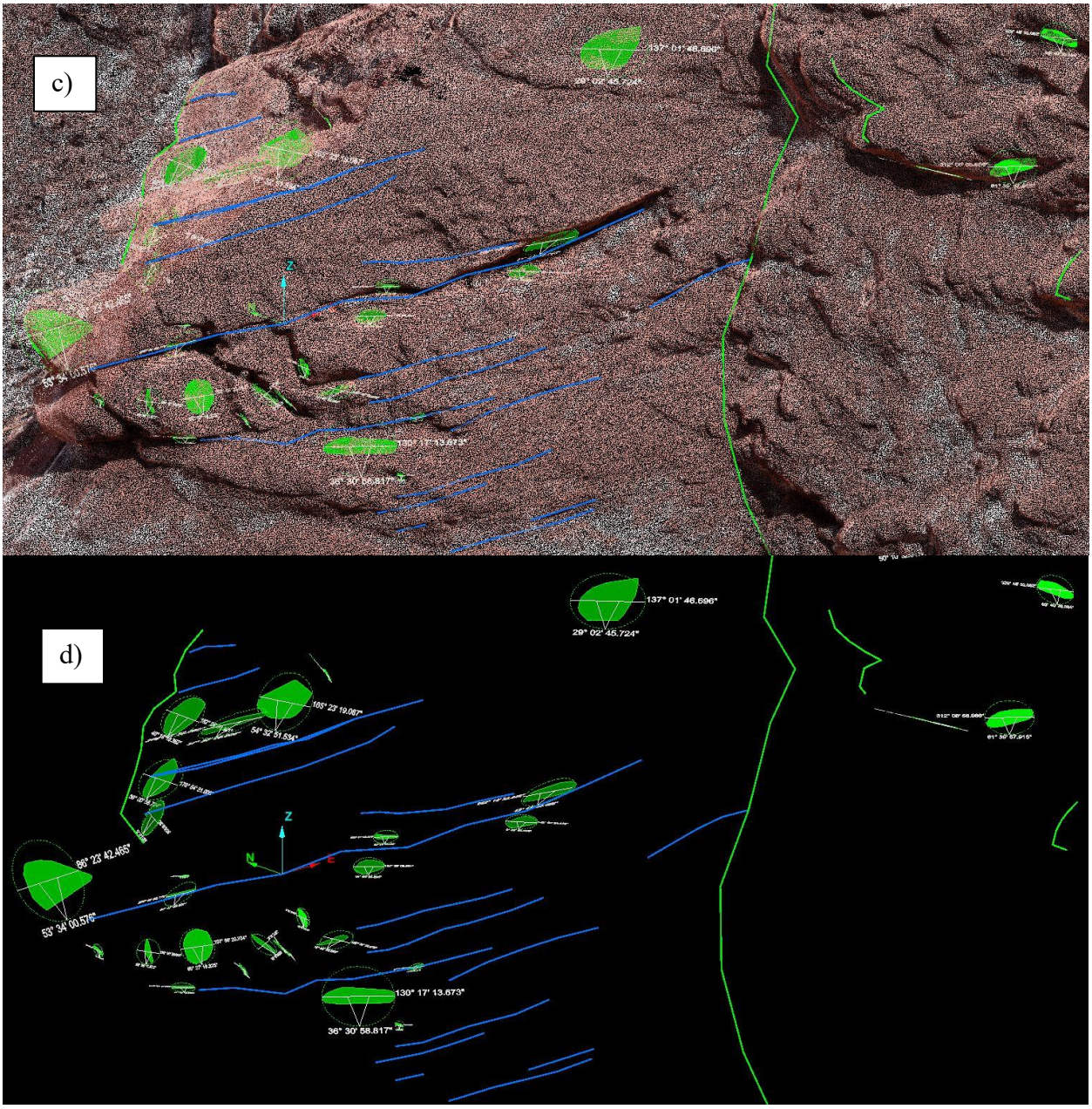


*Figure 15: Intermediate Cutler Side focus site (the fourth station from the diapir). Upper pair of figures (a and b) show zoomed out view of ~30m of the outcrop with bedding (green) and fractures (blue) traced on the outcrop (fractures only mapped at the field in-situ site, outlined as the red circle). Upper figure (a) is a visualization of the point cloud with interpretations on it and the lower figure (b) shows the same area with the point cloud turned off. Lower two figures (c and d) show an enlarged view of the area of the field measurements corresponding to the red circle in the upper figures. Color scheme of lower figure is the same as upper figure. Green patches in all figures*

*are sites of fractures measured on the model using multipoint tools in I-site studio. The stereoplot inserts in a show the fracture orientation data collected from 3D model (left) and in situ (right). (see Appendix 1-2 for the data)*

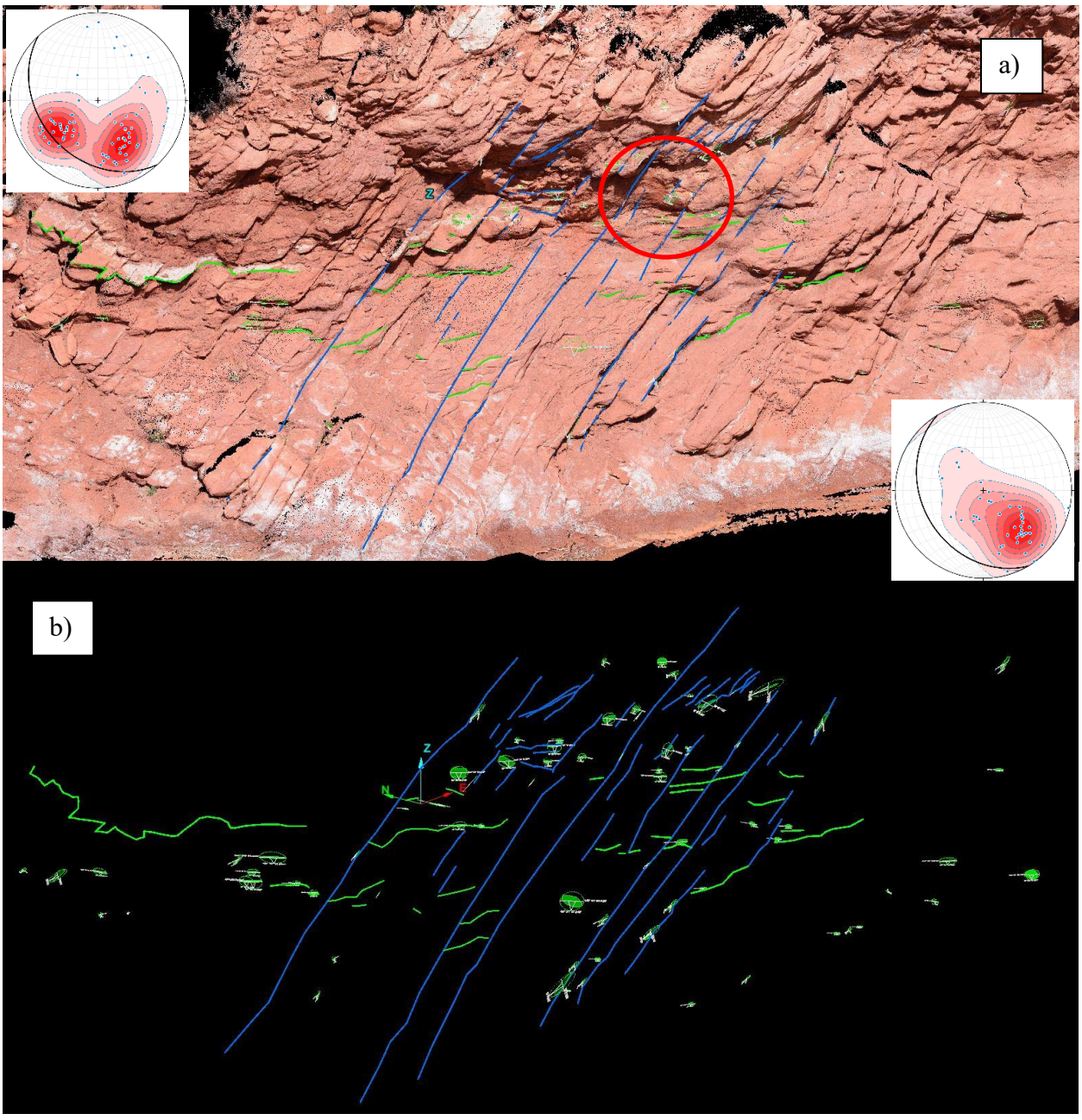

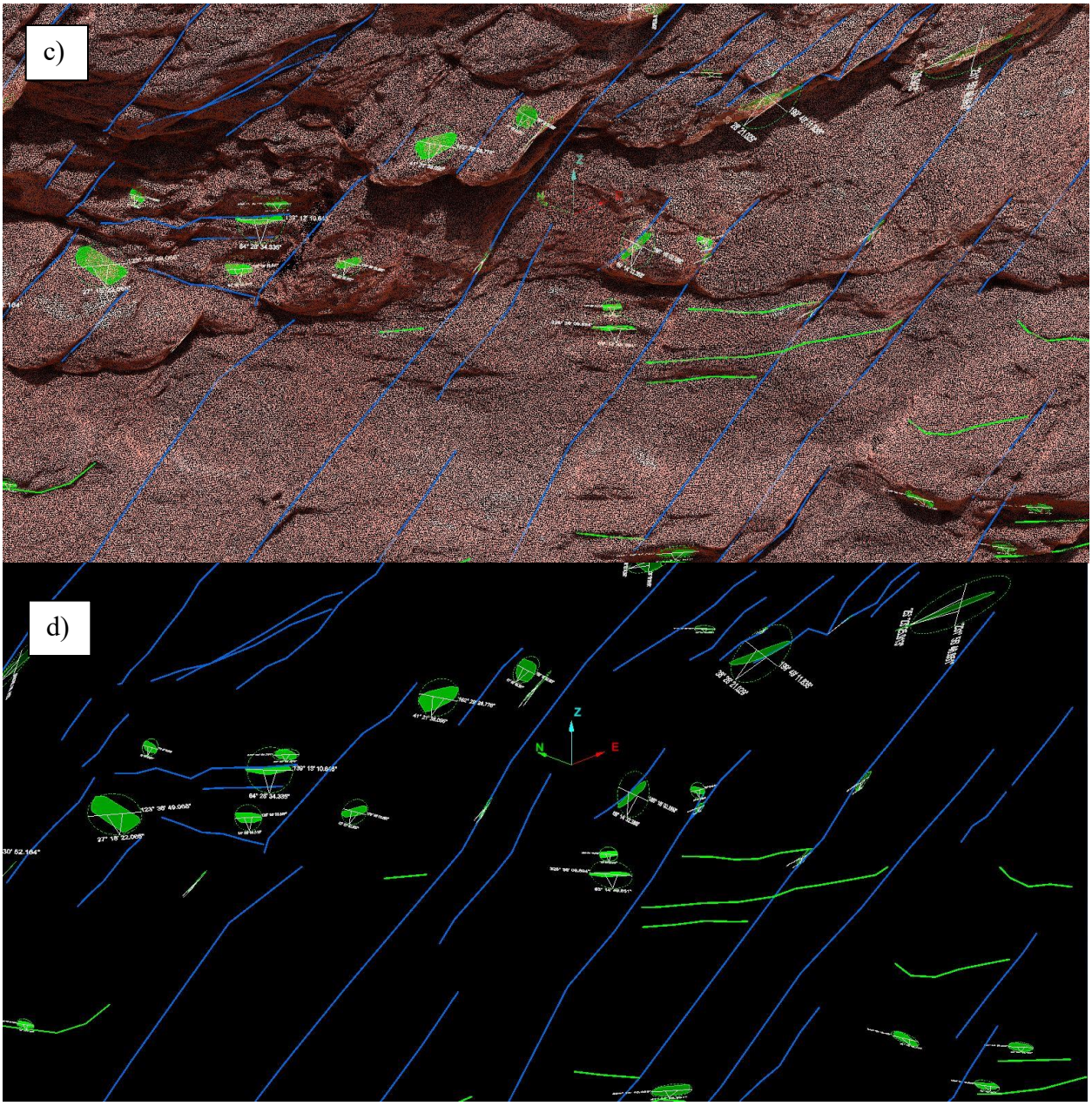


*Figure 16: Cutler-Second Farthest focus site (the fifth station from the diapir on the mouth of the Canyon). Upper pair of figures (a and b) show zoomed out view of ~10m of the outcrop with bedding (green) and fractures (blue) traced on the outcrop. Red circle shows the area where field data were acquired and enlarged in the lower figures. Upper figure (a) is a visualization of the point cloud with interpretations on it and the lower figure (b) shows the same area with the point cloud turned off. Lower two figures (c and d) show an enlarged view of the area of the field measurements corresponding to the red circle in the upper figures. Color scheme of lower figure is the same as upper figure. Green patches in all figures are sites of fractures measured on the model using multipoint tools in*

*I-site studio. The stereoplot inserts in show the fracture orientation data collected from 3D model (left) and in situ (right). (see Appendix 1-2 for the data).*

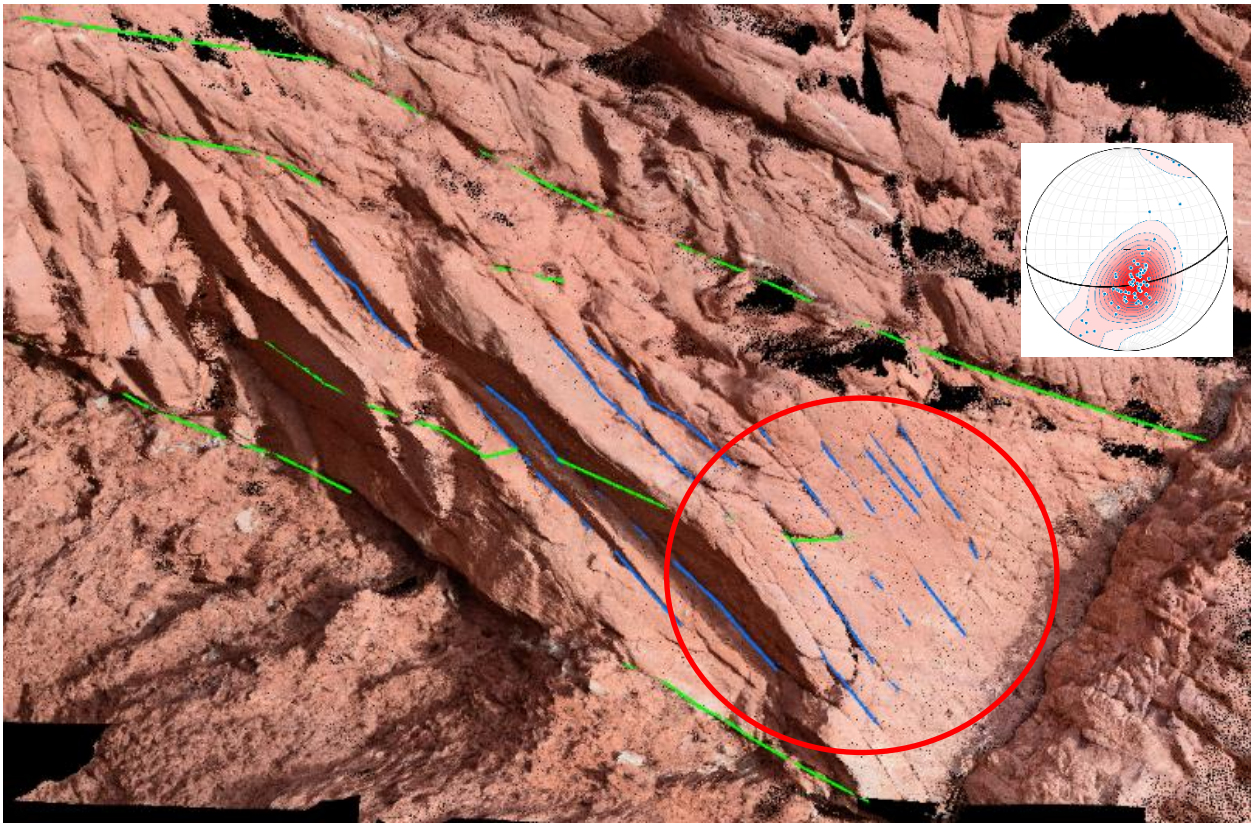

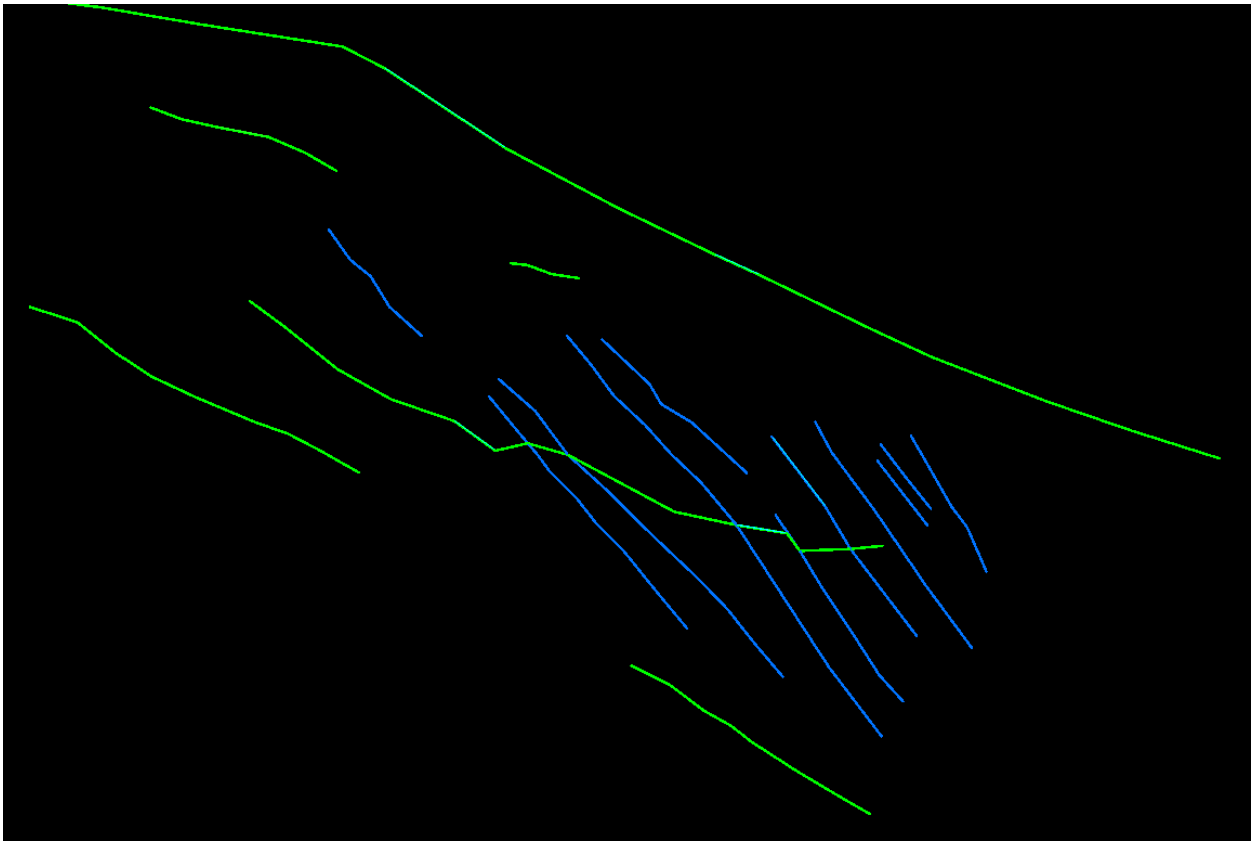

*Figure 17: Cutler-Farthest focus site (the sixth station in the canyon on the cliff from the diapir). Upper Figure shows a visualization of the point cloud with interpretations drawn on it and lower figure shows the interpretation without the point cloud. Red circle shows the position of the in-situ field measurements at this site. Stereograms show orientations measured in situ only. This site could not be properly georeferenced for direct comparison between field and model data. (see text for discussion) (see Appendix 1 for the data).*

*Figure 18: The fault filled with Sulphur oxidation (see Figure 8)*

### *3.2.3. Analysis of Fracture Orientations*

After generating the 3D models in Agisoft Photoscan, I exported the dense point cloud as ".las" format to import them to CloudCompare to merge the data into a single project. I then exported again in the same format for importing to Maptek I-site Studio to digitize and analyze the fracture systems. I-site studio has a "geotech" utility which allows multipoint analysis of a point cloud to determine a best orientation for a plane fitting these points. Thus, this method is an extension of the classic 3-point problem to multi-point analyses. This technique seemed an ideal use of the 3D model to supplement field measurements and I attempted to use the method at several sites within the 3D model.

Although the method seemed ideal, several problems were encountered during this analysis;

1) There was a problem with one of the focus sites from the Intermediate section-*Diapir Side* on the 3D models. At the site, despite care with photo overlap and close spacing, there is a hole in the point cloud, primarily due to shadow (Figure 14), so it left a gap on the model that could not be analyzed as a direct comparison between the field data and model derived data.

2) The 3D model of *Cutler-Farthest* (Figure 10) was run by itself because it was geographically isolated from the main outcrop along the creek. Despite numerous processing schemes to improve this model, it could not be properly georeferenced. The origin of the problem is unknown. A well-defined model was generated relatively easily (Figure 17) and allowed mapping directly on the model, but when ground control points were added to the model they showed large spatial errors and the resultant model was rotated by large amounts from the real world. The origin of this problem is unknown, but it is likely one or more of the GCP's either has a bad position or was somehow mislocated on the model. Thus, I was unable to directly compare field measurements to model measurements at this site.

3) I digitized fractures from the diapir contact site twice, (*On the Contact* in Figure 12 and Figure 20). After digitizing the fractures and using the fracture traces to estimate fracture orientation using the multipoint tool, I made a plot of the data on an equal area stereoplot to compare it with the stereoplot of the data collected for this site in the field (Figure 19). Figure 12 and Figure 19 show the comparison of the stereoplots with a kamb contoured plot and scatter plot respectively. These plots demonstrate that the remote measurement produced a very unsatisfactory result, with apparent fracture orientations nearly 90 degrees from the observed and none of the field fractures recognized. The origin of the problem is discussed below.

Despite these problems, fracture analysis on the 3D model at all other sites produced satisfactory results, and arguably, better results, than field measurements, for reasons discussed

below. Figure 13 and Figure 15 show *Closest to the Contact* and *Intermediate Cutler Side* stations where the results of model based measurements are comparable to the field data, but slightly different. Specifically, at both sites the general fracture patterns are similar in the two methods; in Figure 13, both stereonet plots reveal the pattern seen on the 3D model of two, approximately orthogonal fracture sets perpendicular to bedding and in Figure 15 only one fracture set, perpendicular to bedding, is shown. However, the positions of the maxima in the stereonet plots are clearly shifted slightly between field based and model-based measurements; e.g. in Figure 15, the maxima for poles to fractures in the field based data is located at S (181/64) whereas the maxima from the model is at SW, an angle of ~ 206/76. Similarly, Figure 13, the field based maxima in the poles to fracture plots are at W (260/12) and S (176/70) vs corresponding maxima on the model based plots at NW (111/02) and S (185/50), which differ by angles of 149/10 and 351/20 respectively. Note that although the scalar angular differences among these plots are similar, the direction of the shifts is not, suggesting strongly the source of the distinction is a random, presumably measurement based, error in one or both methods. This conclusion on measurement error is supported by bedding measurements in both the field and on the model, which unlike the fracture data are indistinguishable great circles on the plots (Figure 13 and Figure 15).

Perhaps the most intriguing results is at the "Cutler--second farthest site" (Figure 16). Here, I did the same procedure, with the field and model measurements, and the main fracture set (mapped in blue in Figure 16) yielded indistinguishable orientations using the two methods (pole maxima at 137/35 for the field data and 147/43 for the model based measurements). Similarly, bedding orientations match perfectly for field vs model-based measurements (great circles in the stereonet plots, Figure 16). What is different is the model based measurements revealed a clear,

second fracture set at this site, with a maxima in the pole plot at 236/43, or ~90 degrees from the other fracture set. This fracture set is clearly visible in the larger scale view of the outcrop (upper figures, in Figure 16) as the sub-horizontal steps in the bedding surface.

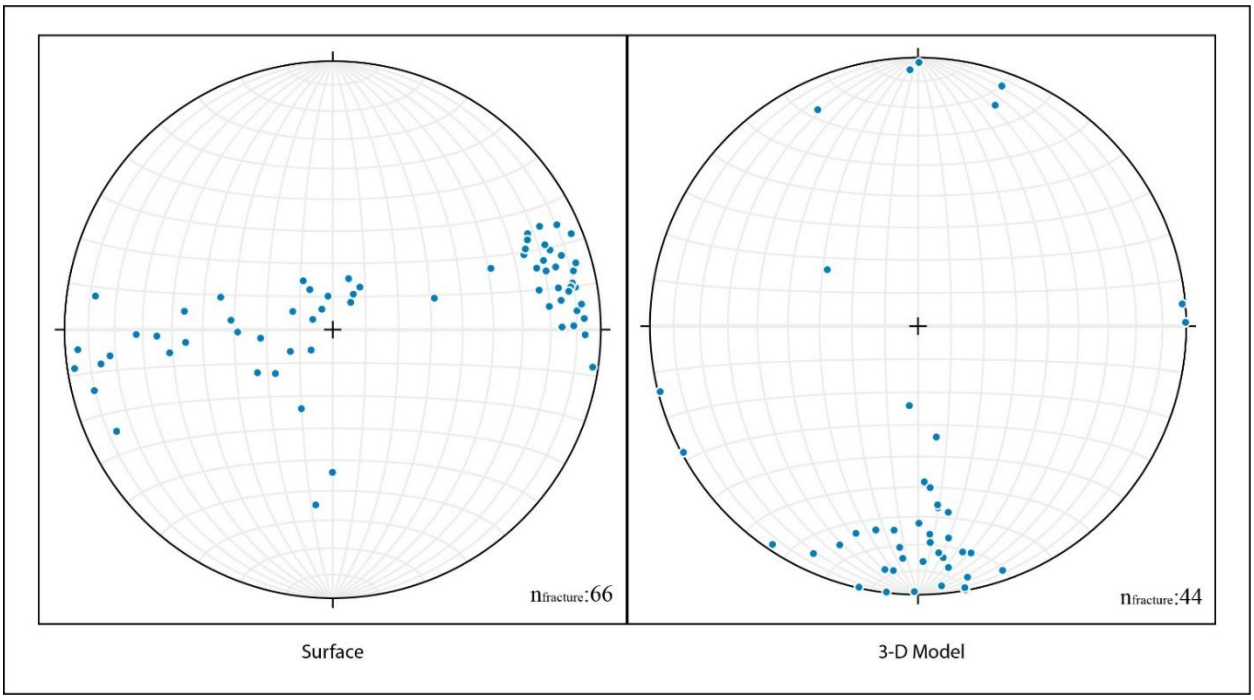


*Figure 19: The comparison of surface and 3-D model On the Contact focus site (see Appendix 4 for the data)*

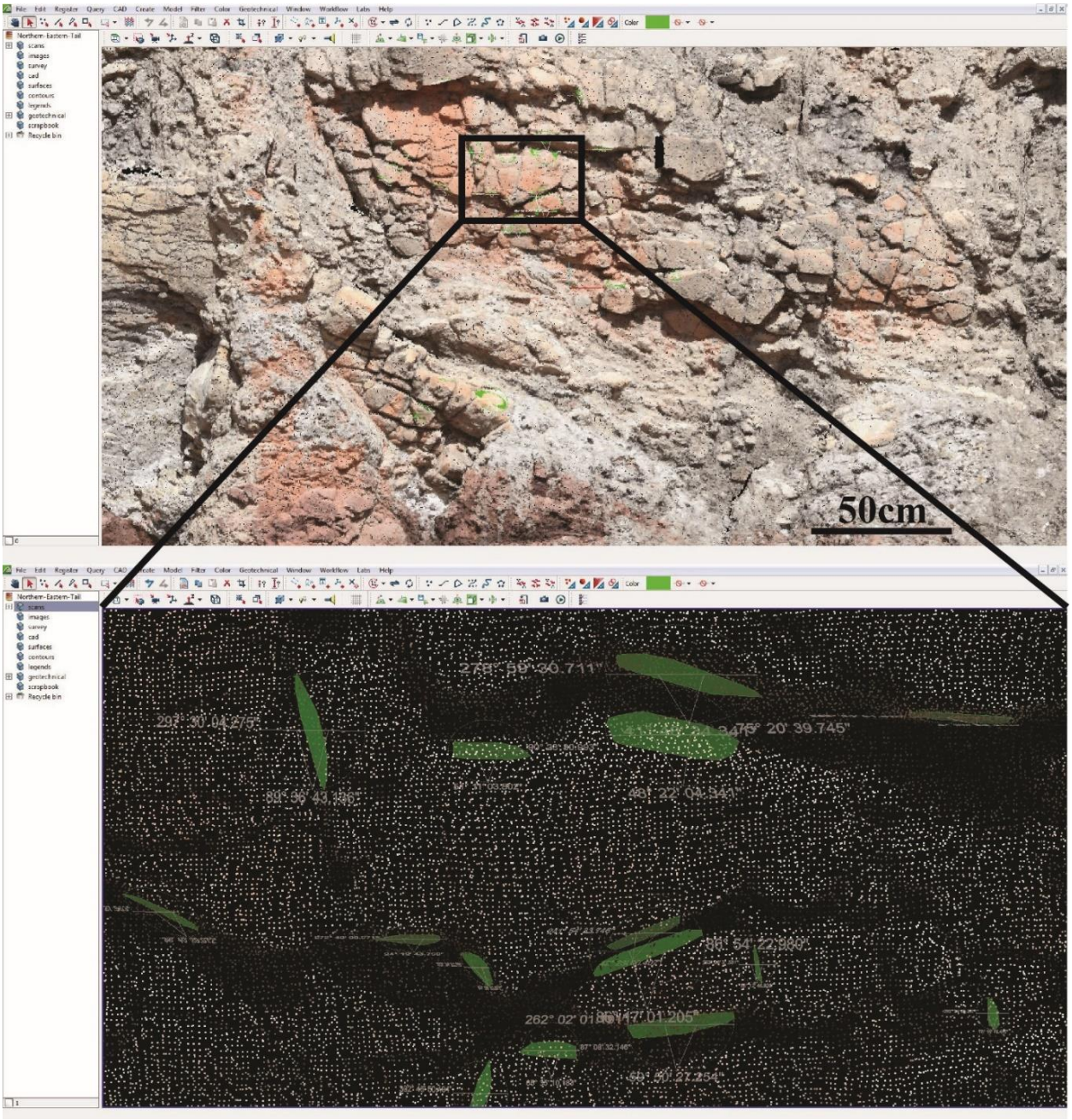


*Figure 20: Diapir contact focus site (the first fracture station from the diapir). The images show the strike and dip measurements of the fractures (green) on the 3D model. When zoomed in, there is a pixel issue on the Maptek. Note that the pixels are larger than original (see Appendix 4 for the data)*

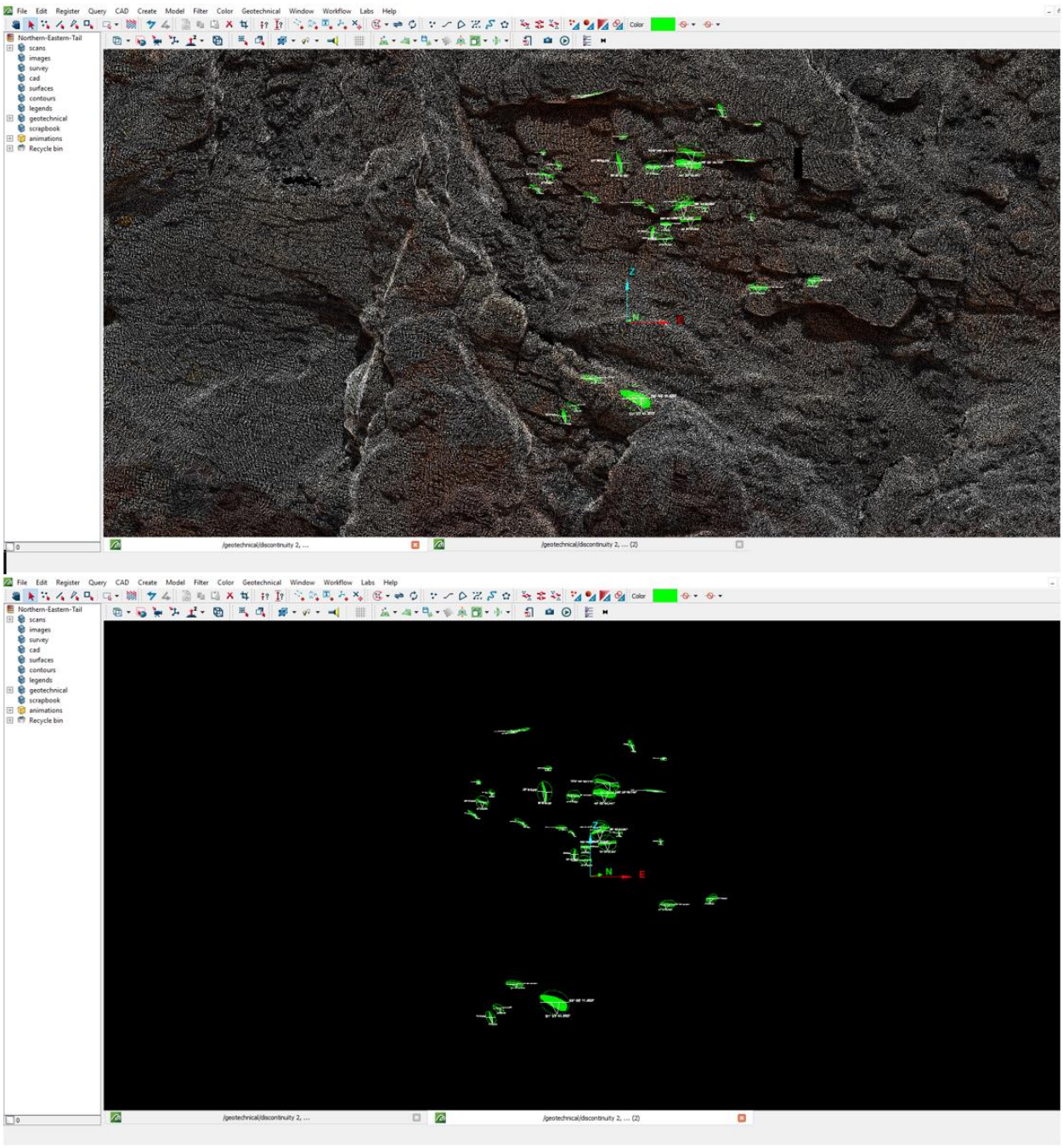


*Figure 21: Maptek surface (Upper figure shows* ***Error! Reference source not found.****'s original figure while lower f igure shows the fracture tracing map) (see Appendix 4 for the data)*

### *3.2.4. Fracture systems*

Figure 22-Figure 23 show stereogram plots of bedding orientations together with fracture orientations for each of the six focus sites. Figure 22 show measurements in modern coordinates while Figure 23 show rotated measurements with bedding restored to horizontal. The purpose of the rotation was to determine if the data were consistent with the fractures forming early in the diapiric history or late. That is, if the fractures formed when the beds were subhorizontal, the orientations should be consistent among the sites when beds are restored to horizontal whereas if they formed late, they should be similar in modern, geographic coordinates. Note that this analysis makes two major assumptions: 1) that all fractures formed at the same time; and 2) that bed rotations occurred along the strike line. Although neither of these assumptions can be fully justified, in the absence of other data, these are the only end members that can be easily evaluated.

Comparing Figure 22 and Figure 23, it is not clear if either end-member assumption is correct. The three inner sites (domain 0) all show the same general pattern of two orthogonal fracture sets approximately perpendicular to bedding, and in modern coordinates these sites show grossly different patterns (Figure 22) but are relatively similar when bedding is restored to horizontal (Figure 23). This suggests that for these sites the fractures either formed early, when beds were near horizontal, or some complex superposition which coincidentally produces this result. In contrast, outer zone sites in the more intact Cutler, are more ambiguous (Figure 22 and Figure 23). That is, in modern coordinates, these sites have similar fracture orientations, but because they also have similar bedding orientations, this pattern remains in restored coordinates. Thus, for these sites, orientation alone is ambiguous on the timing of fracture formation.

One solution to this discrepancy may arise when we incorporate the results analyzing fractures on the 3D model, particularly the *Cutler-Second Farthest* site where this broader scale analysis on the model revealed a second fracture set at ~60 degrees to the main fracture set. This geometry suggests a conjugate shear fracture set, which is consistent with small offsets observed on some fractures in the field (Figure 24). Under that interpretation, the observation that the fractures are generally perpendicular to bedding implies they probably formed early, when the beds were subhorizontal. In addition, if the fractures are a conjugate set in the outer, Cutler exposures, they imply a subhorizontal, bed-parallel maximum stress oriented ~NS to NNE in restored bedding coordinates.

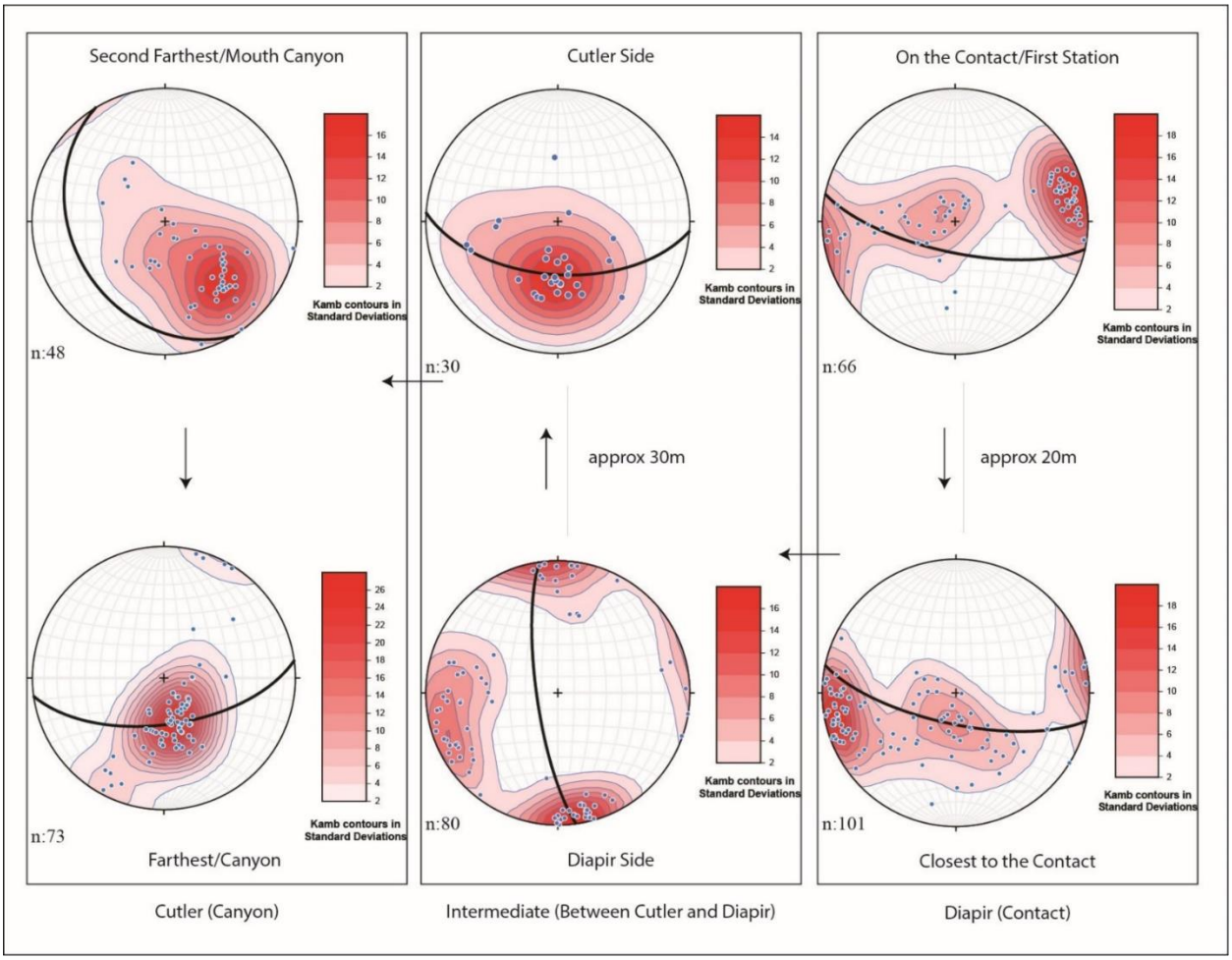


*Figure 22: Kamb contoured equal area stereonet plot of poles to fractures with bedding at each site shown as heavy great circle. (The arrows between stereoplots show distance from diapir contact toward the canyon) (see Appendix 1 for the data)*

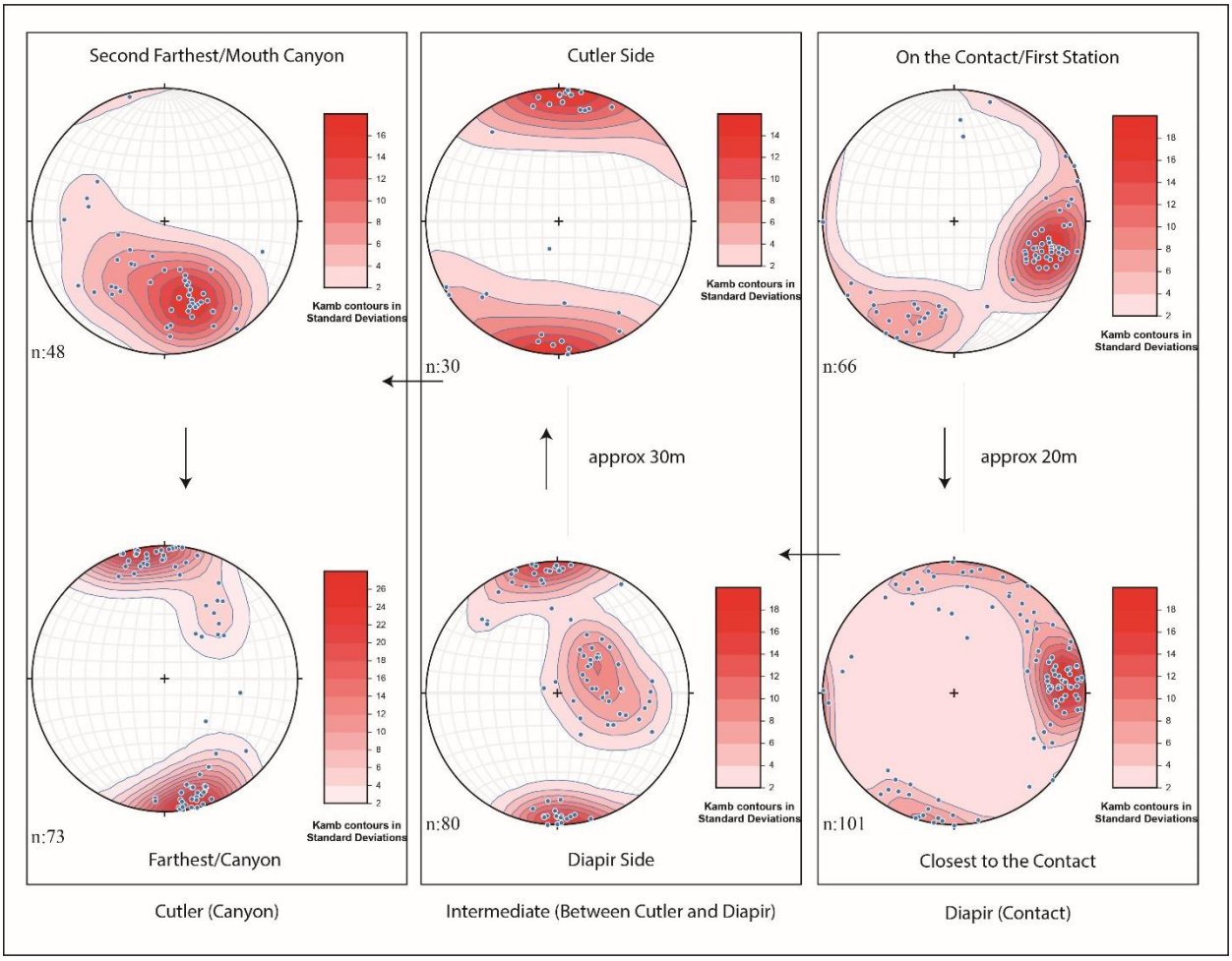


*Figure 23: Kamb contours after bedding rotation to horizontal (The arrows between stereoplots show distance from diapir contact toward the canyon) (see Appendix 1 for the data)*

*Figure 24: Offset around the Cutler-Second Farthest site*

# 4. Discussion

This study was undertaken with a goal of understanding fracture systems surrounding the Onion Creek diapir with a focus on a well exposed deformed zone at the diapir margin. The approach of using a field study combined with new 3D modeling capabilities led to unexpected results with implications for approaches in the use of these field methods Thus, I discuss the implications for use the technology in this type of study as well as the original intent of the study, the evaluation of the facture system and its relation to the formation of the Onion Creek diapir and significance for risking hydrocarbon traps adjacent to diapirs.

## 4.1. Mapping of fracture systems on virtual outcrop models

The 3D models allow spectacular display of the 3D geometry of the study outcrop. Manipulating these models in 3D allowed assessment of structural geometry that would not be possible in the field. For this study, one application of the model was that focus sites, together with adjacent parts of the outcrops could be revisited at will within the visualization of the model. This allowed mapping of surfaces including bedding and fractures by digitizing in 3D, directly on the model as well as acquire measurements for bedding, faults and/or fractures in the models.

An example of an application of using the model to extend field observations is the analysis shown in Figure 16. Here, limitations of access to the outcrop suggested that only one generation of fractures was present, based on field measurements. However, by zooming out to larger areas on the model, and carefully assessing the larger outcrop, it became apparent that a second fracture set was present, displayed particularly prominently on the upper part of the outcrop where it could not be easily reached for field measurements. In addition, the model

allowed routine mapping of bedding and fractures within this exposure, further clarifying the geometry (Figure 16).

## 4.2. Use of 3D outcrop models for remote sensing of fracture orientations

In addition to allowing detailed mapping of fracture traces, the 3D model also afforded an opportunity to dramatically increase the density of strike and dip data relative to data collected in the field, provided the method gave comparable results. To evaluate that question, I measured fractures on the model from the same focus sites that were examined in the field (Figure 30). The model aided in this analysis by allowing analysis across a broader region, including not only the focus site but adjacent areas as well. The result of this analysis was different at different sites with some sites showing reasonable correlations between the field data and the model measurements (e.g. Figure 13 and Figure 15), one site that faithfully reproduced the field result but also revealed a second fracture set (Figure 16), and one site that gave completely unacceptable results (Figure 12). Each of these cases implies different explanations.

In the case of the unacceptable comparison (Figure 12) my hypothesis is that remote analysis failed because of a unique feature of the outcrop geometry and lighting conditions at the time the images were acquired. Specifically, the fracture apertures are small relative to the model resolution (e.g. note the point spacing in Figure 12). Thus, small error in position of points in the point cloud can produce a significant error when a multipoint analysis is used to determine strike and dip. In addition, most of the fractures intersect a relatively planar surface, bedding, with deep shadow obscuring internal surfaces of the fracture. Thus, when attempting to measure the surfaces with remote analysis, there is insufficient 3D control to accurately measure the fractures. This is clear in Figure 12 where most of the measured surfaces are at low angles for the

model surface, yet the fractures that were being measured are at a high angle to the surface. Some of these surfaces are real fractures of other orientations but they then stand out in the analysis because most of the fractures in the dominant set remain unresolvable in the method.

In contrast, other sites, where the fractures are prominent at outcrop scale and are easily seen on the model (Figure 13, Figure 15 and Figure 16) the results of the measurements on the model are comparable to the field measurements. In fact, it could be argued here that the results of measurements on the model are actually superior to the field measurements (Figure 25 and Figure 27). From six focus site, although the *On the Contact* (Figure 12) has tiny fractures and two unsuccessful results, *Intermediate-Diapir Side* focus site (Figure 14) did not appear on the model, and *Cutler-Farthest* station had georeferenced systematic error that I could not figure out (Figure 17), the rest gave spectacular results (Figure 25 and Figure 27). Therefore, it is simply possible that the model measurements are actually better because it works well in larger areas.

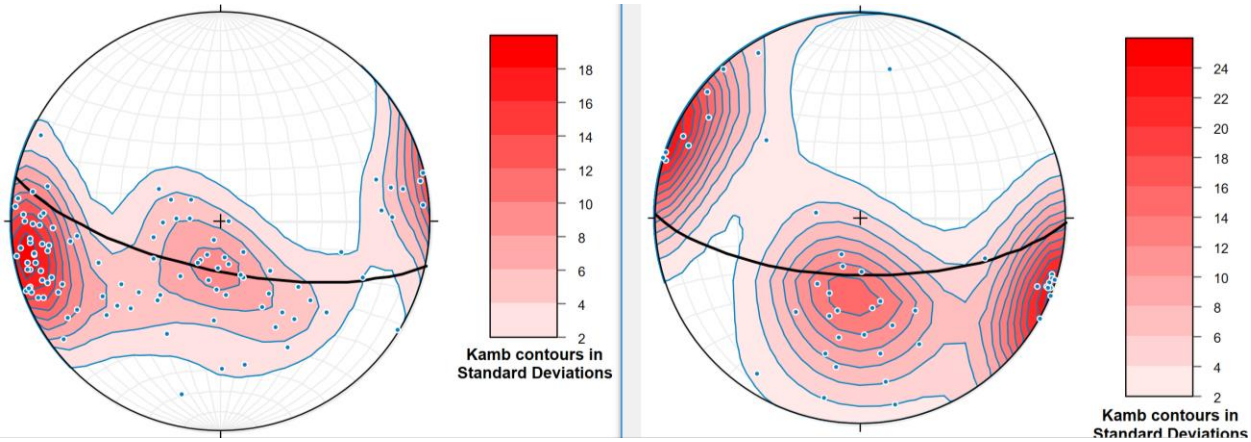


*Figure 25: Closest to the Contact focus site. Stereoplot from field data (Left), from the model (Right)*

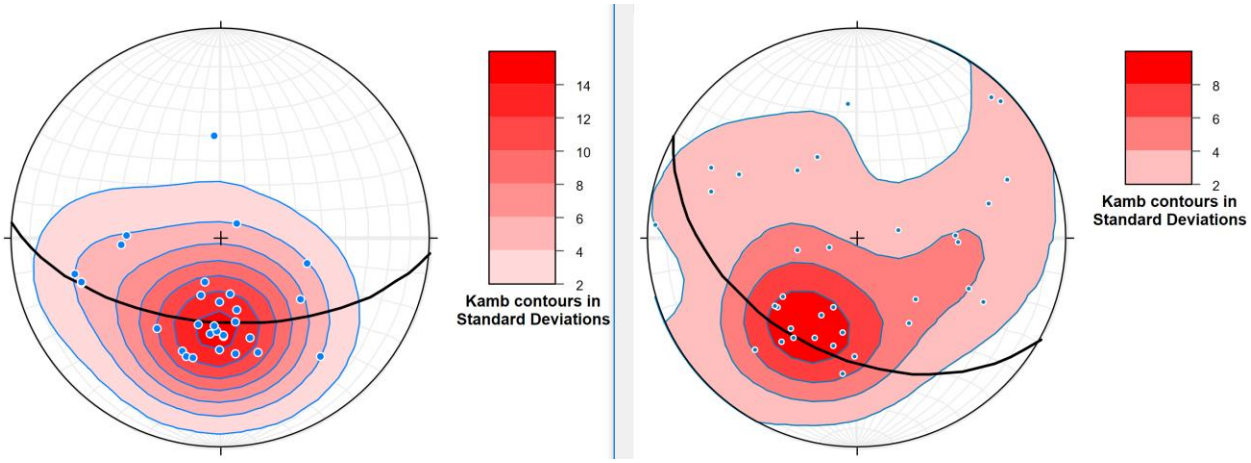


*Figure 26: Intermediate-Cutler Side focus site. Stereoplot from field data (Left), from the model (Right)*

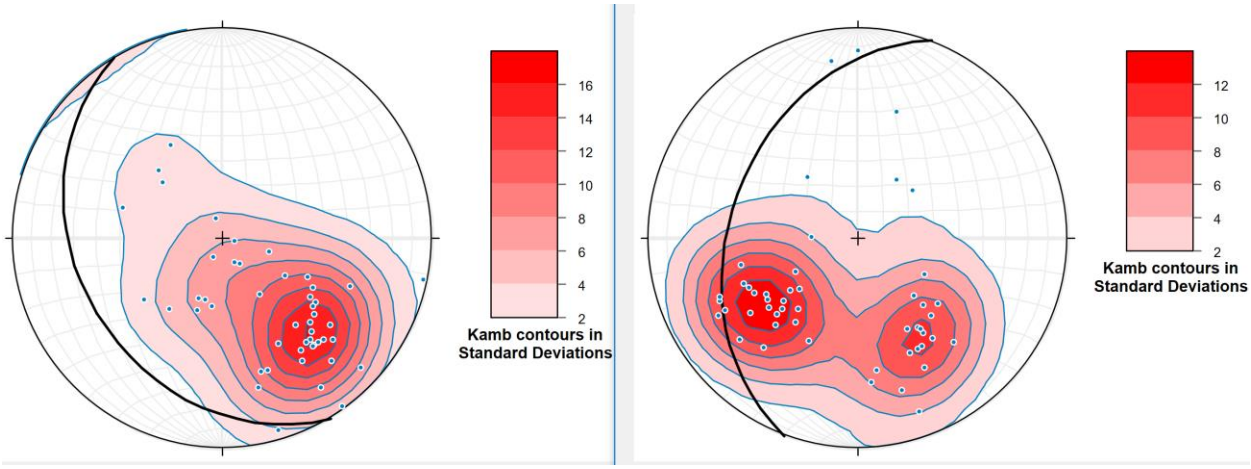


*Figure 27: Cutler-Second Farthest focus site. Stereoplot from field data (Left), from the model (Right)*

In any case, using 3D models remotely saves time and reduces expenses of fieldwork. In addition, it allows whole outcrop analysis. For example, in this study it would have been possible to map every fracture visible down to cm levels throughout the outcrop, extrapolating orientations from these data as well as connectivity. Ideally the could even be extended to 3D by constructing 3D surface from the model elements, although assumptions in surface construction would likely outweigh benefits of this kind of analysis. Nonetheless, future studies should consider this type of approach.

Although promising, the result here indicates caution is needed in using these data. The failure of the method in the site near the contact of the diapir is discouraging, yet not surprising in retrospect when the measurements are seen in the context of the sparsity of the point cloud where the measurements were made (Figure 12). One solution to this problem is apparent from Figure 12. Had we taken more detailed photos, at this specific site, and made a very high-resolution virtual outcrop at the scale of 1-2m, it is likely the smaller fractures could have been resolved. Thus, future studies should consider multiscale approaches; using these methods to make outcrop models of the entire site, as done here, with focused, more detailed models at key sites.

## 4.3. Fracture patterns near the Onion Creek diapir

It is difficult to generalize to larger scales from a small exposure like the outcrop examined here, yet the fracture systems observed are consistent with general models of stresses surrounding salt diapirs. Salt intrusion causes localized high stresses and leads to initiation and propagation of fractures near diapirs (NRC, 1996). Quinta et al. (2012), for example, states that the influence of diapir-related stress decreases away from diapir margin, which is consistent with the observed limited range of fault systems and bed rotations near diapirs. The data sets analyzed here indicate fractures are more abundant near the diapir, including rocks that are basically cataclasites within 20m of the diapir contact. In these close in sites there has been intense deformation, but it is difficult to determine how it relates to diapirism when bedding changes abruptly across numerous faults. Nonetheless, it is important to note that in areas near the contact where bedding is recognizable, the faults form a mutually orthogonal set which is itself perpendicular to bedding. This suggests these fractures are extension fractures and record a stretching within the bedding plane or two superimposed orthogonal extension events.

Farther from the diapir contact, however, the fracture systems are distinctly simpler in the study site shear fractures (Figure 24). Salt diapirs typically show radial faults, concentric faults, or both (Davison et al., 2000; Stewart, 2006) (Figure 28 and Figure 29). Figure 22Figure 23 show that in this study area both radial and concentric fractures are present at the six field sites I examined but vary with position relative to the diapir margin. In particular, in modern coordinates two fracture sets are present at sites near the diapir margin (domain 0) but only one is present farther from the diapir. In all cases, however, the fractures are approximately perpendicular to bedding. In modern, coordinates this pattern is indistinct, but when the fractures are restored with bedding horizontal, a clearer picture emerges (Figure 23). That is, in the sites close to the diapir, the two fracture sets include both a radial and concentric fracture set whereas farther from the diapir, the radial set disappears and only the concentric set is present. This implies that well away from the diapir margin radial extension was dominant whereas near the diapir margin the rocks were stretched in two directions.

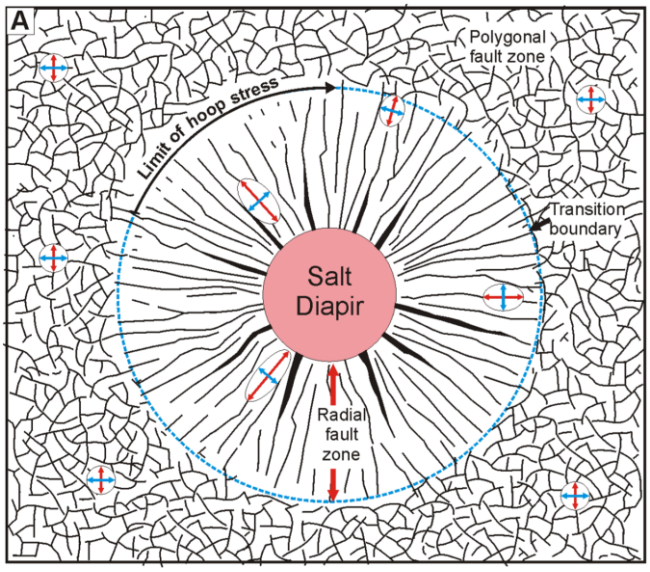


*Figure 28: Polygonal fault zone demonstrates the geometry of a hoop stress field around a salt diapir. The blue dashed circle shows the limit of the hoop stress. The red and blue arrows respectively illustrate the ratio of the maximum and minimum horizontal principal stresses (Carruthers, 2012).*

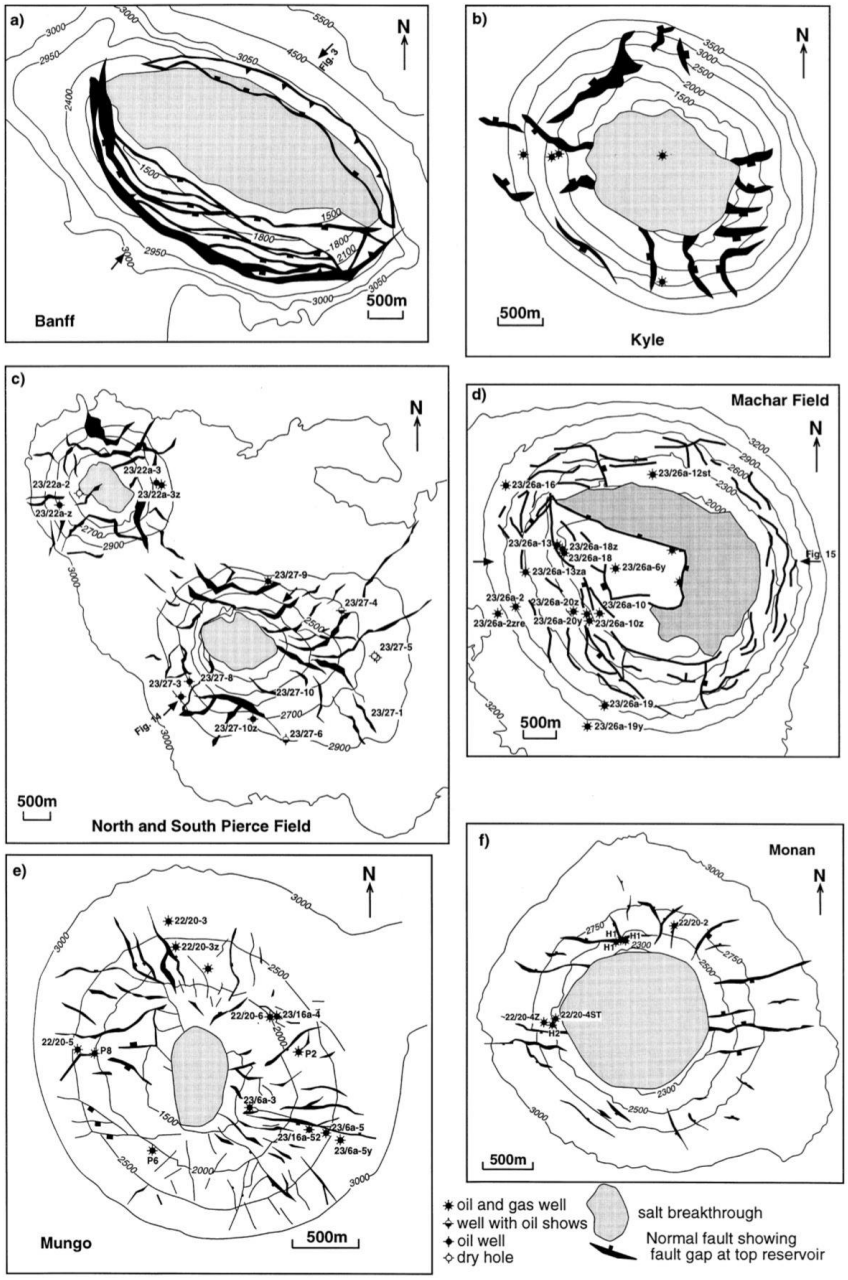


*Figure 29: The figure shows some examples of radial and concentric faults around salt diapirs. Interpreted by oilcompanies such as Conoco, Ranger Oil, Enterprise Oil, and BP Amoco (Davison, 2000).*

## 4.4. Use of a Smart Phone for collecting orientation data

In the last few years the availability of software on smartphones that allow use of these devices as a replacement for a conventional geologist's compass has led to their widespread use,

yet evidence has accumulated that not all devices yield accurate results (Novakova and Pavlis, 2017; Allmendinger et al, 2017). However, the results of my device were positive (Figure 30). Specifically, in a field test of similar fracture sets in the same outcrop (Figure 30) the phone and Brunton compass produced comparable results. The device used is an iPhone 7 Plus (IOS 11) with Field Move Clino 2.3.3 and thus, this result is consistent with the conclusions of Allmendinger et al. (2017) that iPhones, in general, produce good results in these types of analyses.

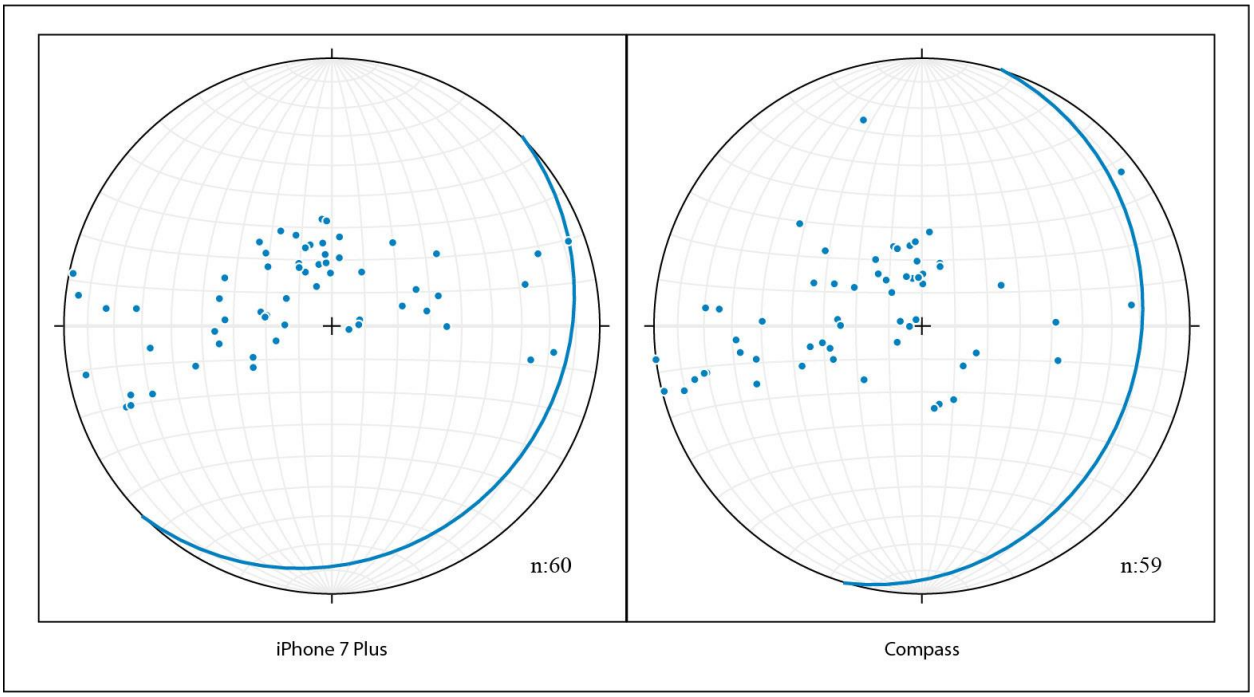


*Figure 30: The comparison of phone data and compass data (the declination of the compass was set up for El Paso which is 8.1º although the phone was set up for Utah that is 10.1º) (Blue circles show the overall fracture orientation while dots show fracture) (see Appendix 3 for the data)*

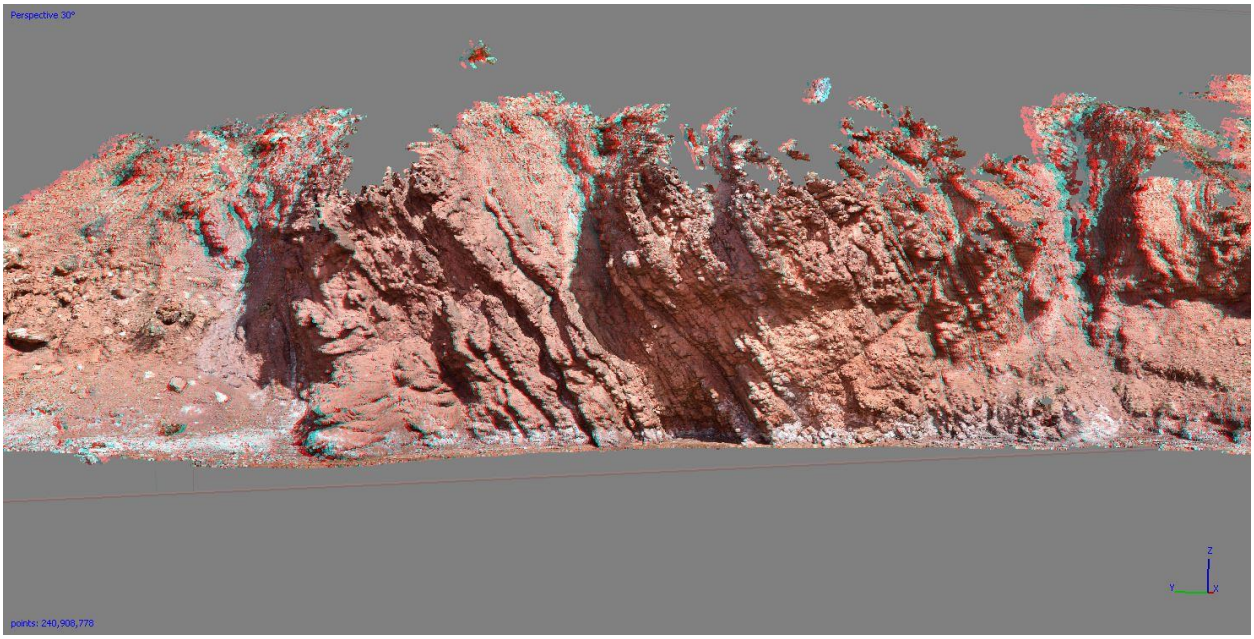


*Figure 31: Cyan-magenta stereo view of the data station of Cutler side in the intermediate section of the walls from Photoscan stereo view (Y shows north, X shows east)*

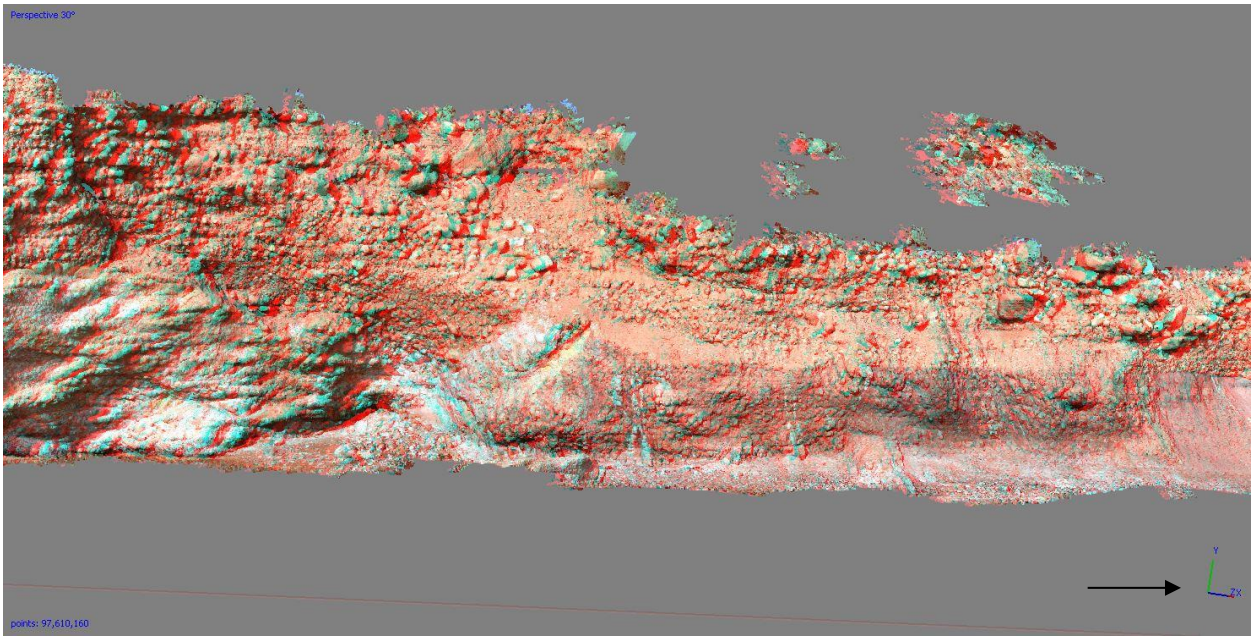


*Figure 32: Southern west section of the walls in cyan-magenta Photoscan stereo view (Black arrow shows north)*

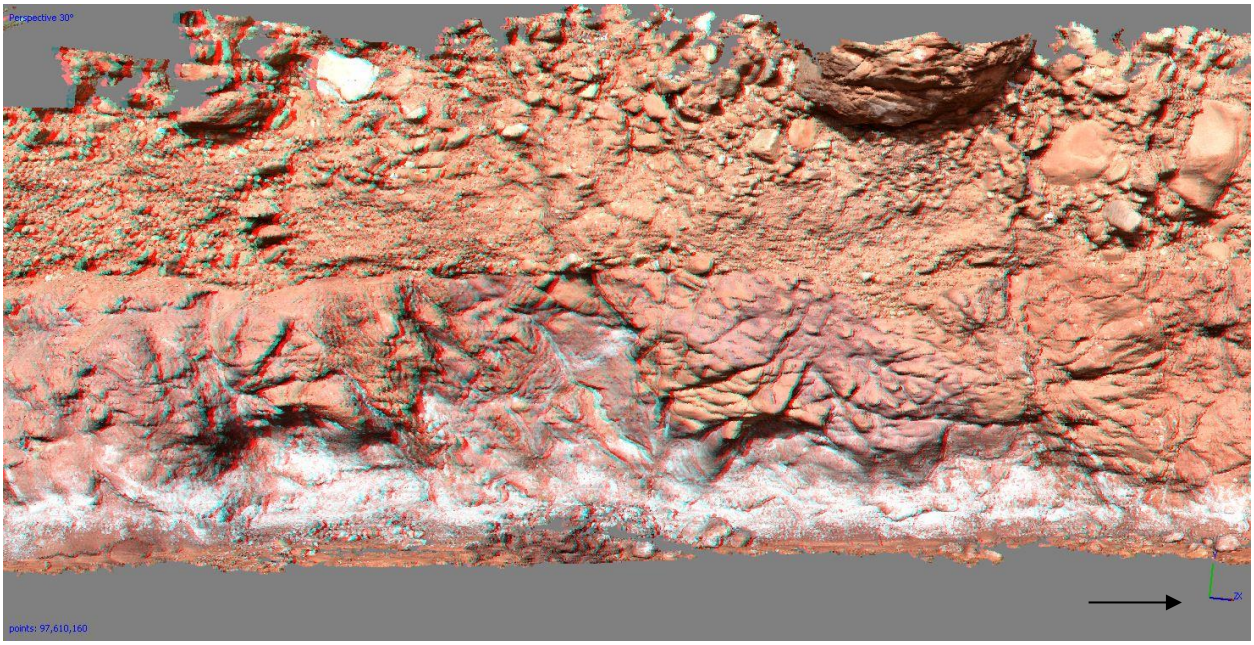


*Figure 33: Northern west section of the walls in cyan-magenta Photoscan stereo view (Black arrow shows north)*

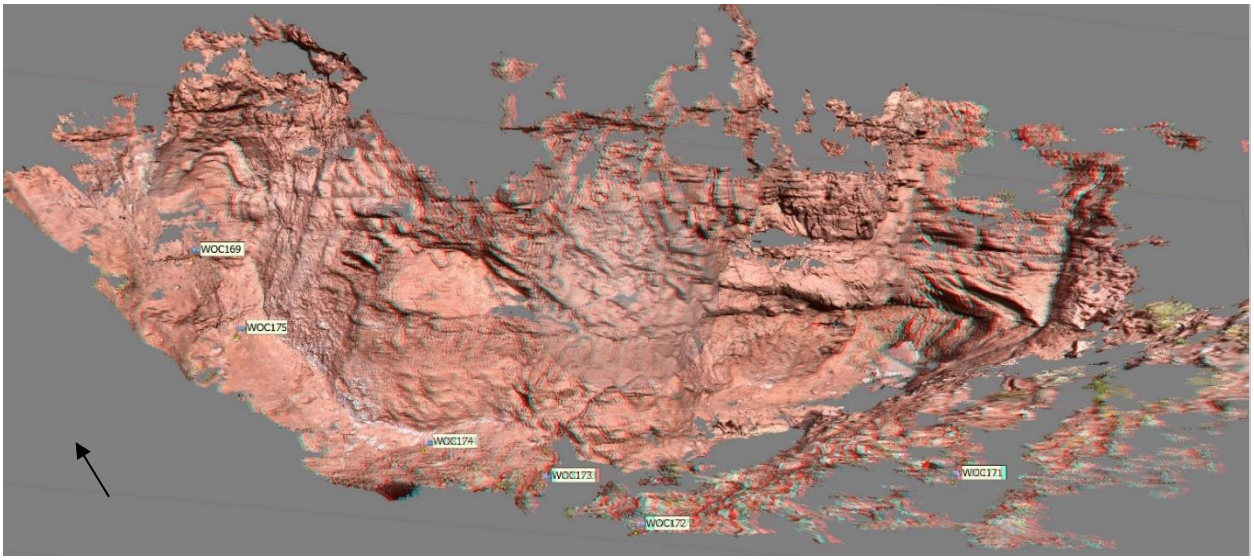


*Figure 34: Canyon in cyan-magenta Photoscan stereo view (Black arrow shows north)*

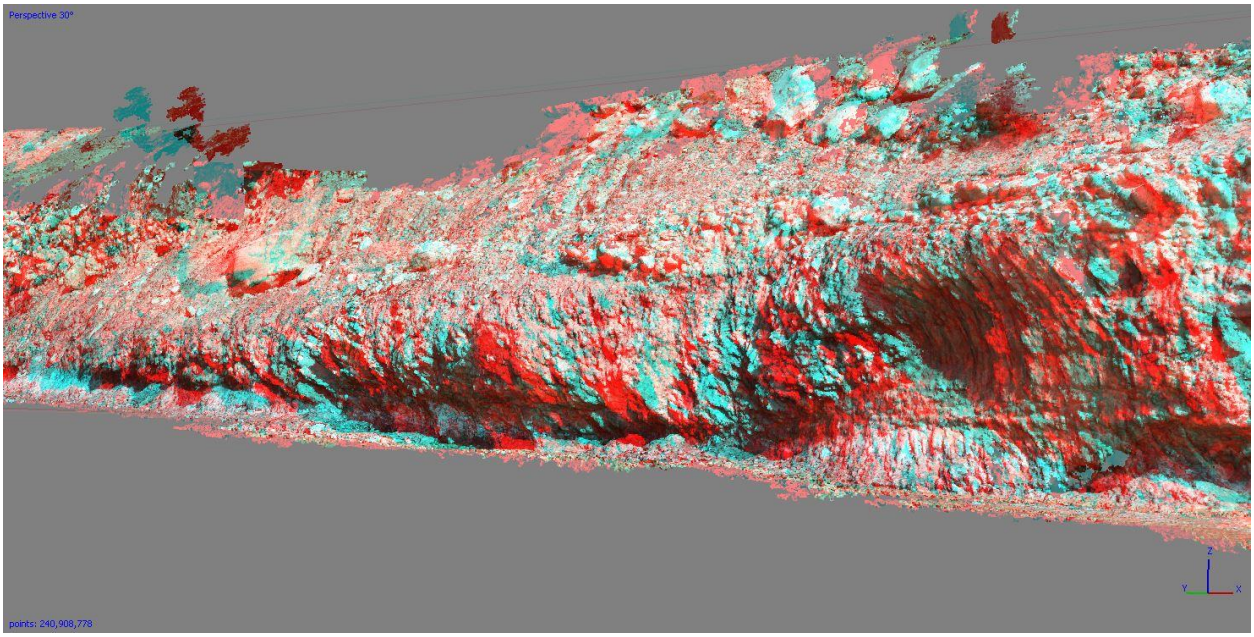


*Figure 35: Southern east side of the walls in cyan-magenta Photoscan stereo view (Y shows north, X shows east)*

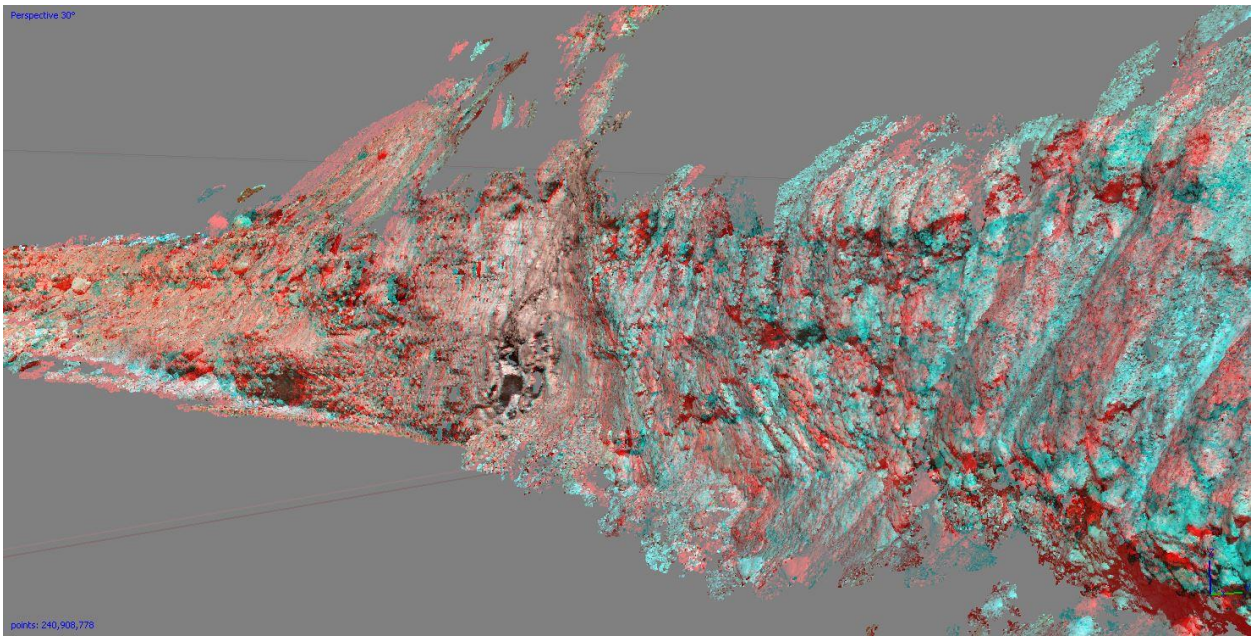


*Figure 36: The data stations of the diapir section of the wall in cyan-magenta Photoscan stereo view (Y shows north, X shows east)*

# 5. Conclusion

Field exposures in the Paradox Basin provide unprecedented detail of the fracture systems and stratigraphic relationships that developed along the margins of salt diapirs, providing potential to understand fracture permeability development in other salt provinces. This study used a new method, 3D terrain models using SfM/MvS, as a base for detailed mapping and fracture analysis to the mm level. Use of these methods produced new insights with important cautionary notes.

Significant results of this study include:

1) Collecting ground control data with only a handheld GPS is -generally not reliable if submeter accuracy is needed. Although horizontal errors were in line with known errors in WAAS corrected differential GPS, a systematic error of more than 8m was seen in the vertical. The origin of this error is unknown, but likely related to weather conditions or local geography disturbing the differential correction in the WAAS signal.
2) Measuring orientations with a cell phone provides reasonable data, provided the cell phone passes simple tests.
3) Remotely measured fracture orientations using multipoint analyses on the model produced mixed results. Where fractures were large and easily observed on the model, the model-based measurements were broadly consistent with the field measurements. Indeed, in one site the model-based measurements were arguably superior because they resolved a second fracture set that was clear on unreachable cliff faces above the field site, but difficult to see at the level of a field observer. In contrast, at one site near the diapir contact the field measurements and model-based

measurements were completely at odds. In this case, however, the origin of the discrepancy is clear from 3D assessment of the model where relatively 2D outcrop geometry and small scale of the fractures prevented routine analysis of 3D geometry.

4) In cases like the site where model measurements failed a solution to the problem is either use standard field measurement techniques for the analysis or to use a camera to second set of very high-resolution photographs of the site of interest, allowing development of a more high resolution model where the fracture systems would be resolved. Which method is used would depend on field time vs lab time.
5) Although the 3D model allowed rapid mapping of fracture traces and bedding traces to show 3D trajectories, fracture connectivity and fracture network assessments proved difficult in this study site because although fractures and faults could be traced through the cliff faces of the model, a large flat area between the cliffs is covered, handicapping tracing feature between the two complete exposures.

## Suggestion for Future work

The salt diapir at Onion Creek needs more fracture sites around it better understand the relationships between faults, fracturing and bedding. Similar techniques could be used elsewhere along the diapir margin from domain 0 sites into intact Cutler to further clarify the origin of the fracture systems. Particularly important is a more regional assessment of the fracture systems, beyond the limited range of this small outcrop.

# References


Allmendinger, W. A., Siron, C. R., & Scott, C. P. (2017) Structural data collection with mobile devices: Accuracy, redundancy, and best practices. *Journal of Strauctural Geology*. 102, 98-112.

Baars, D.L. (1966) Pre-Pennsylvanian paleotectonics - key to basin evolution and petroleum occurrences in Paradox basin, Utah and Colorado. *Am. Assoc. Petrol. Geol. Bull*., 50, 2082-2111.

Baars, D.L. & Stevenson, G.M. (1981) Tectonic evolution of the Paradox basin, Utah and Colorado. In: *Geology of the Paradox Basin* (Ed. by D.L. Wiegand), pp. 23-31. Association of Geologists, Rocky Mount.

Baars, D. L., & Stevenson, G. M., 1982, Subtle stratigraphic traps in Paleozoic rocks of Paradox Basin; in The Deliberate Search for the Subtle Trap, M. T. Halbouty, ed.: American Association of Petroleum Geologists, Memoir 32, p. 131-158.

Banbury, N.J. (2005) The role of salt mobility in the development of supra-salt sedimentary depocentres and structural styles. PhD Thesis, University of Edinburgh, Edinburgh, UK.

Barbeau, D.L. (2003) A flexural model for the Paradox basin: implications for the tectonics of the Ancestral Rocky Mountains. *Basin Res*., 15, 97-115.

Bromley, M.H. (1991) Architectural features of the Kayenta Formation (Lower Jurassic), Colorado Plateau, USA: relationship to salt tectonics in the Paradox Basin. *Sediment. Geol*., 73, 77-99.

Carrivick, J.L., Smith, M.W., Quincey, D.J., 2016, Structure from Motion in the Geosciences, John Wiley and Sons, West Sussex, UK, 197p.

Carruthers, T. D. (2012) Interaction of Polygonal Fault Systems with Salt Diapirs. PhD Thesis, Cardiff University, Cardiff, UK.

Condon, S.M. (1997) Geology of the Pennsylvanian and Permian Cutler Group and Permian Kaibab Limestone in the Paradox Basin, Southeastern Utah and Southwestern Colorado. *US Department of the Interior, US Geological Survey Bulletin*, 2000-P, 46pp.

Cook, E. L. (2017) Near Salt Stratal Geometries and Implications for the Evolution of the Onion Creek Diapir Moab, UT. MS Thesis, Brigham Young University, UT.

Davison, I., Alsop, I., Birch, P., Elders, C., Evans, N., Nicholson, H., Rorison, P., Wade, D., Woodward, J., Young, M., 2000. Geometry and late-stage structural evolution of Central Graben salt diapirs, North Sea. *Marine and Petroleum Geology* 17(4), 499-522.

Dershowitz, W. S., and P. R. LaPointe, 1994, Discrete fracture approaches for oil and gas applications, in R. A. Nelson and S. Laubach, eds., Rock mechanics: Rotterdam, Balkema, p. 19– 30.

Doelling, H. H. (1985) Geologic map of Arches National Park and vicinity, Grand County, Utah. Utah Geological and Mineral Survey Map 74. Utah Geological Survey.

Doelling, H. H. (1988) Geology of Salt Valley anticline and Arches National Park, Grand County, Utah. In: *Salt Deformation in the Paradox Region* (Ed. By H.H. Deolling, C.G. Oviatt & P.W. Huntoon), *Utah Geol. Sırvey Bull*., 122, 1-60.

Doelling, H.H. (2001) Geologic map of the Moab and eastern part of the San Rafael Desert 30'x60' Quadrangles, Grand and Emery Counties, Utah and Mesa County, Colorado. Utah Geological Survey Map 180.

Doelling, H.H. (2002) Geologic map of the Fisher Towers 7.5' quadrangle, Grand County, Utah. Utah Geological Survey Map 183, p.22.

Elston, D.P. & Shoemaker, E.M. (1960) Late Paleozoic and early Mesozoic structural history of the Uncompahgre front. In: *Geology of the Paradox basin fold and fault belt - Four Corners Geol. Soc. 3rd Field Conference* (Ed. by K.G. Smith), pp. 47-55 Four Corners Geological Society, Durango, Colorado.

Elston, D.P., Shoemaker, E.M. & Landis, E.R. (1962) Uncompahgre front and salt anticline region of Paradox Basin, Colorado and Utah. *Am. Assoc. Petrol. Geol. Bull*., 46, 1857-1878.

Elston, D.P. & Shoemaker, E.M. (1963) Salt anticlines of the Paradox Basin, Colorado and Utah. In: *Symposium on Salt - Northern Ohio Geological Society* (Ed. by A.C. Bersticker), pp. 131-146. Northern Ohio Geological Society, Cleveland, Ohio.

Friedman, J.D., Case, J.E. & Simpson, S.L. (1994) Tectonic trends of the northern part of the Paradox Basin, southeastern Utah and southwestern Colorado, as derived from landsat multispectral scanner imaging and geophysical and geologic mapping. *US Department of the Interior, US Geological Survey Bulletin*, 2000-C, p. 34.

Green M. (2014) Own work, CC BY-SA 3.0, https://commons.wikimedia.org/w/index.php?curid=33572534

Goldhammer, R.K., Oswald, E.J. & Dunn, P.A. (1994) High frequency, glacio-eustatic cyclicity in the Middle Pennsylvanian of the Paradox Basin-an evaluation of Milankovitch forcing. In: *Orbital Forcing and Cyclic Sequences. Special publication of International Association of Sedimentologists*, 19 (Ed. by P.L. de Boer &D.G. Smith), 243-283. Blackwell, Oxford.

Grisi, K. C. (2018) Attributes of Fisher Valley Megaflap and Comparison to the Gypsum Valley Megaflap, Paradox Basin, Utah and Colorado: Implications for Controls on Megaflap Formation. MS Thesis, The University of Texas at El Paso, TX.

Hanke, J.R. (2017) *Journal of Structural Geology*. https://doi.org/10.1016/j.jsg.2017.11.012

Hazel, J.E. (1994) Sedimentary response to intrabasinal salt tectonism in the Upper Triassic Chinle Formation, Paradox basin, Utah. US Department of the Interior, US Geological Survey Bulletin, 2000-F, 34pp.

Hite, R.J. & Buckner, D.H. (1981) Stratigraphic correlations, facies concepts, and cyclicity in Pennsylvanian rocks of the Paradox basin. In: *Geology of the Paradox Basin* (Ed. By D.L. Wiegand), pp.147-159. Association of Geologists, Rocky Mount.

Hite, R.J., Anders, D.E., and Ging, T.G., 1984, Organic-rich source rocks of Pennsylvanian age in the Paradox Basin of Utah and Colorado: in Hydrocarbon Source Rocks of the Greater Rocky Mountain Region, Rocky Mountain Association of Geologists, p. 255-271.

Hudec, M.R. (1995) The Onion Creek salt diapir: an exposed diapir fall structure in the Paradox basin, Utah. In: *Salt, Sediment and Hydrocarbons. Gulf Coast Section Society of Economic Paleontologists and Mineralogists 16th Annual Research Conference* (Ed. by C.J. Travis, H. Harrison, M.R. Hudec, B.C. Vendeville, F.J. Peel & B.F. Perkins), pp. 125-134. Gulf Coast Section SEPM Foundation, Houston, Texas.

Kelley, V.C., 1958, Tectonics of the region of the Paradox Basin, in Sanborn, A.F., ed., Guidebook to the Geology of the Paradox Basin: Intermountain Association of Petroleum Geologists, p. 31–38.

Kenroy, P. R. (2013) Fracture-Controlled Paleohydrologic Systems in the Vicinity of Salt Diapirs. MS Thesis, Northern Illinois University.

Kluth, C.F. & Duchene, H.R. (2009) Late Pennsylvanian and early Permian structural geology and tectonic history of the Paradox Basin and Uncompahgre uplift, Colorado and Utah. In: *The Paradox Basin Revisited - New Developments in Petroleum Systems and Basin*

*Analysis* (Ed. by W.S. Houston, L.L. Wray & P.G. Moreland), pp. 178-197. Association of Geologists, Rocky Mount.

Lawton, T.F. & Buck, B.J. (2006) Implications of diapir-derived detritus and gypsic paleosols in Lower Triassic strata near the Castle Valley salt wall, Paradox Basin, Utah. *Geology*, 34, 885-888.

Matthews, N.A., Noble, T.A., and Breithaupt, B.H., 2016, Close-range photogrammetry for 3D ichnology: The basics of photogrammetric ichnology, in Falkingham, P.L., Marty, D., and Richter, A, eds., Dinosaur Tracks – The Next Steps: Bloomington, Indiana, Indiana University Press, 520 p.

Moore, K.D., Soreghan, G.S. & Sweet, D.E. (2008) Stratigraphic and structural relations in the proximal Cutler Formation of the Paradox Basin: implications for timing of movement on the Uncompahgre front. *Mountain Geol.*, 45, 49-68.

Narr, W., Schechter D.S. &Thompson L.B. (2006) Naturally Fractured Reservoir Characterization. Society of Petroleum Engineers, 112.

Nelson, R. A., 1985, Geologic analysis of naturally fractured reservoirs: Houston, Texas, Gulf Publishing, 320 p.

Nicholas, I.P.W., Alves T.M., &Blenkinsop T.G. (2016) Reservoir leakage along concentric faults in the Southern North Sea: Implications for the deployment of CCS and EOR techniques. *Tectonophysics*. 690. 97-116.

NRC (National Research Council) (1996) Rock Fractures and Fluid Flow. National Academy Press, Washington D.C. 551.

Novakova, L. & Pavlis T. L. (2017) Assessment of the precision of smart phones and tablets for measurement of planar orientations: A case study. *Journal of Strauctural Geology*. 97, 93-103.

Nuccio, V.F. & Condon, M. (1996) Burial and thermal history of the Paradox basin, Utah and Colorado, and petroleum potential of the Middle Pennsylvanian Paradox Formation, US Department of the Interior, US Geological Survey Bulletin, 2000-O, p. 41.

Ohlen, H.R. & Mcintyre, L.B. (1965) Stratigraphy and tectonic features of the Paradox Basin, four corners area. *Am. Assoc. Petrol. Geol. Bull.*, 49, 2020-2040.

Online Reference 1, https://www.nikonusa.com/en/nikon-products/product/dslr-cameras/d5300.html

Online Reference 2, http://kb.unavco.org/kb/assets/24/Gb1000_om.pdf

Online Reference 3, www.geo.cornell.edu/geology/faculty/RWA/programs/stereonet.html

Online Reference 4, https://www.faa.gov/about/office_org/headquarters_offices/ato/service_units/techops/navservices/gnss/waas/benefits/

Online Reference 5, http://www.esri.com/news/arcuser/0703/geoid1of3.html

Peacock, D.C.P., Sanderson, D.J. & Rotevatn A. (2018) Relationships between fractures. *Journal of Structural Geology.* 106, 41-53.

Quinta, A., Tavani, S. & Roca E. (2012) Fracture pattern analysis as a tool for constraining the interaction between regional and diapir-related stress fields: Poza de la Sal Diapir (Basque Pyreness Spain). *Salt Tectonics, Sediments and Prospectivity*. Geological Society of London, Special Publications. 363, 521-532.

Rasmussen, D.L. (2006) Escalation of Pennsylvanian-Permian Uncompahgre uplift revealed by progression of siliciclastic wedges in the Paradox basin, Colorado and Utah. In: *Geological Society of America 38th Annual Meeting - Abstracts with Programs Geol. Soc. Am.*, p. 29.

Rasmussen, L. & Rasmussen, D.L. (2009) Burial history analysis of the Pennsylvanian petroleum system in the deep Paradox Basin fold and fault belt, Colorado and Utah. In: *The Paradox Basin Revisited - New Developments in Petroleum Systems and Basin Analysis* (Ed. By W.S. Houston, L.L. Wray & P.G. Moreland), pp. 24-94. Association of Geologists, Rocky Mount.

Raup, O.B. & Hite, R.J. (1992) Lithology of evaporite cycles and cycle boundaries in the upper part of the Paradox Formation of the Hermosa Group of Pennsylvanian age in the Paradox Basin, Utah and Colorado. US Department of the Interior, US Geological Survey Bulletin, 2000-B, p. 37.

Reiss, L. H., 1982, The reservoir engineering aspects of fractured formations: Houston, Texas, Gulf Publishing, 186 p.

Rohrbaugh Jr., M. B., Dunne, W. M., & Mauldon, M. (2002). Estimating fracture trace intensity, density, and mean length using circular scan lines and windows. *AAPG Bulletin.* v. 86, no. 12, p. 2089–2104.

Stewart, S.A., 2006. Implications of passive salt diapir kinematics for reservoir segmentation by radial and concentric faults. *Marine and Petroleum Geology* 23(8), 843-853.

Trudgill, B.D. & Paz, M. (2009) Restoration of mountain front and salt structures in the northern Paradox Basin, SE Utah. In: *The Paradox Basin Revisited - New Developments in Petroleum Systems and Basin Analysis* (Ed. By W.S. Houston, L.L. Wray & P.G. Moreland), pp. 132-177. Association of Geologists, Rocky Mount.

Trudgill B.D., 2011, Evolution of salt structures in the northern Paradox Basin: controls on evaporite deposition, salt wall growth and supra-salt stratigraphic architecture. *Basin Research*, **23**, 208-238.

Venus, J. H., Mountney, N. P., and McCaffrey,W.D., 2015, Syn-sedimentary salt diapirism as a control on fluvial-system evolution: an example from the proximal Permian Cutler Group, SE Utah, USA. *Basin Research*, **27**, 152-182.

Wengerd, S.A. (1962) Pennsylvanian sedimentation in Paradox Basin, Four Corners region. In: *Pennsylvanian system in the United States - A symposium* (Ed. by C.C. Branson), pp. 264-330. Am. Assoc. Petrol. Geol., Tulsa, Oklahoma.

White, M.A. & Jacobson, M.I. (1983) Structures associated with the southwest margin of the ancestral Uncompahgre Uplift. In: *Northern Paradox Basin - Uncompahgre Uplift* (Ed. By W.R. Averett), pp. 33-39. Grand Junction Geological Society, Grand Junction, Colorado.

# Appendix

Note: Right Arm (Hand) rule is applied for all the data collected.

## Appendix 1

| Location Name | Plane Type | Dip | Strike |
|---|---|---|---|
| On the Contact | Joint | 86.93184 | 188.0206 |
| On the Contact | Joint | 78.43345 | 8.237022 |
| On the Contact | Joint | 9.942538 | 121.3026 |
| On the Contact | Joint | 74.6913 | 153.1973 |
| On the Contact | Joint | 46.5691 | 7.359779 |
| On the Contact | Joint | 74.72725 | 159.6113 |
| On the Contact | Joint | 81.03471 | 166.0405 |
| On the Contact | Joint | 22.23876 | 354.0491 |
| On the Contact | Joint | 17.58585 | 58.61084 |
| On the Contact | Joint | 79.88213 | 175.3539 |
| On the Contact | Joint | 74.75798 | 164.0471 |
| On the Contact | Joint | 52.78524 | 158.4556 |
| On the Contact | Joint | 76.27741 | 351.847 |
| On the Contact | Joint | 12.49043 | 118.5608 |
| On the Contact | Joint | 84.75092 | 355.7199 |
| On the Contact | Joint | 65.16581 | 158.2955 |
| On the Contact | Joint | 72.48669 | 353.5581 |
| On the Contact | Joint | 74.23563 | 172.4541 |
| On the Contact | Joint | 80.51147 | 169.8446 |
| On the Contact | Joint | 79.60308 | 168.7347 |
| On the Contact | Joint | 84.81478 | 157.8499 |
| On the Contact | Joint | 80.82881 | 345.9218 |
| On the Contact | Joint | 81.91376 | 173.9259 |
| On the Contact | Joint | 32.30918 | 162.1965 |
| On the Contact | Joint | 14.27886 | 59.86685 |
| On the Contact | Joint | 10.48571 | 80.75381 |
| On the Contact | Joint | 7.325335 | 61.34114 |
| On the Contact | Joint | 66.43555 | 156.9999 |
| On the Contact | Joint | 73.95701 | 169.2721 |
| On the Contact | Joint | 78.32726 | 178.8651 |
| On the Contact | Joint | 54.78507 | 275.8413 |
| On the Contact | Joint | 43.69757 | 270.4276 |
| On the Contact | Joint | 21.8984 | 323.5857 |
| On the Contact | Joint | 26.42608 | 331.0451 |

| | | | |
|---|---|---|---|
| On the Contact | Joint | 45.90946 | 355.4197 |
| On the Contact | Joint | 15.33203 | 121.2265 |
| On the Contact | Joint | 55.38374 | 358.2066 |
| On the Contact | Joint | 62.48687 | 358.8654 |
| On the Contact | Joint | 7.113765 | 28.24515 |
| On the Contact | Joint | 70.89864 | 164.3468 |
| On the Contact | Joint | 78.63577 | 169.5912 |
| On the Contact | Joint | 8.956587 | 319.066 |
| On the Contact | Joint | 29.20736 | 359.0963 |
| On the Contact | Joint | 31.43262 | 5.780457 |
| On the Contact | Joint | 77.86917 | 335.1301 |
| On the Contact | Joint | 13.58762 | 25.10345 |
| On the Contact | Joint | 16.33319 | 106.1944 |
| On the Contact | Joint | 80.95529 | 154.6776 |
| On the Contact | Joint | 36.0332 | 16.44467 |
| On the Contact | Joint | 51.52423 | 352.2583 |
| On the Contact | Joint | 66.83234 | 168.8799 |
| On the Contact | Joint | 73.8407 | 179.1206 |
| On the Contact | Joint | 82.81068 | 180.9504 |
| On the Contact | Joint | 69.58707 | 173.6232 |
| On the Contact | Joint | 82.55633 | 177.2373 |
| On the Contact | Joint | 25.61653 | 292.4061 |
| On the Contact | Joint | 14.48073 | 334.2122 |
| On the Contact | Joint | 77.61931 | 170.5388 |
| On the Contact | Joint | 71.12614 | 161.5626 |
| On the Contact | Joint | 78.17944 | 161.7873 |
| On the Contact | Joint | 82.74725 | 164.4059 |
| On the Contact | Joint | 69.49313 | 153.517 |
| On the Contact | Joint | 68.43951 | 154.971 |
| On the Contact | Joint | 73.63914 | 157.9221 |
| On the Contact | Joint | 67.89931 | 162.9387 |
| On the Contact | Joint | 86.92583 | 351.6616 |
| Closest to the Contact | Joint | 89 | 211.603 |
| Closest to the Contact | Joint | 74.38967 | 1.758194 |
| Closest to the Contact | Joint | 73.10008 | 11.20316 |
| Closest to the Contact | Joint | 83.43986 | 2.11496 |
| Closest to the Contact | Joint | 69.0992 | 357.7215 |
| Closest to the Contact | Joint | 68.77864 | 357.746 |
| Closest to the Contact | Joint | 17.33647 | 3.521133 |
| Closest to the Contact | Joint | 18.13592 | 272.7873 |
| Closest to the Contact | Joint | 78.12278 | 344.585 |
| Closest to the Contact | Joint | 16.83441 | 259.0238 |

| | | | |
|---|---|---|---|
| Closest to the Contact | Joint | 23.37774 | 248.0939 |
| Closest to the Contact | Joint | 79.36705 | 347.5238 |
| Closest to the Contact | Joint | 71.68233 | 351.8221 |
| Closest to the Contact | Joint | 83.19112 | 345.8605 |
| Closest to the Contact | Joint | 89 | 166.6301 |
| Closest to the Contact | Joint | 73.4901 | 282.4685 |
| Closest to the Contact | Joint | 22.22611 | 249.0123 |
| Closest to the Contact | Joint | 65.47832 | 165.2102 |
| Closest to the Contact | Joint | 65.94545 | 176.0228 |
| Closest to the Contact | Joint | 49.74899 | 194.5033 |
| Closest to the Contact | Joint | 51.47725 | 341.3108 |
| Closest to the Contact | Joint | 47.41932 | 221.1824 |
| Closest to the Contact | Joint | 40.20081 | 219.7929 |
| Closest to the Contact | Joint | 73.21349 | 336.3447 |
| Closest to the Contact | Joint | 39.00541 | 274.2021 |
| Closest to the Contact | Joint | 83.21065 | 347.6457 |
| Closest to the Contact | Joint | 86.77541 | 168.5401 |
| Closest to the Contact | Joint | 37.63688 | 309.3112 |
| Closest to the Contact | Joint | 50.22749 | 315.883 |
| Closest to the Contact | Joint | 26.74869 | 273.1642 |
| Closest to the Contact | Joint | 34.44733 | 236.178 |
| Closest to the Contact | Joint | 69.30959 | 328.5171 |
| Closest to the Contact | Joint | 53.20942 | 320.5961 |
| Closest to the Contact | Joint | 59.89247 | 320.5243 |
| Closest to the Contact | Joint | 85.77098 | 352.2072 |
| Closest to the Contact | Joint | 15.03163 | 234.0423 |
| Closest to the Contact | Joint | 80.35434 | 353.7656 |
| Closest to the Contact | Joint | 73.12293 | 2.447838 |
| Closest to the Contact | Joint | 86.50249 | 175.625 |
| Closest to the Contact | Joint | 27.30751 | 27.41409 |
| Closest to the Contact | Joint | 7.813634 | 288.2897 |
| Closest to the Contact | Joint | 21.22074 | 23.85633 |
| Closest to the Contact | Joint | 27.00196 | 346.241 |
| Closest to the Contact | Joint | 11.79474 | 4.802628 |
| Closest to the Contact | Joint | 16.68446 | 297.0478 |
| Closest to the Contact | Joint | 86.85181 | 6.430305 |
| Closest to the Contact | Joint | 85.49409 | 340.7939 |
| Closest to the Contact | Joint | 88.01561 | 4.266548 |
| Closest to the Contact | Joint | 56.07086 | 220.8775 |
| Closest to the Contact | Joint | 59.7705 | 269.5155 |
| Closest to the Contact | Joint | 74.87854 | 327.5915 |
| Closest to the Contact | Joint | 71.70718 | 168.8557 |

| | | | |
|---|---|---|---|
| Closest to the Contact | Joint | 57.92996 | 354.288 |
| Closest to the Contact | Joint | 82.84657 | 323.2185 |
| Closest to the Contact | Joint | 47.35606 | 242.7017 |
| Closest to the Contact | Joint | 62.01241 | 201.4467 |
| Closest to the Contact | Joint | 69.9558 | 338.3342 |
| Closest to the Contact | Joint | 70.73573 | 178.7818 |
| Closest to the Contact | Joint | 61.54294 | 352.1941 |
| Closest to the Contact | Joint | 78.20707 | 359.2153 |
| Closest to the Contact | Joint | 79.69637 | 8.993164 |
| Closest to the Contact | Joint | 74.34502 | 352.5594 |
| Closest to the Contact | Joint | 76.38618 | 340.2262 |
| Closest to the Contact | Joint | 74.93105 | 358.8836 |
| Closest to the Contact | Joint | 88.09032 | 340.1355 |
| Closest to the Contact | Joint | 14.02628 | 37.28598 |
| Closest to the Contact | Joint | 22.62389 | 358.7997 |
| Closest to the Contact | Joint | 3.236838 | 181.2697 |
| Closest to the Contact | Joint | 14.2286 | 263.506 |
| Closest to the Contact | Joint | 84.44711 | 25.51603 |
| Closest to the Contact | Joint | 18.40886 | 299.1305 |
| Closest to the Contact | Joint | 30.22222 | 330.6487 |
| Closest to the Contact | Joint | 79.06699 | 349.7332 |
| Closest to the Contact | Joint | 84.26547 | 345.7835 |
| Closest to the Contact | Joint | 23.5894 | 281.293 |
| Closest to the Contact | Joint | 58.55408 | 260.3865 |
| Closest to the Contact | Joint | 42.66602 | 318.7894 |
| Closest to the Contact | Joint | 29.00778 | 265.3836 |
| Closest to the Contact | Joint | 88.60589 | 350.4198 |
| Closest to the Contact | Joint | 57.46929 | 241.7545 |
| Closest to the Contact | Joint | 76.95856 | 170.0732 |
| Closest to the Contact | Joint | 82.5064 | 359.8226 |
| Closest to the Contact | Joint | 80.35164 | 354.9059 |
| Closest to the Contact | Joint | 13.93991 | 292.0927 |
| Closest to the Contact | Joint | 26.37685 | 306.2669 |
| Closest to the Contact | Joint | 49.56755 | 295.3436 |
| Closest to the Contact | Joint | 48.79955 | 233.2788 |
| Closest to the Contact | Joint | 37.15688 | 244.3333 |
| Closest to the Contact | Joint | 43.47303 | 235.7245 |
| Closest to the Contact | Joint | 46.64288 | 327.3669 |
| Closest to the Contact | Joint | 27.41118 | 225.4261 |
| Closest to the Contact | Joint | 85.65697 | 339.3006 |
| Closest to the Contact | Joint | 72.7849 | 350.3296 |
| Closest to the Contact | Joint | 56.51685 | 327.5405 |

| | | | |
|---|---|---|---|
| Closest to the Contact | Joint | 39.63931 | 308.5441 |
| Closest to the Contact | Joint | 81.20385 | 336.6258 |
| Closest to the Contact | Joint | 83.47166 | 337.4212 |
| Closest to the Contact | Joint | 86.67258 | 340.8282 |
| Closest to the Contact | Joint | 78.38163 | 341.7267 |
| Closest to the Contact | Joint | 73.83311 | 341.385 |
| Closest to the Contact | Joint | 79.49355 | 350.0431 |
| Closest to the Contact | Bedding | 66.3919 | 107.4412 |
| Closest to the Contact | Bedding | 71.84866 | 96.96304 |
| Closest to the Contact | Bedding | 74.49491 | 101.5121 |
| Intermediate-Diapir Side | Joint | 78.90175 | 81.24908 |
| Intermediate-Diapir Side | Joint | 85.51373 | 117.6112 |
| Intermediate-Diapir Side | Joint | 89 | 269.5485 |
| Intermediate-Diapir Side | Joint | 80.33014 | 256.8501 |
| Intermediate-Diapir Side | Joint | 45.66456 | 7.611664 |
| Intermediate-Diapir Side | Joint | 41.72137 | 352.8376 |
| Intermediate-Diapir Side | Joint | 43.91322 | 0.681587 |
| Intermediate-Diapir Side | Joint | 81.49525 | 270.1371 |
| Intermediate-Diapir Side | Joint | 84.65822 | 268.7297 |
| Intermediate-Diapir Side | Joint | 74.32809 | 258.1646 |
| Intermediate-Diapir Side | Joint | 86.19447 | 342.7787 |
| Intermediate-Diapir Side | Joint | 85.07203 | 257.6231 |
| Intermediate-Diapir Side | Joint | 85.86127 | 177.8627 |
| Intermediate-Diapir Side | Joint | 74.66614 | 331.6125 |
| Intermediate-Diapir Side | Joint | 77.8469 | 264.6998 |
| Intermediate-Diapir Side | Joint | 89 | 189.0116 |
| Intermediate-Diapir Side | Joint | 83.94551 | 346.4731 |
| Intermediate-Diapir Side | Joint | 74.3252 | 333.5776 |
| Intermediate-Diapir Side | Joint | 79.20492 | 352.3483 |
| Intermediate-Diapir Side | Joint | 62.99045 | 355.2895 |
| Intermediate-Diapir Side | Joint | 83.62292 | 267.0508 |
| Intermediate-Diapir Side | Joint | 66.56654 | 327.1881 |
| Intermediate-Diapir Side | Joint | 78.9804 | 318.4383 |
| Intermediate-Diapir Side | Joint | 86.1389 | 307.5062 |
| Intermediate-Diapir Side | Joint | 86.65659 | 95.81642 |
| Intermediate-Diapir Side | Joint | 81.60965 | 352.0054 |
| Intermediate-Diapir Side | Joint | 67.89848 | 254.5378 |
| Intermediate-Diapir Side | Joint | 84.99313 | 327.3287 |
| Intermediate-Diapir Side | Joint | 83.38138 | 331.4136 |
| Intermediate-Diapir Side | Joint | 75.85271 | 358.3398 |
| Intermediate-Diapir Side | Joint | 78.29082 | 96.75488 |
| Intermediate-Diapir Side | Joint | 86.69809 | 81.51573 |

| | | | |
|---|---|---|---|
| Intermediate-Diapir Side | Joint | 86.4196 | 255.6288 |
| Intermediate-Diapir Side | Joint | 80.37498 | 337.3206 |
| Intermediate-Diapir Side | Joint | 83.90166 | 78.44525 |
| Intermediate-Diapir Side | Joint | 68.97829 | 167.3194 |
| Intermediate-Diapir Side | Joint | 66.25835 | 10.49249 |
| Intermediate-Diapir Side | Joint | 75.66156 | 333.4166 |
| Intermediate-Diapir Side | Joint | 62.8471 | 338.801 |
| Intermediate-Diapir Side | Joint | 82.07809 | 255.4357 |
| Intermediate-Diapir Side | Joint | 88.11795 | 254.1507 |
| Intermediate-Diapir Side | Joint | 63.5294 | 354.4421 |
| Intermediate-Diapir Side | Joint | 73.93779 | 88.57458 |
| Intermediate-Diapir Side | Joint | 65.76099 | 89.49855 |
| Intermediate-Diapir Side | Joint | 51.79741 | 103.3762 |
| Intermediate-Diapir Side | Joint | 50.46798 | 98.30371 |
| Intermediate-Diapir Side | Joint | 50.72488 | 104.9934 |
| Intermediate-Diapir Side | Joint | 47.23248 | 30.76091 |
| Intermediate-Diapir Side | Joint | 49.52287 | 11.26071 |
| Intermediate-Diapir Side | Joint | 54.34226 | 17.67897 |
| Intermediate-Diapir Side | Joint | 79.86938 | 334.3727 |
| Intermediate-Diapir Side | Joint | 72.81657 | 355.897 |
| Intermediate-Diapir Side | Joint | 87.74935 | 84.00899 |
| Intermediate-Diapir Side | Joint | 75.64494 | 257.2453 |
| Intermediate-Diapir Side | Joint | 86.48572 | 98.57056 |
| Intermediate-Diapir Side | Joint | 74.73204 | 258.9835 |
| Intermediate-Diapir Side | Joint | 82.06952 | 256.9012 |
| Intermediate-Diapir Side | Joint | 79.46844 | 243.0808 |
| Intermediate-Diapir Side | Joint | 73.38313 | 245.3608 |
| Intermediate-Diapir Side | Joint | 70.40596 | 321.8748 |
| Intermediate-Diapir Side | Joint | 87.66964 | 270.6133 |
| Intermediate-Diapir Side | Joint | 81.72563 | 262.4959 |
| Intermediate-Diapir Side | Joint | 85.17966 | 89.25388 |
| Intermediate-Diapir Side | Joint | 76.22958 | 82.27763 |
| Intermediate-Diapir Side | Joint | 78.30201 | 252.0404 |
| Intermediate-Diapir Side | Joint | 54.52566 | 277.8014 |
| Intermediate-Diapir Side | Joint | 62.6143 | 12.19942 |
| Intermediate-Diapir Side | Joint | 81.76582 | 262.8541 |
| Intermediate-Diapir Side | Joint | 72.17008 | 1.240196 |
| Intermediate-Diapir Side | Joint | 71.06689 | 16.43361 |
| Intermediate-Diapir Side | Joint | 86.52545 | 95.89961 |
| Intermediate-Diapir Side | Joint | 76.69234 | 164.5347 |
| Intermediate-Diapir Side | Joint | 82.11655 | 338.2299 |
| Intermediate-Diapir Side | Joint | 74.531 | 15.64977 |

| | | | |
|---|---|---|---|
| Intermediate-Diapir Side | Joint | 77.21186 | 267.7764 |
| Intermediate-Diapir Side | Joint | 83.24171 | 261.2152 |
| Intermediate-Diapir Side | Joint | 77.57741 | 327.089 |
| Intermediate-Diapir Side | Joint | 88.52773 | 199.0355 |
| Intermediate-Diapir Side | Joint | 79.75354 | 256.1294 |
| Intermediate-Diapir Side | Joint | 83.46064 | 271.6438 |
| Intermediate-Diapir Side | Bedding | 78.6042 | 267.5342 |
| Intermediate-Diapir Side | Bedding | 75.96758 | 76.21291 |
| Intermediate-Cutler Side | Joint | 40.27813 | 86.82098 |
| Intermediate-Cutler Side | Joint | 43.90811 | 304.5864 |
| Intermediate-Cutler Side | Joint | 47.67201 | 288.32 |
| Intermediate-Cutler Side | Joint | 49.16245 | 285.6515 |
| Intermediate-Cutler Side | Joint | 49.25606 | 282.5595 |
| Intermediate-Cutler Side | Joint | 29.13193 | 256.674 |
| Intermediate-Cutler Side | Joint | 22.0894 | 260.1385 |
| Intermediate-Cutler Side | Joint | 33.38575 | 259.8147 |
| Intermediate-Cutler Side | Joint | 59.10919 | 341.6437 |
| Intermediate-Cutler Side | Joint | 40.14435 | 217.3633 |
| Intermediate-Cutler Side | Joint | 23.85224 | 288.3937 |
| Intermediate-Cutler Side | Joint | 58.63402 | 342.1318 |
| Intermediate-Cutler Side | Joint | 46.45857 | 262.2452 |
| Intermediate-Cutler Side | Joint | 41.11604 | 253.384 |
| Intermediate-Cutler Side | Joint | 39.01506 | 268.0264 |
| Intermediate-Cutler Side | Joint | 48.05645 | 251.8519 |
| Intermediate-Cutler Side | Joint | 44.39362 | 270.6625 |
| Intermediate-Cutler Side | Joint | 35.17915 | 283.8887 |
| Intermediate-Cutler Side | Joint | 35.82637 | 196.759 |
| Intermediate-Cutler Side | Joint | 63.57046 | 229.8501 |
| Intermediate-Cutler Side | Joint | 38.95605 | 355.5377 |
| Intermediate-Cutler Side | Joint | 36.98277 | 1.192863 |
| Intermediate-Cutler Side | Joint | 18.14006 | 289.2512 |
| Intermediate-Cutler Side | Joint | 24.8288 | 271.1459 |
| Intermediate-Cutler Side | Joint | 8.508178 | 139.1251 |
| Intermediate-Cutler Side | Joint | 60.53428 | 345.9532 |
| Intermediate-Cutler Side | Joint | 38.09842 | 276.2594 |
| Intermediate-Cutler Side | Joint | 38.4075 | 267.999 |
| Intermediate-Cutler Side | Joint | 36.61438 | 272.174 |
| Intermediate-Cutler Side | Joint | 34.45826 | 273.6054 |
| Intermediate-Cutler Side | Bedding | 57.29176 | 109.1294 |
| Intermediate-Cutler Side | Bedding | 57.49846 | 79.40802 |
| Canyon-Second Farthest | Bedding | 29.35419 | 147.2179 |
| Canyon-Second Farthest | Joint | 19.10887 | 196.5447 |

| | | | |
|---|---|---|---|
| Canyon-Second Farthest | Joint | 26.39067 | 235.7036 |
| Canyon-Second Farthest | Joint | 28.45381 | 210.9834 |
| Canyon-Second Farthest | Joint | 67.42216 | 228.0133 |
| Canyon-Second Farthest | Joint | 47.70707 | 219.292 |
| Canyon-Second Farthest | Joint | 44.69303 | 214.5069 |
| Canyon-Second Farthest | Joint | 44.78344 | 216.8981 |
| Canyon-Second Farthest | Joint | 45.24349 | 229.7761 |
| Canyon-Second Farthest | Joint | 52.16948 | 226.2637 |
| Canyon-Second Farthest | Joint | 53.849 | 228.7015 |
| Canyon-Second Farthest | Joint | 36.93391 | 204.6988 |
| Canyon-Second Farthest | Joint | 12.34341 | 236.3306 |
| Canyon-Second Farthest | Joint | 47.60762 | 241.6208 |
| Canyon-Second Farthest | Joint | 55.13077 | 234.8273 |
| Canyon-Second Farthest | Joint | 60.50264 | 222.4768 |
| Canyon-Second Farthest | Joint | 56.85497 | 229.4628 |
| Canyon-Second Farthest | Joint | 55.14408 | 200.3871 |
| Canyon-Second Farthest | Joint | 53.65765 | 231.1853 |
| Canyon-Second Farthest | Joint | 27.00332 | 278.7956 |
| Canyon-Second Farthest | Joint | 56.22416 | 253.4966 |
| Canyon-Second Farthest | Joint | 62.70671 | 256.2444 |
| Canyon-Second Farthest | Joint | 39.12247 | 321.106 |
| Canyon-Second Farthest | Joint | 30.06549 | 288.6241 |
| Canyon-Second Farthest | Joint | 10.92845 | 242.9874 |
| Canyon-Second Farthest | Joint | 87.46092 | 191.682 |
| Canyon-Second Farthest | Joint | 48.84378 | 223.7761 |
| Canyon-Second Farthest | Joint | 7.784497 | 72.7395 |
| Canyon-Second Farthest | Joint | 8.033218 | 294.463 |
| Canyon-Second Farthest | Joint | 85.02206 | 253.5732 |
| Canyon-Second Farthest | Joint | 79.49735 | 223.0456 |
| Canyon-Second Farthest | Joint | 56.96312 | 227.4567 |
| Canyon-Second Farthest | Joint | 56.03085 | 218.7663 |
| Canyon-Second Farthest | Joint | 40.56883 | 16.71011 |
| Canyon-Second Farthest | Joint | 41.13172 | 208.8376 |
| Canyon-Second Farthest | Joint | 34.45322 | 306.7082 |
| Canyon-Second Farthest | Joint | 59.48649 | 236.8348 |
| Canyon-Second Farthest | Joint | 56.03232 | 250.663 |
| Canyon-Second Farthest | Joint | 25.1353 | 285.008 |
| Canyon-Second Farthest | Joint | 88.29825 | 234.6545 |
| Canyon-Second Farthest | Joint | 74.28445 | 236.3994 |
| Canyon-Second Farthest | Joint | 25.38513 | 291.0316 |
| Canyon-Second Farthest | Joint | 41.8953 | 61.10728 |
| Canyon-Second Farthest | Joint | 36.25359 | 46.34106 |

| | | | |
|---|---|---|---|
| Canyon-Second Farthest | Joint | 4.96365 | 194.0903 |
| Canyon-Second Farthest | Joint | 31.66067 | 43.28693 |
| Canyon-Second Farthest | Joint | 42.13549 | 213.4944 |
| Canyon-Second Farthest | Joint | 57.60256 | 224.9394 |
| Canyon-Second Farthest | Joint | 56.71742 | 229.771 |
| Canyon-Second Farthest | Bedding | 31.87736 | 151.3948 |
| Canyon-Farthest | Joint | 21.57814 | 296.0702 |
| Canyon-Farthest | Joint | 23.41538 | 158.9892 |
| Canyon-Farthest | Joint | 17.36576 | 178.7625 |
| Canyon-Farthest | Joint | 33.23157 | 284.1706 |
| Canyon-Farthest | Joint | 25.02855 | 258.0387 |
| Canyon-Farthest | Joint | 33.66731 | 281.5063 |
| Canyon-Farthest | Joint | 21.58548 | 241.1544 |
| Canyon-Farthest | Joint | 79.49654 | 296.273 |
| Canyon-Farthest | Joint | 34.88399 | 268.159 |
| Canyon-Farthest | Joint | 21.45983 | 227.6596 |
| Canyon-Farthest | Joint | 26.36443 | 265.1959 |
| Canyon-Farthest | Joint | 35.2357 | 251.9789 |
| Canyon-Farthest | Joint | 32.67936 | 239.8276 |
| Canyon-Farthest | Joint | 45.41766 | 286.7774 |
| Canyon-Farthest | Joint | 40.42323 | 297.4745 |
| Canyon-Farthest | Joint | 31.07386 | 251.6371 |
| Canyon-Farthest | Joint | 30.02276 | 248.8743 |
| Canyon-Farthest | Joint | 39.30988 | 260.5481 |
| Canyon-Farthest | Joint | 44.81803 | 255.5728 |
| Canyon-Farthest | Joint | 85.30583 | 107.9164 |
| Canyon-Farthest | Joint | 86.99842 | 104.3452 |
| Canyon-Farthest | Joint | 43.06992 | 244.9853 |
| Canyon-Farthest | Joint | 49.55643 | 240.8705 |
| Canyon-Farthest | Joint | 40.91513 | 272.924 |
| Canyon-Farthest | Joint | 29.15745 | 233.087 |
| Canyon-Farthest | Joint | 28.23899 | 253.272 |
| Canyon-Farthest | Joint | 38.4818 | 272.9633 |
| Canyon-Farthest | Joint | 20.29613 | 221.8706 |
| Canyon-Farthest | Joint | 24.01116 | 244.3437 |
| Canyon-Farthest | Joint | 21.90931 | 248.2742 |
| Canyon-Farthest | Joint | 20.06557 | 262.3645 |
| Canyon-Farthest | Joint | 33.53745 | 289.715 |
| Canyon-Farthest | Joint | 23.52654 | 292.8325 |
| Canyon-Farthest | Joint | 12.51727 | 193.547 |
| Canyon-Farthest | Joint | 17.19106 | 176.8939 |
| Canyon-Farthest | Joint | 18.72604 | 219.4823 |

| | | | |
|---|---|---|---|
| Canyon-Farthest | Joint | 71.45715 | 299.5462 |
| Canyon-Farthest | Joint | 75.09755 | 292.1397 |
| Canyon-Farthest | Joint | 71.50311 | 302.7888 |
| Canyon-Farthest | Joint | 59.81118 | 303.2517 |
| Canyon-Farthest | Joint | 10.35397 | 238.9887 |
| Canyon-Farthest | Joint | 13.80909 | 235.1027 |
| Canyon-Farthest | Joint | 19.25791 | 235.7335 |
| Canyon-Farthest | Joint | 14.7776 | 258.813 |
| Canyon-Farthest | Joint | 14.29234 | 233.1546 |
| Canyon-Farthest | Joint | 28.8089 | 261.3554 |
| Canyon-Farthest | Joint | 27.7242 | 263.9151 |
| Canyon-Farthest | Joint | 21.96915 | 260.8155 |
| Canyon-Farthest | Joint | 58.2325 | 139.3162 |
| Canyon-Farthest | Joint | 35.98254 | 260.4971 |
| Canyon-Farthest | Joint | 32.74182 | 241.2232 |
| Canyon-Farthest | Joint | 33.30564 | 253.5287 |
| Canyon-Farthest | Joint | 35.68517 | 120.4176 |
| Canyon-Farthest | Joint | 39.19192 | 246.8119 |
| Canyon-Farthest | Joint | 38.63824 | 178.2515 |
| Canyon-Farthest | Joint | 85.75241 | 298.6631 |
| Canyon-Farthest | Joint | 42.98409 | 257.8492 |
| Canyon-Farthest | Joint | 49.59664 | 251.2373 |
| Canyon-Farthest | Joint | 29.20035 | 242.7045 |
| Canyon-Farthest | Joint | 41.96989 | 271.2112 |
| Canyon-Farthest | Joint | 22.27531 | 234.9883 |
| Canyon-Farthest | Joint | 19.4533 | 219.8324 |
| Canyon-Farthest | Joint | 34.05413 | 278.66 |
| Canyon-Farthest | Joint | 21.58517 | 229.8192 |
| Canyon-Farthest | Joint | 87.53558 | 121.5181 |
| Canyon-Farthest | Joint | 44.28306 | 260.3294 |
| Canyon-Farthest | Joint | 54.13665 | 280.1805 |
| Canyon-Farthest | Joint | 47.9461 | 278.8083 |
| Canyon-Farthest | Joint | 26.35475 | 261.2547 |
| Canyon-Farthest | Joint | 34.00388 | 272.3958 |
| Canyon-Farthest | Joint | 32.11048 | 253.3575 |
| Canyon-Farthest | Joint | 34.61721 | 252.6123 |
| Canyon-Farthest | Joint | 87.56047 | 117.8605 |
| Canyon-Farthest | Bedding | 33.35604 | 172.8015 |
| Canyon-Farthest | Bedding | 17.48084 | 183.6611 |
| Canyon-Farthest | Bedding | 28.81878 | 140.2048 |
| Canyon-Farthest | Bedding | 36.24105 | 161.766 |
| Canyon-Farthest | Bedding | 28.41006 | 201.5909 |

# Appendix 2

| Location Name | Plane Type | Dip | Strike |
|---|---|---|---|
| On the Contact | Joint | 76.559 | 260.916 |
| On the Contact | Joint | 13.65 | 172.2 |
| On the Contact | Joint | 85.532 | 275.177 |
| On the Contact | Joint | 88.335 | 119.292 |
| On the Contact | Joint | 69.662 | 271.842 |
| On the Contact | Joint | 41.86 | 280.986 |
| On the Contact | Joint | 54.967 | 271.62 |
| On the Contact | Joint | 66.138 | 314.681 |
| On the Contact | Joint | 7.209 | 84.204 |
| On the Contact | Joint | 75.678 | 265.789 |
| On the Contact | Joint | 88.022 | 85.327 |
| On the Contact | Joint | 56.757 | 249.827 |
| On the Contact | Joint | 46.444 | 265.013 |
| On the Contact | Joint | 56.403 | 293.547 |
| On the Contact | Joint | 38.204 | 324.698 |
| On the Contact | Joint | 86.087 | 273.083 |
| On the Contact | Joint | 54.005 | 258.559 |
| On the Contact | Joint | 86.044 | 84.579 |
| On the Contact | Joint | 89.014 | 81.944 |
| On the Contact | Joint | 86.846 | 96.255 |
| On the Contact | Joint | 84.956 | 272.435 |
| On the Contact | Joint | 68.064 | 74.29 |
| On the Contact | Joint | 43.129 | 55.384 |
| On the Contact | Joint | 59.657 | 276.885 |
| On the Contact | Joint | 47.855 | 255.809 |
| On the Contact | Joint | 83.956 | 285.395 |
| On the Contact | Joint | 77.373 | 260.514 |
| On the Contact | Joint | 62.141 | 30.122 |
| On the Contact | Joint | 25.458 | 271.278 |
| On the Contact | Joint | 9.043 | 286.984 |
| On the Contact | Joint | 82.158 | 129.345 |
| On the Contact | Joint | 24.189 | 264.196 |
| On the Contact | Joint | 64.799 | 315.769 |
| On the Contact | Joint | 63.26 | 58.123 |
| On the Contact | Joint | 50.39 | 105.757 |
| On the Contact | Joint | 19.648 | 309.163 |
| On the Contact | Joint | 79.3 | 132.111 |
| On the Contact | Joint | 88.741 | 266.291 |
| On the Contact | Joint | 57.802 | 278.856 |

| | | | |
|---|---|---|---|
| On the Contact | Joint | 80.4 | 53.429 |
| Closest to the Contact | Bedding | 65.321 | 98.505 |
| Closest to the Contact | Bedding | 68.6 | 102.778 |
| Closest to the Contact | Bedding | 68.54 | 71.82 |
| Closest to the Contact | Joint | 45.574 | 253.105 |
| Closest to the Contact | Joint | 38.482 | 284.159 |
| Closest to the Contact | Joint | 62.328 | 279.435 |
| Closest to the Contact | Joint | 31.509 | 303.415 |
| Closest to the Contact | Joint | 55.993 | 261.309 |
| Closest to the Contact | Joint | 86.551 | 196.459 |
| Closest to the Contact | Joint | 89.589 | 18.55 |
| Closest to the Contact | Joint | 88.565 | 199.955 |
| Closest to the Contact | Joint | 47.542 | 268.261 |
| Closest to the Contact | Joint | 16.269 | 297.175 |
| Closest to the Contact | Joint | 78.098 | 281.576 |
| Closest to the Contact | Joint | 21.11 | 269.159 |
| Closest to the Contact | Joint | 69.031 | 261.329 |
| Closest to the Contact | Joint | 33.893 | 256.564 |
| Closest to the Contact | Joint | 87.587 | 197.411 |
| Closest to the Contact | Joint | 85.819 | 39.46 |
| Closest to the Contact | Joint | 81.432 | 201.064 |
| Closest to the Contact | Joint | 83.884 | 24.825 |
| Closest to the Contact | Joint | 87.083 | 198.89 |
| Closest to the Contact | Joint | 89.912 | 202.081 |
| Closest to the Contact | Joint | 57.297 | 244.988 |
| Closest to the Contact | Joint | 88.376 | 16.338 |
| Closest to the Contact | Joint | 89.798 | 16.888 |
| Closest to the Contact | Joint | 32.512 | 292.559 |
| Closest to the Contact | Joint | 36.358 | 262.133 |
| Closest to the Contact | Joint | 49.379 | 280.469 |
| Closest to the Contact | Joint | 89.97 | 209.44 |
| Closest to the Contact | Joint | 57.461 | 284.478 |
| Closest to the Contact | Joint | 45.827 | 304.562 |
| Closest to the Contact | Joint | 17.639 | 6.888 |
| Closest to the Contact | Joint | 43.363 | 238.944 |
| Closest to the Contact | Joint | 81.04 | 259.307 |
| Closest to the Contact | Joint | 62.705 | 101.464 |
| Closest to the Contact | Joint | 79.866 | 303.661 |
| Closest to the Contact | Joint | 41.557 | 287.692 |
| Closest to the Contact | Joint | 79.756 | 22.689 |
| Closest to the Contact | Joint | 86.139 | 200.227 |
| Closest to the Contact | Joint | 86.842 | 200.552 |

| | | | |
|---|---|---|---|
| Closest to the Contact | Joint | 53.795 | 197.945 |
| Closest to the Contact | Joint | 88.977 | 197.758 |
| Closest to the Contact | Joint | 77.515 | 33.678 |
| Closest to the Contact | Joint | 49.342 | 39.757 |
| Closest to the Contact | Joint | 87.775 | 47.343 |
| Closest to the Contact | Joint | 20.144 | 290.347 |
| Closest to the Contact | Joint | 83.374 | 58.37 |
| Intermediate-Cutler Side | Bedding | 50.176 | 110.301 |
| Intermediate-Cutler Side | Bedding | 51.791 | 110.051 |
| Intermediate-Cutler Side | Bedding | 29.046 | 137.03 |
| Intermediate-Cutler Side | Bedding | 55.622 | 107.94 |
| Intermediate-Cutler Side | Bedding | 59.001 | 103.256 |
| Intermediate-Cutler Side | Joint | 37.502 | 278.209 |
| Intermediate-Cutler Side | Joint | 43.81 | 282.309 |
| Intermediate-Cutler Side | Joint | 85.705 | 3.454 |
| Intermediate-Cutler Side | Joint | 40.221 | 182.416 |
| Intermediate-Cutler Side | Joint | 53.567 | 86.395 |
| Intermediate-Cutler Side | Joint | 61.914 | 17.52 |
| Intermediate-Cutler Side | Joint | 53.474 | 28.108 |
| Intermediate-Cutler Side | Joint | 65.603 | 159.141 |
| Intermediate-Cutler Side | Joint | 39.016 | 178.906 |
| Intermediate-Cutler Side | Joint | 65.747 | 25.624 |
| Intermediate-Cutler Side | Joint | 35.319 | 64.123 |
| Intermediate-Cutler Side | Joint | 51.394 | 305.517 |
| Intermediate-Cutler Side | Joint | 16.647 | 169.77 |
| Intermediate-Cutler Side | Joint | 54.548 | 165.389 |
| Intermediate-Cutler Side | Joint | 57.239 | 207.093 |
| Intermediate-Cutler Side | Joint | 43.268 | 292.794 |
| Intermediate-Cutler Side | Joint | 84.013 | 136.649 |
| Intermediate-Cutler Side | Joint | 47.059 | 302.384 |
| Intermediate-Cutler Side | Joint | 54.797 | 275.831 |
| Intermediate-Cutler Side | Joint | 41.701 | 318.594 |
| Intermediate-Cutler Side | Joint | 28.582 | 288.207 |
| Intermediate-Cutler Side | Joint | 33.393 | 226.471 |
| Intermediate-Cutler Side | Joint | 11.102 | 340.801 |
| Intermediate-Cutler Side | Joint | 44.617 | 305.711 |
| Intermediate-Cutler Side | Joint | 35.095 | 48.562 |
| Intermediate-Cutler Side | Joint | 61.666 | 312.15 |
| Intermediate-Cutler Side | Joint | 47.495 | 270.892 |
| Intermediate-Cutler Side | Joint | 81.932 | 133.884 |
| Intermediate-Cutler Side | Joint | 39.828 | 238.588 |
| Intermediate-Cutler Side | Joint | 37.067 | 320.874 |

| | | | |
|---|---|---|---|
| Intermediate-Cutler Side | Joint | 42.07 | 320.008 |
| Intermediate-Cutler Side | Joint | 49.285 | 204.436 |
| Intermediate-Cutler Side | Joint | 33.384 | 293.952 |
| Intermediate-Cutler Side | Joint | 23.507 | 348.459 |
| Intermediate-Cutler Side | Joint | 66.677 | 329.809 |
| Intermediate-Cutler Side | Joint | 42.45 | 342.968 |
| Intermediate-Cutler Side | Joint | 29.637 | 335.794 |
| Intermediate-Cutler Side | Joint | 59.87 | 340.416 |
| Intermediate-Cutler Side | Joint | 56.88 | 30.517 |
| Intermediate-Cutler Side | Joint | 57.063 | 338.326 |
| Intermediate-Cutler Side | Joint | 49.788 | 276.766 |
| Intermediate-Cutler Side | Joint | 68.11 | 295.683 |
| Intermediate-Cutler Side | Joint | 43.097 | 30.497 |
| Intermediate-Cutler Side | Joint | 78.504 | 3.543 |
| Intermediate-Cutler Side | Joint | 8.498 | 142.058 |
| Intermediate-Cutler Side | Joint | 16.977 | 134.469 |
| Intermediate-Cutler Side | Joint | 36.516 | 130.287 |
| Intermediate-Cutler Side | Joint | 33.758 | 308.042 |
| Intermediate-Cutler Side | Joint | 28.79 | 65.206 |
| Intermediate-Cutler Side | Joint | 61.592 | 204.23 |
| Intermediate-Cutler Side | Joint | 81.564 | 293.083 |
| Intermediate-Cutler Side | Joint | 14.085 | 278.306 |
| Intermediate-Cutler Side | Joint | 46.143 | 339.075 |
| Intermediate-Cutler Side | Joint | 69.458 | 296.883 |
| Intermediate-Cutler Side | Joint | 71.521 | 336.022 |
| Intermediate-Cutler Side | Joint | 22.544 | 208.142 |
| Intermediate-Cutler Side | Joint | 23.042 | 190.745 |
| Intermediate-Cutler Side | Joint | 21.904 | 4.879 |
| Intermediate-Cutler Side | Joint | 47.977 | 342.95 |
| Intermediate-Cutler Side | Joint | 33.655 | 327.79 |
| Intermediate-Cutler Side | Joint | 44.934 | 344.578 |
| Intermediate-Cutler Side | Joint | 77.286 | 169.583 |
| Intermediate-Cutler Side | Joint | 36.54 | 313.598 |
| Second Farthest | Bedding | 33.53 | 145.032 |
| Second Farthest | Bedding | 27.306 | 123.614 |
| Second Farthest | Bedding | 28.577 | 139.514 |
| Second Farthest | Bedding | 45.576 | 140.639 |
| Second Farthest | Joint | 45.645 | 229.577 |
| Second Farthest | Joint | 37.178 | 226.595 |
| Second Farthest | Joint | 58.648 | 264.622 |
| Second Farthest | Joint | 50.464 | 245.519 |
| Second Farthest | Joint | 53.347 | 261.91 |

| | | | |
|---|---|---|---|
| Second Farthest | Joint | 31.389 | 225.352 |
| Second Farthest | Joint | 29.917 | 208.681 |
| Second Farthest | Joint | 78.245 | 90.268 |
| Second Farthest | Joint | 52.604 | 107.194 |
| Second Farthest | Joint | 76.809 | 250.25 |
| Second Farthest | Joint | 73.851 | 81.515 |
| Second Farthest | Joint | 42.314 | 226.37 |
| Second Farthest | Joint | 36.951 | 225.938 |
| Second Farthest | Joint | 42.799 | 236.081 |
| Second Farthest | Joint | 40.949 | 219.494 |
| Second Farthest | Joint | 50.021 | 233.158 |
| Second Farthest | Joint | 50.282 | 241.519 |
| Second Farthest | Joint | 40.834 | 316.387 |
| Second Farthest | Joint | 60.919 | 336.632 |
| Second Farthest | Joint | 47.267 | 335.522 |
| Second Farthest | Joint | 44.348 | 321.807 |
| Second Farthest | Joint | 38.14 | 319.246 |
| Second Farthest | Joint | 57.92 | 310.364 |
| Second Farthest | Joint | 43.273 | 325.44 |
| Second Farthest | Joint | 45.383 | 295.28 |
| Second Farthest | Joint | 52.292 | 324.864 |
| Second Farthest | Joint | 36.034 | 309.582 |
| Second Farthest | Joint | 47.331 | 346.972 |
| Second Farthest | Joint | 61.138 | 331.527 |
| Second Farthest | Joint | 30.145 | 318.176 |
| Second Farthest | Joint | 44.099 | 316.512 |
| Second Farthest | Joint | 61.191 | 335.442 |
| Second Farthest | Joint | 62.768 | 319.14 |
| Second Farthest | Joint | 46.31 | 331.45 |
| Second Farthest | Joint | 42.32 | 327.981 |
| Second Farthest | Joint | 64.939 | 330.592 |
| Second Farthest | Joint | 27.668 | 331.205 |
| Second Farthest | Joint | 17.763 | 0.235 |
| Second Farthest | Joint | 47.714 | 313.238 |
| Second Farthest | Joint | 41.141 | 306.236 |
| Second Farthest | Joint | 58.821 | 242.735 |
| Second Farthest | Joint | 50.321 | 239.324 |
| Second Farthest | Joint | 48.602 | 338.051 |
| Second Farthest | Joint | 45.794 | 235.358 |
| Second Farthest | Joint | 43.513 | 235.41 |
| Second Farthest | Joint | 41.018 | 241.67 |
| Second Farthest | Joint | 33.568 | 322.214 |

| | | | |
|---|---|---|---|
| Second Farthest | Joint | 30.709 | 50.94 |
| Second Farthest | Joint | 57.144 | 227.636 |
| Second Farthest | Joint | 64.393 | 253.831 |
| Second Farthest | Joint | 69.242 | 186.267 |
| Second Farthest | Joint | 64.739 | 244.451 |
| Second Farthest | Joint | 62.418 | 267.506 |
| Second Farthest | Joint | 64.691 | 106.229 |
| Second Farthest | Joint | 63.247 | 325.603 |
| Second Farthest | Joint | 38.473 | 199.82 |
| Second Farthest | Joint | 40.834 | 317.336 |
| Second Farthest | Joint | 51.478 | 264.815 |
| Second Farthest | Joint | 42.848 | 251.746 |
| Second Farthest | Joint | 61.877 | 255.136 |
| Second Farthest | Joint | 25.391 | 231.93 |
| Second Farthest | Joint | 57.929 | 229.951 |
| Second Farthest | Joint | 64.476 | 139.22 |
| Second Farthest | Joint | 54.152 | 126.443 |
| Second Farthest | Joint | 16.926 | 228.258 |
| Second Farthest | Joint | 41.729 | 190.309 |
| Second Farthest | Joint | 69.496 | 201.094 |
| Second Farthest | Joint | 41.361 | 162.491 |
| Second Farthest | Joint | 75.915 | 319.086 |
| Second Farthest | Joint | 55.557 | 259.911 |
| Second Farthest | Joint | 57.915 | 171.127 |
| Second Farthest | Joint | 54.44 | 246.785 |
| Second Farthest | Joint | 45.348 | 170.601 |
| Second Farthest | Joint | 49.619 | 312.1 |

# Appendix 3

| Tool | Dip | Strike |
|---|---|---|
| Phone | 4.948235 | 188.8965 |
| Phone | 71.62321 | 186.5846 |
| Phone | 30.13729 | 68.16112 |
| Phone | 18.54878 | 63.49782 |
| Phone | 22.27633 | 11.7323 |
| Phone | 36.3609 | 24.42918 |
| Phone | 27.80125 | 155.783 |
| Phone | 33.36781 | 61.55971 |
| Phone | 34.31878 | 49.22037 |
| Phone | 26.90308 | 42.90192 |
| Phone | 30.36902 | 47.8577 |
| Phone | 20.25322 | 9.875694 |
| Phone | 25.91556 | 339.083 |
| Phone | 27.16047 | 332.9358 |
| Phone | 14.5024 | 2.386642 |
| Phone | 84.75029 | 7.09938 |
| Phone | 63.73704 | 189.4639 |
| Phone | 18.79341 | 117.8147 |
| Phone | 22.02708 | 163.2516 |
| Phone | 33.64728 | 163.5974 |
| Phone | 34.92154 | 179.8282 |
| Phone | 25.67582 | 83.19408 |
| Phone | 31.58885 | 125.4419 |
| Phone | 39.01783 | 144.8111 |
| Phone | 62.42533 | 167.5327 |
| Phone | 16.45887 | 31.51407 |
| Phone | 29.07506 | 170.4008 |
| Phone | 21.84569 | 61.87312 |
| Phone | 19.38584 | 77.45442 |
| Phone | 71.22604 | 338.7667 |
| Phone | 19.5227 | 84.13745 |
| Phone | 33.11543 | 84.29301 |
| Phone | 32.43503 | 86.71559 |
| Phone | 20.73262 | 8.234489 |
| Phone | 73.44069 | 4.649513 |
| Phone | 16.302 | 87.56659 |
| Phone | 8.412468 | 165.382 |
| Phone | 25.88165 | 74.62738 |
| Phone | 7.87179 | 175.1519 |

| | | |
|---|---|---|
| Phone | 68.20924 | 341.3586 |
| Phone | 60.76585 | 339.5681 |
| Phone | 20.66308 | 60.50365 |
| Phone | 13.16547 | 68.11871 |
| Phone | 35.78185 | 14.02145 |
| Phone | 69.44563 | 338.7291 |
| Phone | 69.93477 | 160.384 |
| Phone | 17.65869 | 346.136 |
| Phone | 82.54185 | 160.0206 |
| Phone | 82.79329 | 348.9674 |
| Phone | 44.05102 | 344.017 |
| Phone | 62.4877 | 5.330338 |
| Phone | 21.0619 | 95.44962 |
| Phone | 25.46165 | 70.90918 |
| Phone | 27.45781 | 94.2907 |
| Phone | 22.10174 | 84.05116 |
| Phone | 36.19484 | 357.8251 |
| Phone | 33.01919 | 3.743591 |
| Phone | 35.15741 | 351.5049 |
| Phone | 57.80047 | 353.3727 |
| Phone | 88.40904 | 11.64263 |
| Compass | 90 | 353 |
| Compass | 59 | 356 |
| Compass | 39 | 342 |
| Compass | 35 | 350 |
| Compass | 16 | 90 |
| Compass | 50 | 2 |
| Compass | 20 | 105 |
| Compass | 25 | 81 |
| Compass | 29 | 94 |
| Compass | 53 | 349 |
| Compass | 65 | 5 |
| Compass | 89 | 346 |
| Compass | 76 | 347 |
| Compass | 15 | 78 |
| Compass | 69 | 74 |
| Compass | 18 | 52 |
| Compass | 55 | 341 |
| Compass | 19 | 106 |
| Compass | 26 | 70 |
| Compass | 13 | 90 |
| Compass | 7 | 14 |

| | | |
|---|---|---|
| Compass | 71 | 348 |
| Compass | 3 | 47 |
| Compass | 26 | 85 |
| Compass | 27 | 152 |
| Compass | 81 | 345 |
| Compass | 31 | 351 |
| Compass | 24 | 258 |
| Compass | 72 | 348 |
| Compass | 15 | 85 |
| Compass | 16 | 72 |
| Compass | 83 | 142 |
| Compass | 25 | 72 |
| Compass | 20 | 85 |
| Compass | 14 | 48 |
| Compass | 58 | 352 |
| Compass | 29 | 339 |
| Compass | 24 | 30 |
| Compass | 4 | 2 |
| Compass | 25 | 55 |
| Compass | 29 | 347 |
| Compass | 41 | 178 |
| Compass | 67 | 174 |
| Compass | 17 | 224 |
| Compass | 43 | 194 |
| Compass | 18 | 206 |
| Compass | 25 | 262 |
| Compass | 29 | 340 |
| Compass | 26 | 5 |
| Compass | 50 | 40 |
| Compass | 38 | 38 |
| Compass | 21 | 50 |
| Compass | 24 | 318 |
| Compass | 30 | 26 |
| Compass | 36 | 22 |
| Compass | 24 | 247 |
| Compass | 25 | 1 |
| Compass | 70 | 5 |
| Compass | 9 | 329 |

# Appendix 4

| Dip | Strike |
|---|---|
| 86.93183899 | 188.0206 |
| 78.43344879 | 8.237022 |
| 9.94253826 | 121.3026 |
| 74.69129944 | 153.1973 |
| 46.56910324 | 7.359779 |
| 74.72724915 | 159.6113 |
| 81.03470612 | 166.0405 |
| 22.23875618 | 354.0491 |
| 17.58584785 | 58.61084 |
| 79.88212585 | 175.3539 |
| 74.75798035 | 164.0471 |
| 52.78524017 | 158.4556 |
| 76.27741241 | 351.847 |
| 12.49042988 | 118.5608 |
| 84.75091553 | 355.7199 |
| 65.16580963 | 158.2955 |
| 72.48669434 | 353.5581 |
| 74.23563385 | 172.4541 |
| 80.51147461 | 169.8446 |
| 79.60308075 | 168.7347 |
| 84.81478119 | 157.8499 |
| 80.82881165 | 345.9218 |
| 81.91376495 | 173.9259 |
| 32.30918121 | 162.1965 |
| 14.27886486 | 59.86685 |
| 10.48571396 | 80.75381 |
| 7.32533503 | 61.34114 |
| 66.4355545 | 156.9999 |
| 73.95700836 | 169.2721 |
| 78.32726288 | 178.8651 |
| 54.78507233 | 275.8413 |
| 43.6975708 | 270.4276 |
| 21.89840126 | 323.5857 |
| 26.42608261 | 331.0451 |
| 45.90945816 | 355.4197 |
| 15.33202553 | 121.2265 |
| 55.38374329 | 358.2066 |
| 62.48686981 | 358.8654 |
| 7.11376524 | 28.24515 |

| | |
|---|---|
| 70.89863586 | 164.3468 |
| 78.63576508 | 169.5912 |
| 8.95658684 | 319.066 |
| 29.20736122 | 359.0963 |
| 31.432621 | 5.780457 |
| 77.86917114 | 335.1301 |
| 13.58761501 | 25.10345 |
| 16.3331871 | 106.1944 |
| 80.95529175 | 154.6776 |
| 36.0331955 | 16.44467 |
| 51.52423477 | 352.2583 |
| 66.83234406 | 168.8799 |
| 73.84069824 | 179.1206 |
| 82.8106842 | 180.9504 |
| 69.58707428 | 173.6232 |
| 82.55632782 | 177.2373 |
| 25.61652756 | 292.4061 |
| 14.48073006 | 334.2122 |
| 77.61930847 | 170.5388 |
| 71.12614441 | 161.5626 |
| 78.17943573 | 161.7873 |
| 82.74724579 | 164.4059 |
| 69.49313354 | 153.517 |
| 68.43950653 | 154.971 |
| 73.63913727 | 157.9221 |
| 67.89931488 | 162.9387 |
| 86.92583466 | 351.6616 |
| 89 | 277 |
| 68 | 262 |
| 65 | 277 |
| 57 | 264 |
| 62 | 270 |
| 80 | 276 |
| 89 | 332 |
| 34 | 261 |
| 88 | 271 |
| 82 | 295 |
| 80 | 278 |
| 66 | 282 |
| 75 | 264 |
| 86 | 265 |
| 56 | 264 |

| | |
|---|---|
| 71 | 275 |
| 73 | 265 |
| 76 | 109 |
| 66 | 267 |
| 79 | 263 |
| 88 | 90 |
| 89 | 260 |
| 59 | 261 |
| 89 | 346 |
| 75 | 290 |
| 69 | 287 |
| 84 | 259 |
| 89 | 283 |
| 48 | 268 |
| 75 | 274 |
| 88 | 260 |
| 85 | 251 |
| 89 | 179 |
| 75 | 257 |
| 84 | 109 |
| 69 | 267 |
| 85 | 88 |
| 74 | 259 |
| 50 | 266 |
| 76 | 269 |
| 88 | 175 |
| 33 | 32 |
| 78 | 65 |
| 24 | 277 |

# Vita

Muhammed Tarik Iraz, the oldest of four children by Faruk and Rakiye, was born in 1991 in Istanbul, Turkey. He was always curious of man-made items and this made him interested in engineering. Because of his father's job, he went to school in many different cities, and he finally completed his high school, Midyat Aziz Onen Lisesi, Mardin, in 2009. Later, he began studying Geological Engineering in Akdeniz University, Antalya and graduated in 2013. Once he was a senior, he wrote his seminar study and completing thesis on Remote Sensing.

To start working in national companies, he prepared for the national exam that is written once in two years and placed 94$^{th}$ from over 12000 people in his major, in 2014. While he was waiting for the results, he started his graduate studies in Akdeniz University and applied for a study abroad scholarship sponsored by the Ministry of National Education. After he placed 3$^{rd}$ from 57 people, he started studying English in Akdeniz University, Yildiz Technical University and University of Texas at Arlington from March 2015 to December 2016.

In the spring of 2017, he started his master's degree in University of Texas at El Paso. Based on his agreement with Turkish Petroleum Corporation, he focused on fractures and completed his thesis on fractures of Western Onion Creek, Moab, UT.

Contact information: mtiraz@miners.utep.edu

+90 531 855 47 47

This thesis/dissertation was typed by Muhammed Tarik Iraz.